Design of a 4wd-4ws robot vehicle for the VEHIL test facility of TNO Automotive

van den Boer, M.C.

Award date:
2006

TU/e technische universiteit eindhoven

Design of a 4wd-4ws robot vehicle for the VEHIL test facility of TNO Automotive

M.C. van den Boer

DCT 2006.06

Master's Thesis

Supervisor: Prof.dr. H. Nijmeijer
Coaches: Dr.ir. P.C.J.N. Rosielle
Ir. J. Ploeg (TNO)

Technische Universiteit Eindhoven
Department of Mechanical Engineering
Section Dynamics and Control

Eindhoven, January 2006

/ faculteit werktuigbouwkunde

Table of contents

Summary

Safety related vehicle systems are tested in a simulated traffic situation in the VEHIL test facility of TNO automotive in Helmond. The traffic around the vehicle under test is simulated with highly dynamic robot vehicles. The unsprung robot vehicles that are currently being used are analyzed and, as a result of this analysis, design requirements for a new robot vehicle are made. An investigation is done to find out which components can be used in the new vehicle design considering performance and costs.

The robot vehicle must be redesigned to have wheel suspension and unlimited steering angles on all four wheels. While designing the various vehicle components, calculations and finite element analyses have been made to assure these components are suitable. Basic vehicle dynamic simulations in Matlab are performed to verify subsystem functionality. With the use of 3D CAD software a new robot vehicle is constructed.

The new robot vehicle with double wishbone suspension is designed to the same performance as the existing vehicle, but at reduced cost. It is anticipated that further cost reduction is possible in the near future because of the ongoing development of motors, batteries and electronics.

Direct cost per new robot vehicle is estimated to be around € 130.000,-

Introduction

The number of passenger cars in the Netherlands has increased over the last twenty years from 4,5 million in 1985 to 7 million in 2005. Because of this, driving a car nowadays is more demanding for the driver than it used to be. A lot of development is done to help the drivers while they are on the road. There are, for example, already systems in use which automatically adapt the vehicle speed to the distance between two vehicles. Other systems monitor the surroundings, other vehicles and even the driver of the vehicle and take actions if necessary to avoid accidents. So the use of these systems can help to increase the safety on the road.

In the developments phase of such vehicle systems, testing is necessary. The Netherlands Organisation for Applied Scientific Research TNO develops and tests such vehicle systems at the automotive department which is part of the business unit "Science and Industry". Within the automotive department is the division Advanced Chassis and Transport Systems, ACTS. This division, located in Helmond, works mainly in the field of vehicle dynamics and advanced vehicle control. For the testing of new vehicle systems ACTS has built the VEHIL test facility. This facility is used for testing of vehicle systems in a controlled simulated traffic environment. In this test facility, robot vehicles are used for the simulation of traffic around the vehicle under test.

For the use in VEHIL, these robot vehicles can be further developed. In addition, these robots can be used in other applications. For this purpose a new design for these robot vehicles, with wheel suspension and unlimited steering angles at relative low cost is desired. This report describes the design of this new robot vehicle.

Those who are new to the VEHIL test facility: In chapter 1 the VEHIL test facility and its robots are explained in more detail. The existing robot vehicle is analysed and described in chapter 2. Design requirements: chapter 3. Energy source for the new robot vehicle: chapter 4. Motors, wheels and tires: Chapter 5. The suspension and the steering: chapter 6 and chapter 7. Vehicle assembly: chapter 8, followed by conclusions and recommendations. **Design engineers**: detailed design data have been placed in appendices in a separate cover.

Chapter 1 VEHIL and the Moving Base

§ 1.1 VEHIL

The VEHIL test laboratory is used for testing intelligent vehicle systems, like adaptive cruise control, lane keeping sensors, pre crash sensing systems and so on. In this laboratory realistic traffic situations can be simulated in a controlled environment and without high vehicle speeds.

VEHIL is short for Vehicle Hardware-In-the-Loop. It means the actual vehicle (hardware) is used in the simulation control loop. The VEHIL laboratory is 200 meters long and 40 meters wide, see figure 1.1.1.

The vehicle under test is placed on a roller bench with a dynamometer and is operated automatically or by a human driver. Other road users are simulated by robot vehicles called "Moving Base". There is also a control room from where all the vehicles are controlled and where data from each test is logged.

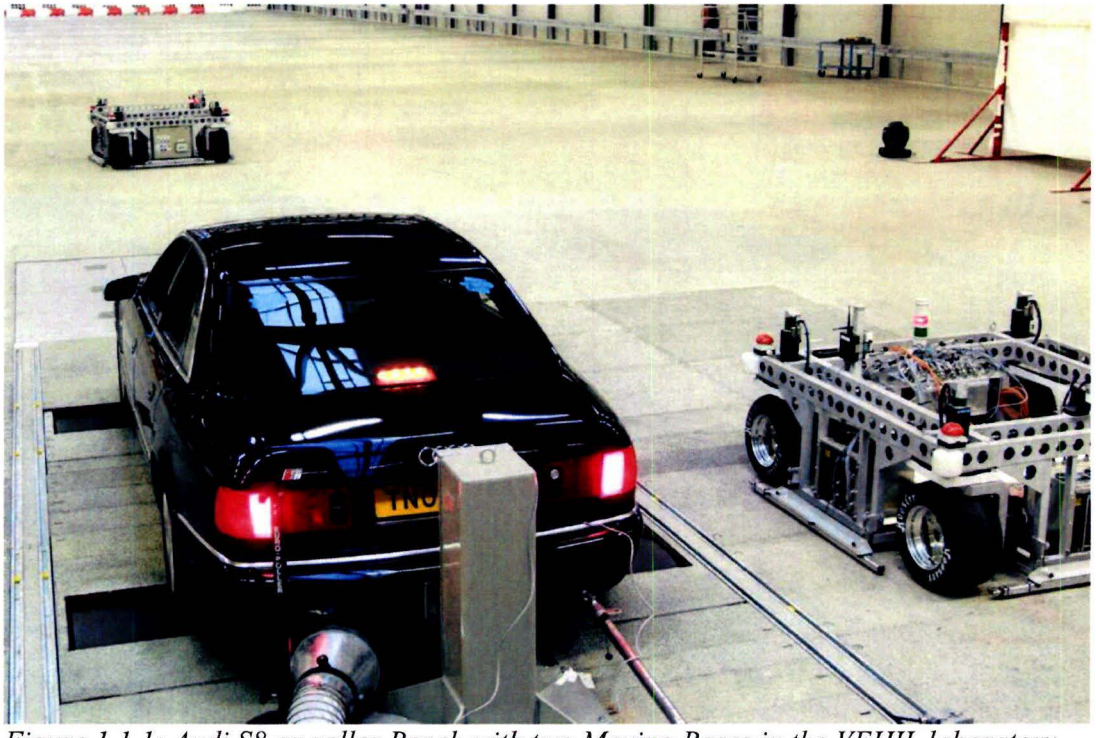

Figure 1.1.1: Audi S8 on roller Bench with two Moving Bases in the VEHIL laboratory

Because the vehicle under test is on a roller bench, it does not move in the real world. The Moving Bases move relative to the test vehicle to simulate a realistic road situation. When for example the vehicle under test is "driving" 100 [km/h] behind another vehicle, simulated by a Moving Base, that has the same speed, the Moving Base does not move

and the distance between the two stays the same. If there is a difference in speed between the two vehicles in simulation, the Moving Base has to move with the difference of the two velocities in the real world. Normal passenger cars can decelerate up to 10 [m/s^2], which is a lot more than their ability to accelerate. Because of this, the Moving Base has to be able to accelerate 10 [m/s^2]. In the case of a lane change simulation, the Moving Base also has to make the relative movement between the two vehicles. This means the Moving Base has to move crab-like, because there is no longitudinal speed component, see figure 1.1.2.

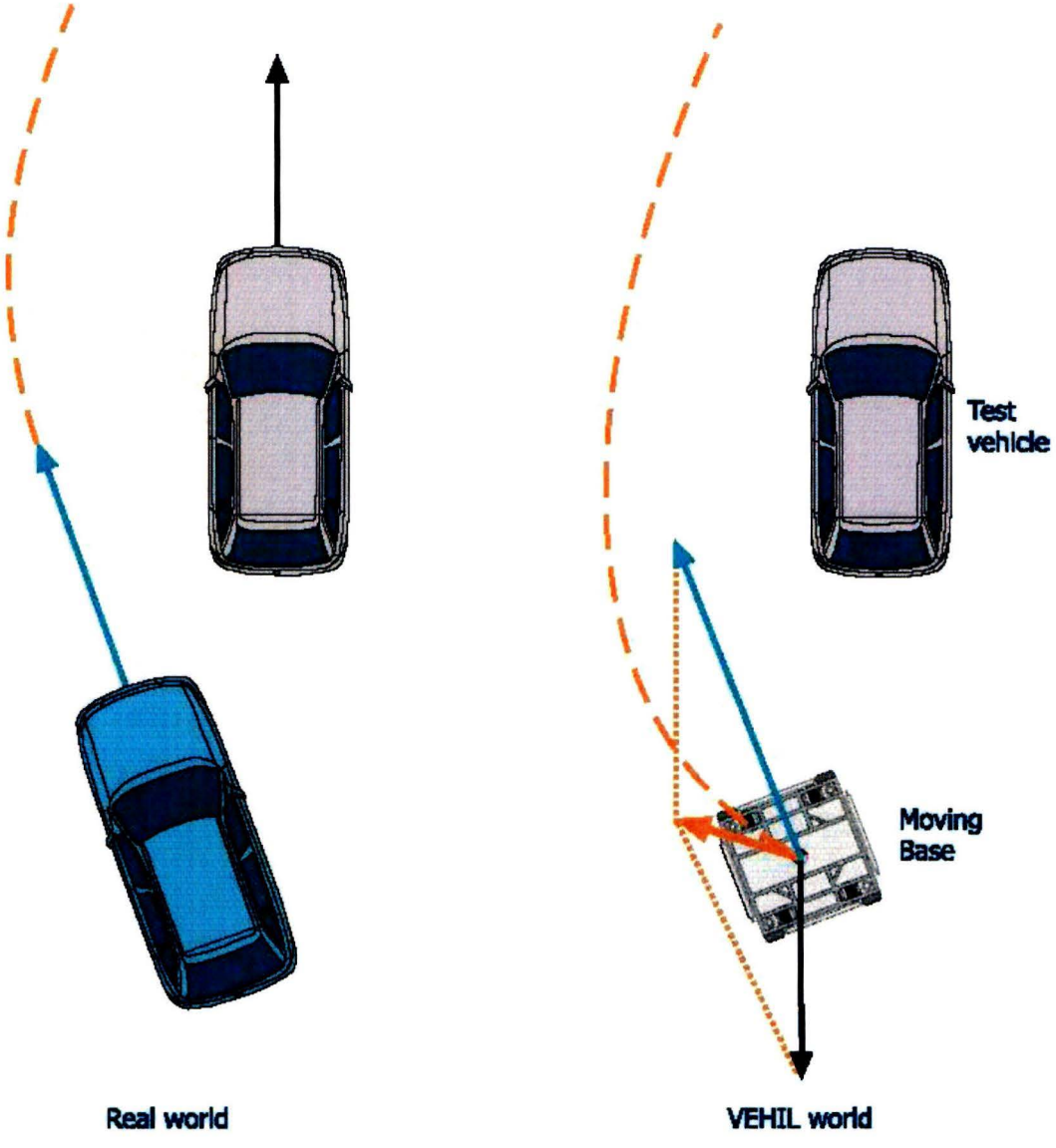

Figure 1.1.2: Comparison of the real and relative movements in a VEHIL test

More information about VEHIL can be found in [TNO VEHIL]

§ 1.2 Moving Base

In the development phase of the VEHIL test facility it turned out that no vehicle had the specifications that were needed. A new automatic guided vehicle, AGV, had to be developed.

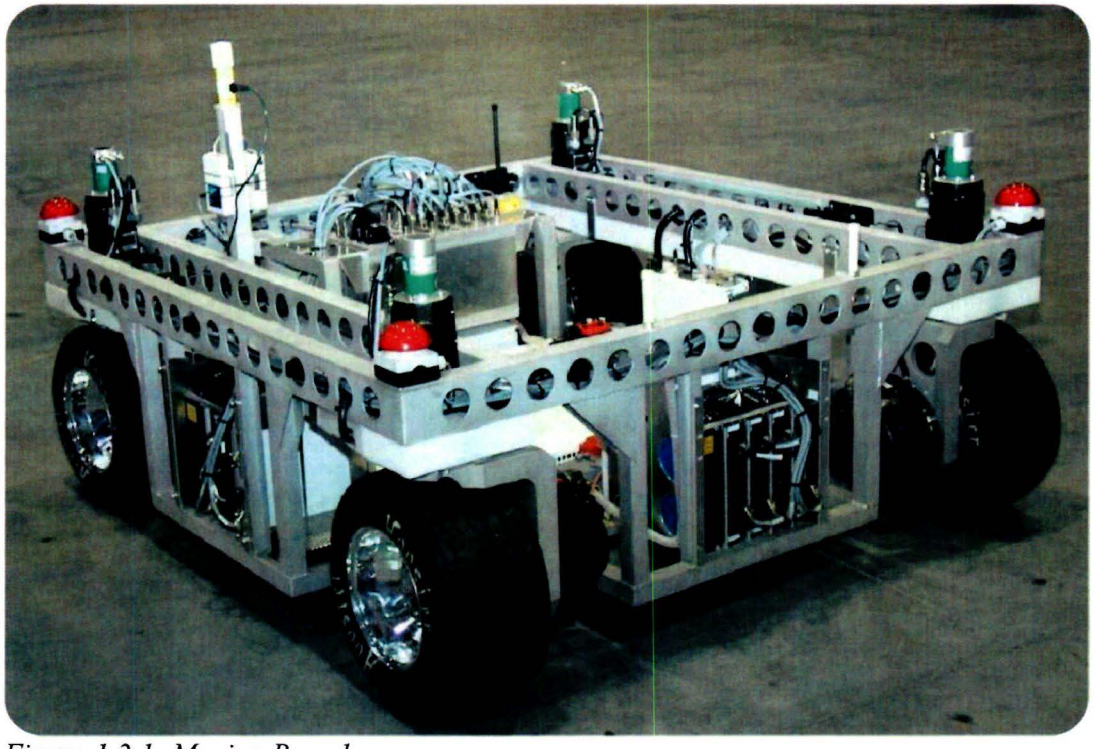

Figure 1.2.1: Moving Base 1

The new AGV, called "Moving Base" is a high performance robot vehicle, see figure 1.2.1. The Moving Base has four wheels with racing tires. Each wheel is driven by a disc armature servomotor with a planetary reduction and steered by a servomotor with a cycloid reduction. All four wheels of the Moving Base can be steered -350° to +350° from the initial position until a stop, which makes complex movements possible, see figure 1.2.2.

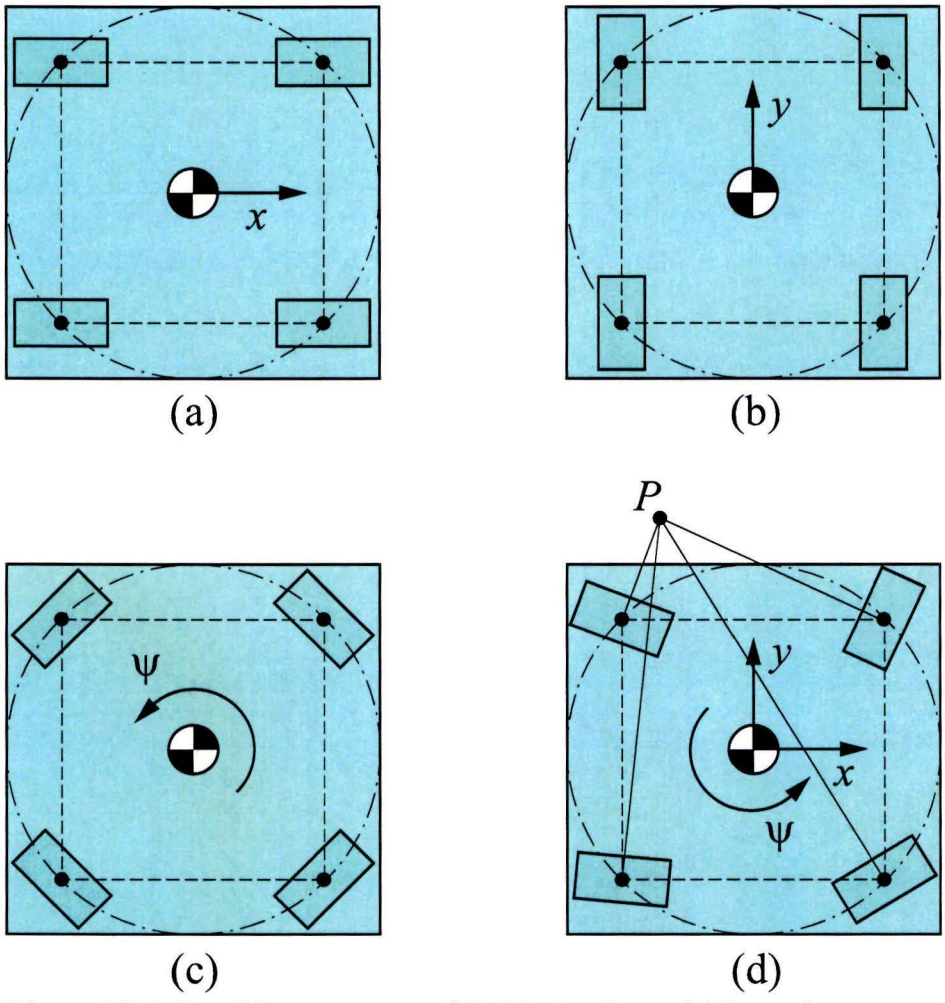

Figure 1.2.2: Possible movements of the Moving Base. (a) Lateral movement; (b) Longitudinal movement; (c) Rotation about vehicle centre; (d) Rotate about an arbitrary pole, P

The motors receive their energy from a custom made battery pack that was developed by TNO Environment, Energy and Process Innovation. This battery has a high charge and discharge rate and a high energy density. The centre of gravity of the Moving Base is almost in the middle of the four wheels and an effort is made to keep it as low as possible. The lower the centre of gravity, the better is the distribution of all the forces on the wheels.

For simplicity, all the motors and their reductions are placed directly on the axis of the component they drive. Each wheel is directly mounted to the reduction, so the bearings in this gear unit function as wheel bearings.

The Moving Base can operate very quietly, because the electric motors produce little noise. Besides this, there is only noise of cooling fans and the squeaking of the tires.

The Moving Base and all of its components are controlled by "ControlCIT", which is an acronym for Control Computer for Intelligent Transport systems. This is a small, lightweight, PC/104 based control system that is developed by TNO Automotive for the control of AGV's and other transport systems. [TNO ControlCIT]

The floor in the VEHIL laboratory has a magnet grid which is used for the positioning of the Moving Base that can detect the magnets by means of four magnet detection rulers. The position is also calculated from the odometry data, which are the signals from the wheel encoders, steering encoders, gyroscope and accelerometers. The position calculated by this method has an error because of tire slip.

In table 1.2.1 some specifications of the Moving Base are summarized. More detailed information about the Moving Base can be found in appendix A [Specifications current Moving Base] and [TNO MB].

vehicle mass	621 [kg]
wheel base	1.4 [m]
track width	1.4 [m]
maximum driving speed	50 [km/h]
maximum acceleration	10 [m/s^2]
installed power	52 [kW]
acceleration time from 0 to 50 km/h	2.1 [s]
Battery pack with NIMH cells	336 [V] / 138 [kg]

Table 1.2.1 Specifications of the Moving Base

§ 1.3 Assignment definition

Due to its unique specifications the Moving Base can be adapted for other applications that share one or more characteristics with the Moving Base in VEHIL. Some important characteristics of the Moving Base are:

- Manoeuvrability
- High acceleration in all directions
- Short response time
- Driving of programmed paths
- Remotely controllable

The Moving Base can, for example, be adapted for use as a "fun race vehicle", "attraction in a theme park", "camera robot" or for the use in a "driving simulator". More information about alternative applications for the Moving Base can be found in [Tertoolen].

When the Moving Base will be used in other applications, it may need some other features. An important feature that is required for most applications is suspension. The new Moving Base will operate in environments where the underground may not be as flat as in the VEHIL-laboratory. For more freedom of movement it is also desirable to have an unlimited steering angle.

The assignment is to make a design for a new robot vehicle which has the same performance as the existing Moving Bases and also has primary suspension and unlimited steering as mentioned above. Besides the production costs should be less than for the current Moving Bases.

Chapter 2 Analysis of the existing Moving Bases

Before starting with the design of the robot vehicle, an analysis of the current Moving Bases is made. The information from this analysis can be very useful when designing a new Moving Base.

§ 2.1 Tires and wheels

The Moving Bases are equipped with Formula Student racing tires with a relatively small diameter: 18 [inch]. The small wheel diameter helps to lower the centre of gravity of the vehicle in this design. Racing tires are designed for optimal grip and to cope with forces in all directions. Unlike in racing conditions, where the tyres are warmed up before and in the beginning of a race, the Moving Base operates with relatively cold tyres. To assure that the vehicle has enough grip, the floor in the VEHIL-laboratory has been coursed with a special coating, with gravel.

The VEHIL laboratory should have a flat floor and therefore the current Moving Bases don't have primary suspension. All the suspension comes from the tires. For this reason 10 [inch] rims are used so the tire height is about 4 [inch].

A tire can act like a spring but, when rolling, the damping is only about 50 [Ns/m], [Besselink]. The vibrations of the Moving Base swing up at a speed of about 25 [km/h], because at this speed an eigenfrequency is excited. These heavy vibrations have a negative effect on the construction and the electronic parts of the vehicle and can even cause parts to fail.

A quarter Moving base can be seen as a spring with a mass that has an eigenfrequency:

$$\omega = \sqrt{\frac{k}{m}} = \sqrt{\frac{1{,}4 \cdot 10^5}{621/4}} = 30[rad/s] = 4{,}78[Hz]$$

At 25 [km/h] the Moving Base moves 6,94 [m/s], so it can be seen that each $\frac{6{,}94}{4{,}78} = 1{,}45[m]$ an excitation occurs.
Since the circumference of the tires is 1,4 [m], the unroundness and unbalance of the tires can be a source that excites the Moving Base in its eigenfrequency. Besides this, the bumps in the laboratory floor also act as a source that excites the Moving Base.

§ 2.2 Electric drive

Each wheel of the Moving Base is driven by a disc armature electric motor with a planetary reduction. The rims are directly connected to this reduction, so the bearings in the reduction also function as wheel bearings. As can be seen in figure 2.2.1, the electric

motor is placed completely beside the wheel and the reduction is mounted partly inside the wheel. With the moment of inertia about the steering axis defined as $J_z = \frac{1}{2}mr^2$ the

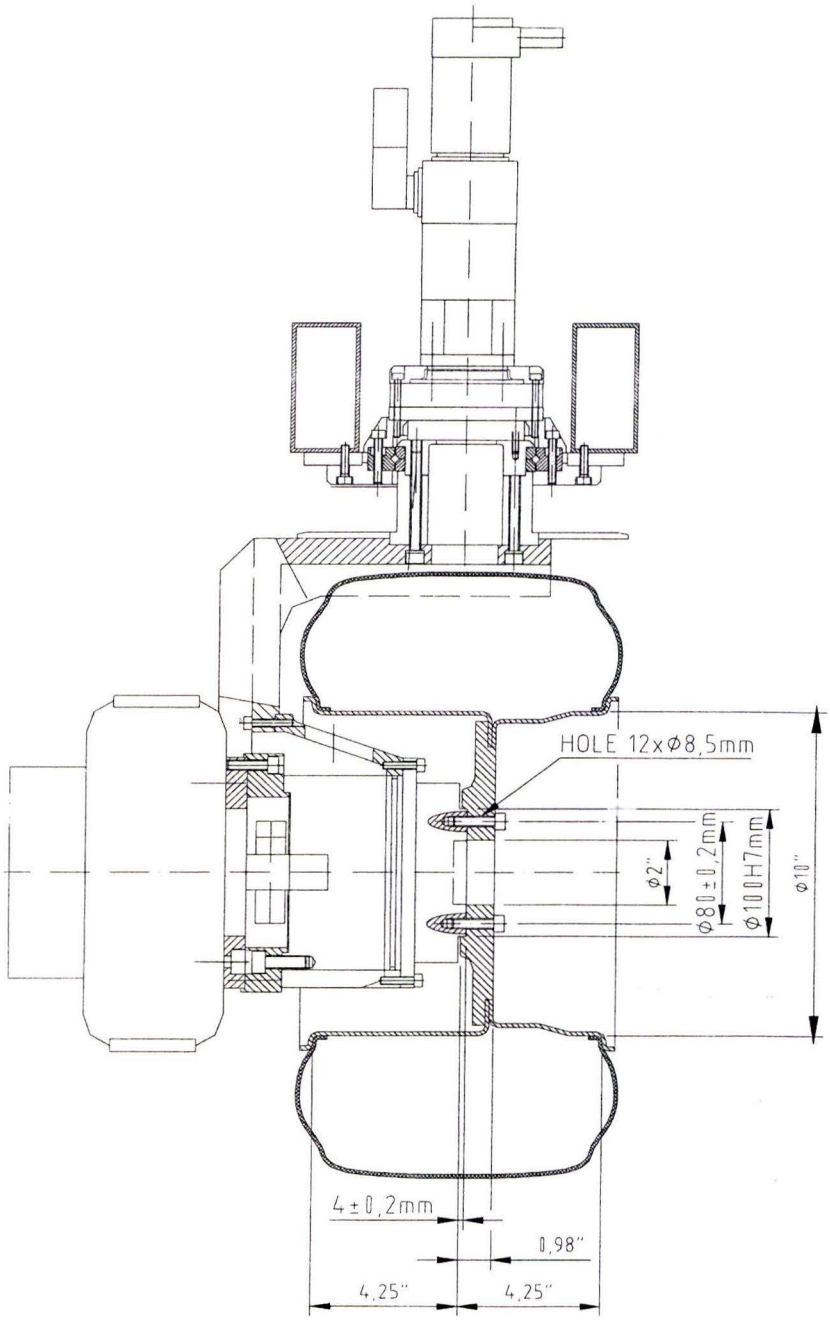

Figure 2.2.1 cross-section of a wheel unit from Moving Base 2

disc armature motor has a high contribution to the inertia of the wheel unit about the steering axis. The higher this inertia the more power is needed to steer the wheel unit.

Due to the unevenly distributed mass around the steering axis, steering produces lateral forces, which causes undesired movements of the Moving Base during steering.

§ 2.3 Wheel carrying arm

The wheel carrying arm is milled out of a solid piece of aluminium. It holds the disc armature motor and the reduction. It is connected to the main frame through a crossed roller bearing as can be seen in figure 2.2.1.

A milled wheel carrying arm is relative expensive for series production, because a lot of material is lost in production and an expensive CNC machine is used. In this wheel carrying arm a lot of material is in a neutral area where the contribution to the stiffness is relatively low.

§ 2.4 Cable guiding system

The power supply for the drive motor and the data signals have to be transferred between the main frame and the rotating wheel unit. For this purpose a cable guiding system is used. The cables are directly attached to the wheel unit and are guided by this system to wind around a part of the wheel unit while steering. Due to the length of the cables, the steering angle is limited to plus and minus 350 degrees. When a limit is reached, micro switches trigger a safety system that stops the Moving Base.

§ 2.5 Steering

Above the cable guiding system a cycloid reduction is located. Its output shaft is connected to the wheel carrying arm and a servo motor is directly connected to the input side. On top of the servo motor is an absolute rotary encoder.
The housing of the reduction and the housing of the servo motor are connected to the main frame with the same flange. To reduce the effect of this over determined connection the flange is machined in one operation. Besides this, the crossed roller bearing also works against the bearing of the cycloid reduction, because they are both rigidly connected to the main frame and the wheel carrying arm.

§ 2.6 Main frame

The upper main frame consists of aluminium box girders with dimensions 100 x 50 x 3 [mm] (h x w x t), figure 2.6.1. The four wheel units are connected to this part of the main frame.

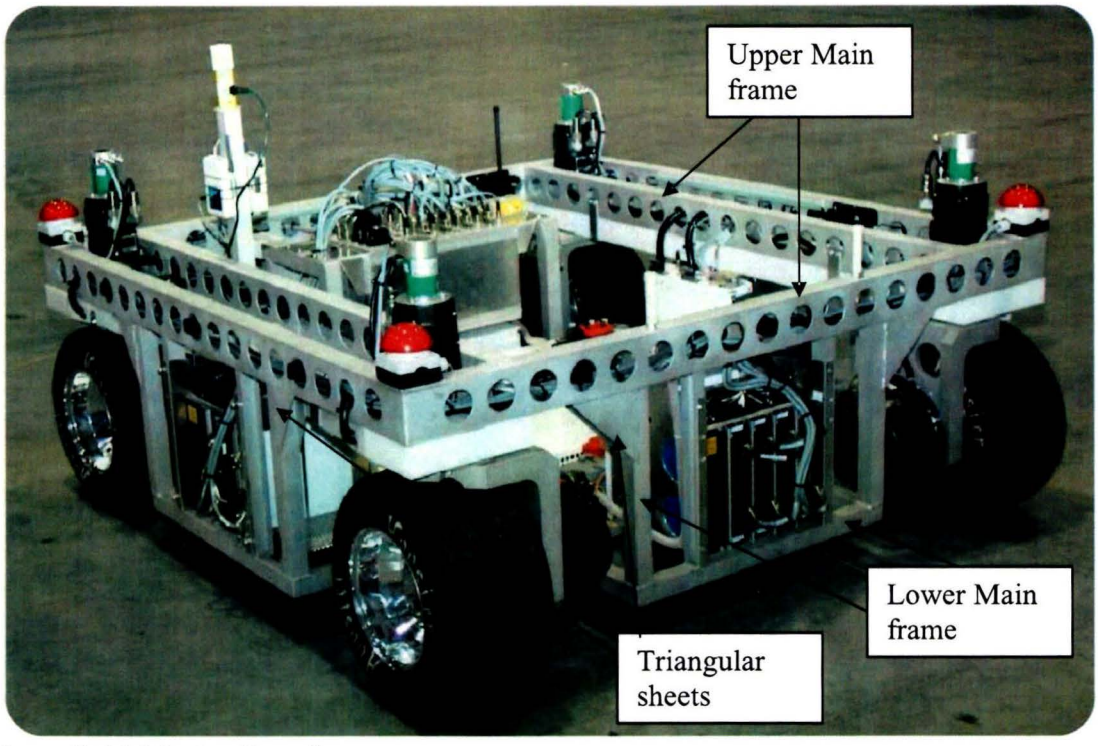

Figure 2.6.1 Moving Base 1

All other components are mounted to the lower part of the main frame. This part is made of aluminium box girders with dimensions 40 x 40 x 3 [mm] (h x w x t). All of these girders that are connected to the upper frame are in vertical position. The centre of gravity of the Moving Base is 0,33 [m] above the ground, so all the lateral and longitudinal forces have to go from the tires through the wheel unit, the upper main frame and through the vertical girders of the lower main frame to the centre of gravity. Those forces will cause the vertical girders to bend. To help the vertical girders a bit, triangular sheets of aluminium are welded between the upper main frame and the vertical girders. Nevertheless large forces are exerted at the welds connecting the upper and the lower main frame. These high forces and the difference in stiffness between the large girder and the sheet cause the frame to fail at this point, see figure 2.6.2

Figure 2.6.2 Cracked aluminium welds

§ 2.7 Electronics

Almost all electronic components are located in the lower main frame, see figure 2.7.1 and 2.7.2. There are two racks with power electronics for the drive motors, each on a side between two wheels. One rack at another side between two wheels contains the electronics for the four steering motors. Opposite of this rack are the computer for the control of the moving base, two power converters for the power supply from the battery to the computer and the racks and an adapter box that is used for connecting various electronic components. In the middle of the frame, close to the floor is the custom made battery pack. Besides this there are some relatively small components like gyroscope, accelerometer, W-lan, brake resistors and a box for the remote control.

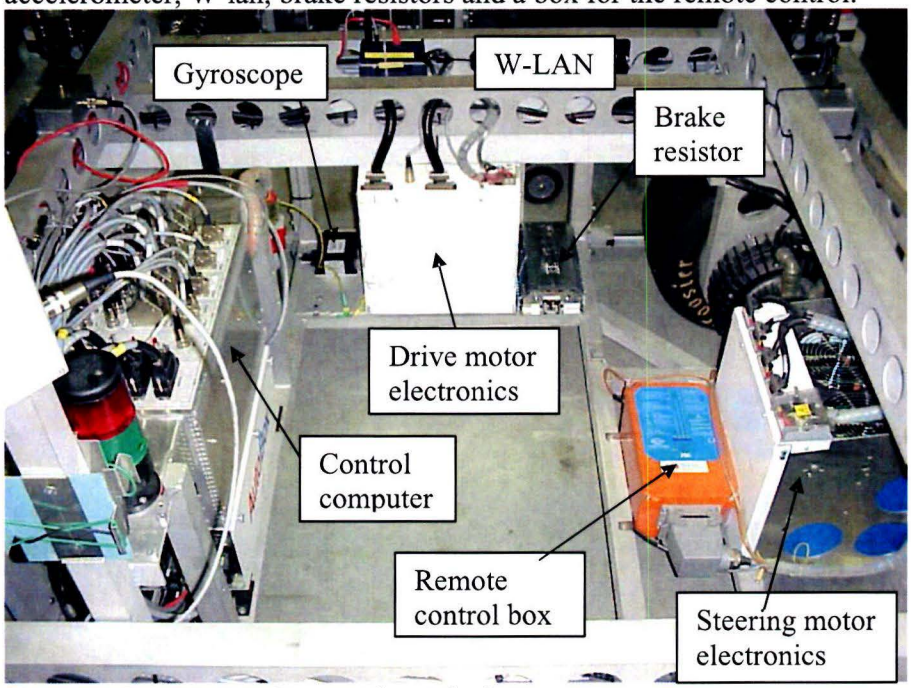

Figure 2.7.1: Moving Base without the battery

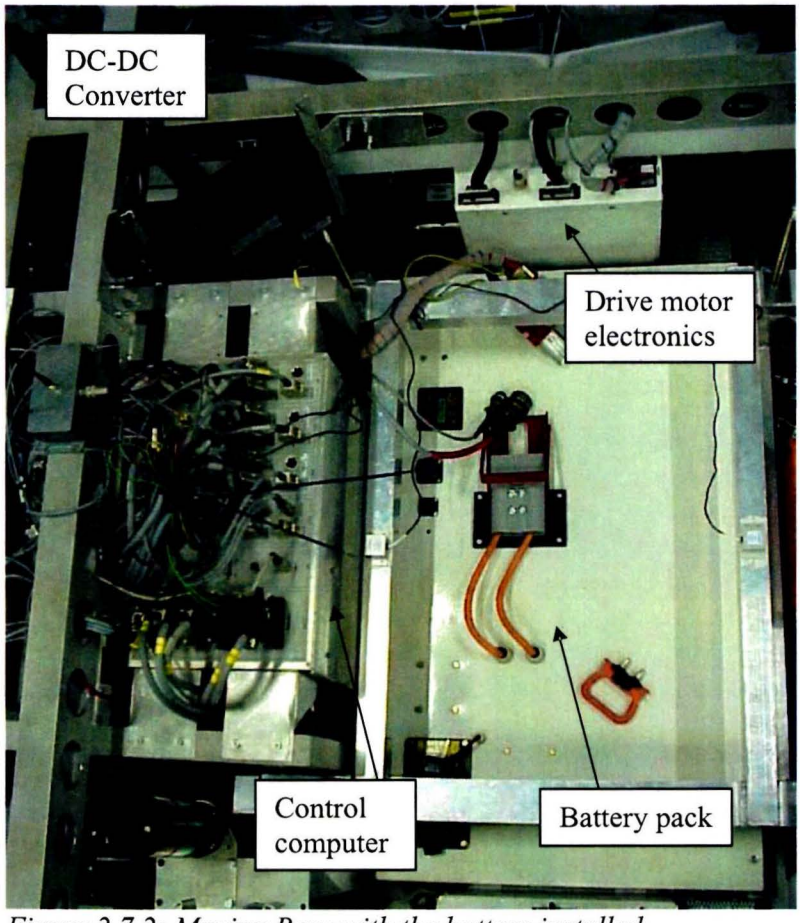

Figure 2.7.2: Moving Base with the battery installed

More information about all the components used in the Moving Base can be found in appendix A [Specifications current Moving Base].

Chapter 3 Design requirements

The basic purpose of a Moving Base is to move a mass in the horizontal plane. In the VEHIL application this is a mass that simulates a midsize passenger car and therefore has the dimensions as mentioned in chapter 1. In other applications a Moving Base can be used to precisely move tools, people or goods.

There are various ways to move a mass in the horizontal plane, but to be independent of the environment and for the freedom of movement it is obvious to use a wheeled vehicle. The number of wheels used is arbitrary. When using a vehicle with one or two wheels, balancing of the vehicle could become a problem. With three wheels at the corners of an equal sided triangle this problem is solved. However, the movement in x and y direction is not the same, because not all wheels can transfer the same amount of torque onto the road due to their position and weight transfer. A vehicle with four wheels is more symmetrical, but would need something to keep all four wheels on the ground. This could be done by creating a weak connection frame between the wheels or by a suspension system. A vehicle with more than four wheels can be more symmetrical, but it would also be more complex compared to a vehicle with four wheels.

In the following paragraphs design requirements for various parts of the design will be described. At the end all the values will be summarized.

§ 3.1 General dimensions

The vehicle has to be able to move in all directions in the horizontal plane. Whether it is moving pure longitudinal or pure lateral, the dynamic behaviour of the vehicle should be the same. Therefore the vehicle has to be as symmetrical as possible both in dimensions as in weight distribution. A four wheeled vehicle will be designed, because it is relative symmetric compared to its complexity. The track width and wheelbase are chosen to be comparable to the track width of a midsize passenger car and are set to 1,4 [m]. The coordinate system that will be used is the ISO coordinate system, because this system is generally used for automotive applications, see figure 3.1.1.

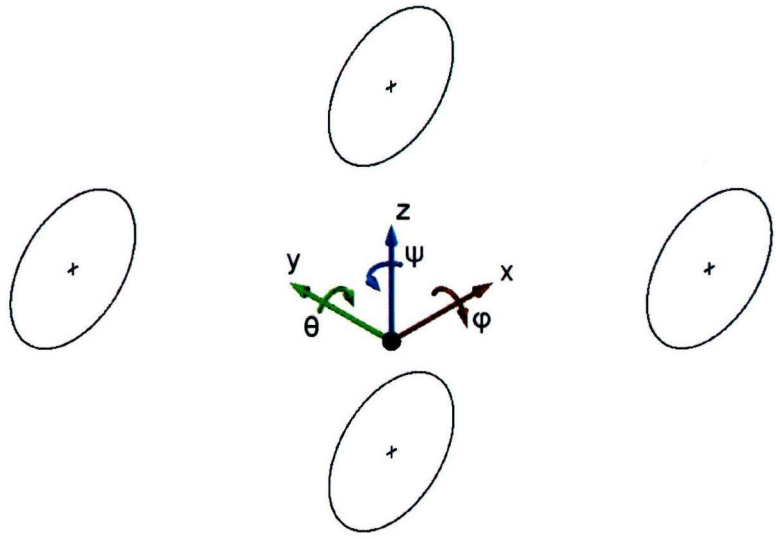

Figure3.1.1: The ISO coordinate system

In this system the x axis, in red, represents the longitudinal direction, the y axis, in green, the lateral direction and the z axis, in blue, the vertical direction. The rotations about these axes are: φ, in red, is roll, θ, in green, is pitch and ψ, in blue, is yaw.

§ 3.2 Handling

For the handling of the vehicle it is important that all four wheels follow the road and have enough grip to transfer forces that can influence the position or behaviour of the vehicle. This can be achieved by a suspension system between the wheels and the frame that connects the four wheels. Furthermore suspension lowers the vibrations and vertical acceleration forces on the various components of the robot vehicle. With a suspension system it can also be possible to change the ride height and to adjust the system for different tasks or roads.

To achieve maximum manoeuvrability with a four-wheeled robot vehicle, all wheels should be steered. In addition to this, each wheel has to be able to steer without a limit in the steering angle. With this steering configuration the robot vehicle could, for example, drive in circles without changing the orientation of the main frame.

§ 3.3 Performance

The total mass of the vehicle should be as low as possible, since the mass is proportional to the force required for acceleration of the vehicle as can be seen from Newton's second law of motion.

$$F = m \cdot a \tag{3.1}$$

The lower the total vehicle mass the less powerful the motors and energy source can be.

The vehicle mass, m = 550 [kg] has to be accelerated from standstill to 20 [km/h] or 5,6 [m/s] with an acceleration, a = 10 [m/s^2]. This requires a force, F = 5500 [N]. With the average velocity, v_{av} = (0 + 5,6)/2 = 2,8 [m/s], the required power is:

$$P = F \cdot v_{av} = 15400[W] \tag{3.2}$$

From 20 [km/h] to the maximum speed of 50 [km/h] or 13,9 [m/s], the acceleration has to be a = 4 [m/s^2]. The required power for this acceleration is calculated to be P = 21450 [W]

Forces due to rolling resistance, F_R are:

$$F_R = \mu_R F_v \tag{3.3}$$

With F_v, the vertical tire force and μ_R, the coefficient of rolling resistance, ranging from 0,01 to 0,025, these forces are very small compared to the forces required for acceleration, so they will be neglected.

The force to overcome the air resistance, F_{air} is:

$$F_{air} = \tfrac{1}{2} \rho_{air} C_w A v_{air}^2 \tag{3.4}$$

With the density of air, ρ_{air} = 1,29 [kg/m^3], the air resistance coefficient, $C_w \approx 1$, the frontal vehicle area, A ≈ 1.2 [m^2]. This force is also relative small compared to the forces required for acceleration, because the maximum speed of the vehicle is 50 [km/h] and most of the operation time the speed is below this maximum speed. The air resistance at 50 [km/h] and in a windless environment is calculated with formula 3.4:

$$F_{air} = \tfrac{1}{2} \cdot 1{,}29 \cdot 1 \cdot 1{,}2 \cdot 13{,}9^2 = 149[N]$$

Besides a low total mass of the vehicle, the centre of gravity should be as low as possible to minimize weight transfer. The current Moving Base has its centre of gravity at 0,331 [m] above the ground. Due to the suspension system, the new Moving Base will have more ground clearance so the centre of gravity will probably be higher than 0,331 [m]. The weight transfer is described in appendix B [Weight transfer and the centre of gravity].

The centre of gravity should be in the middle of the vehicle and thus be on the yaw axis of the vehicle. A low inertia around the yaw axis, i.e. much mass in the centre of the vehicle, would result in a more manoeuvrable vehicle.

Each of the four wheel units has a large contribution to the inertia of the total vehicle around the yaw axis, so it is important that their mass is low. Each wheel unit is steered separately. The inertia of the steered part of the wheel unit determines the amount of torque that is needed for a steering operation and therefore the requirements for the

steering system. If the mass of a wheel unit is not distributed symmetrically around its steering axis, this will cause undesired lateral forces while steering. These forces can cause undesired movements of the Moving Base.

During acceleration large forces have to be transferred from the road to the centre of gravity. It is important for this transfer that the various components in the path of the forces have enough stiffness and do not dissipate energy that should be used for acceleration.

The required energy for the operation of the robot vehicle can be supplied in various ways. The energy source can be at a fixed position outside the vehicle, with a connection between the two for the transfer of energy. It is also possible to have an energy source inside the vehicle. For both situations there are various types of energy sources. With the energy source outside the vehicle, the operation area is limited due to the connection for energy transfer. With the energy source inside the vehicle the operation area is not limited, but the continuous operation time is limited, dependent on the energy capacity of the energy source. Because of the freedom of movement the robot vehicle will have an inside energy source.

The mobile robot can be used for transporting of various things, so it should have a certain load capacity. The maximum load capacity is set to 300 [kg].

§ 3.4 Design requirements summary

- Four wheel drive
- Four wheel unlimited steering
- Track width: 1,4 [m]
- Wheel base: 1,4 [m]
- Primary suspension adaptable for different ride heights
- Centre of gravity on the yaw axis and as low as possible
- Maximum acceleration: 10 [m/s^2]
- Maximum driving speed: 50 [km/h]
- Inside energy source
- Maximum load capacity: 300 [kg]

Chapter 4 Energy source

Since electric motors will be used, an energy source that provides electric energy is required. Sources that provide direct electric energy are:

- Battery
- Super capacitor

It is also possible to use an energy source that converts its energy into electric energy.

- Fuel cell: For example hydrogen from a fuel tank is converted in the fuel cell
- Electric aggregate: A fossil fuel from a fuel tank is converted into kinetic energy by the combustion engine and this energy is converted into electric energy by a generator.
- Flywheel storage: Kinetic energy from the flywheel is converted into electric energy by a generator.

The volume and mass of systems with an extra conversion step are relative high for the power that is needed for acceleration. For applications where driving range is more important than acceleration, these systems can be considered, because the energy density of fossil fuels is high compared to the energy density of batteries. For now, only batteries and super capacitors are discussed. A flywheel storage might be used, without the conversion step. Each wheel unit would have a separate flywheel which directly exchanges kinetic energy with the wheels. This type of energy storage will be discussed in chapter 5, because it would be part of the driveline.

§ 4.1 Battery

In this paragraph various battery types are described with their characteristics and a choice is made for the battery that will be used in the robot vehicle.

- Lead-acid: This battery type is commonly used in the automotive and other industries. It can supply a high power, but it has a low energy density. The cold temperature performance is poor and it has a short calendar and cycle life. This battery type is relatively low cost.
- NiCad Nickel-Cadmium batteries are well developed and relatively low cost, they have a higher energy density and cycle life than lead-acid batteries, but their power capacity is relatively low. Besides Cadmium is a heavy metal that is toxic. This battery type is used in various cordless consumer products.
- NiMH Nickel-Metal-Hydride batteries have a higher energy density than lead-acid and NiCad batteries; the mass is 60% less than lead-acid batteries for the same amount of energy storage. They have a higher life cycle than lead-acid batteries. Moreover this battery type is safe and abuse tolerant. They are however more expensive

than NiCad batteries and have a high self discharge rate. This battery type is most used in commercial hybrid electric vehicles and is good commercial available.

- Li-ion — Lithium-ion batteries have a higher energy density and power compared to the battery types above, but they are also more expensive. This battery type is most used for small electric devices like digital camera's and mobile phones. There are little electric or hybrid vehicles equipped with this battery type, because of the high cost.
- Zinc-air — These batteries have a very high energy density, higher than Li-ion batteries. They are most used for hearing aids. For vehicle applications this battery type is not commercially available.
- NaNiCl / ZEBRA — This is a Sodium Nickel Chloride battery produced by "Beta research". It is still in development, but complete functional packages are available. The energy density is comparable to Li-ion batteries. A drawback of this battery is the high operating temperature.

Batteries in development and not available yet:

- BILAPS — Bipolar Lead Acid Power Source. This battery is developed by TNO for hybrid vehicles and 42 [V] infrastructure in cars. The specific power of this battery is above 500 [W/kg]. Besides the used materials are cheap and well developed.
- E-light — This is a lightweight thermal battery developed by "Stork Product Engineering". The E-light converts various fluid and possibly solid fuels into electric energy. The energy density will be between 1000 and 3000 [Wh/kg].

There are many other battery types in development, but it can take a long time for these batteries to become commercially available.

For a better comparison of the different battery types, some characteristics are listed in table 4.1.1.

Type:	Specific energy density [Wh/kg]	Energy density [Wh/l]	Specific power [W/kg]	Cycle life [number of recycles]	Price[1.) [€/kWh]
VRLA (sealed lead-acid)	30-45	60-90	200-300	400-600	150
Ni-Cd	40-60	80-110	150-350	600-1200	300
Ni-MH	60-70	130-170	150-300	600-1200	200-350
Li-ion	90-130	140-200	250-450	800-1200	>200
Zn/air	230	269	105	n/a[2.)	90-120
$Na/NiCl_2$	86-99	149-154	150-180	1000	230-350

This table is based on table 6.2 from [Modern electric vehicle technology]

1.) Prices are relative and are subject to continuous change. Prices depend most on production quantity.

2.) This cell is reloaded mechanically

Table 4.1.1: Comparison of battery types

A research is done to find out which available batteries can be used as an energy source for the robot vehicle. Special attention is paid to mass produced batteries that are used in hybrid vehicles. A list of these batteries is in appendix C [Battery]. For a comparison of these commercial available batteries and the theoretical values from table 4.1.1 the specific energy density as a function of price is displayed in figure 4.1.1 and the mass versus price of a unit is displayed in figure 4.1.2.

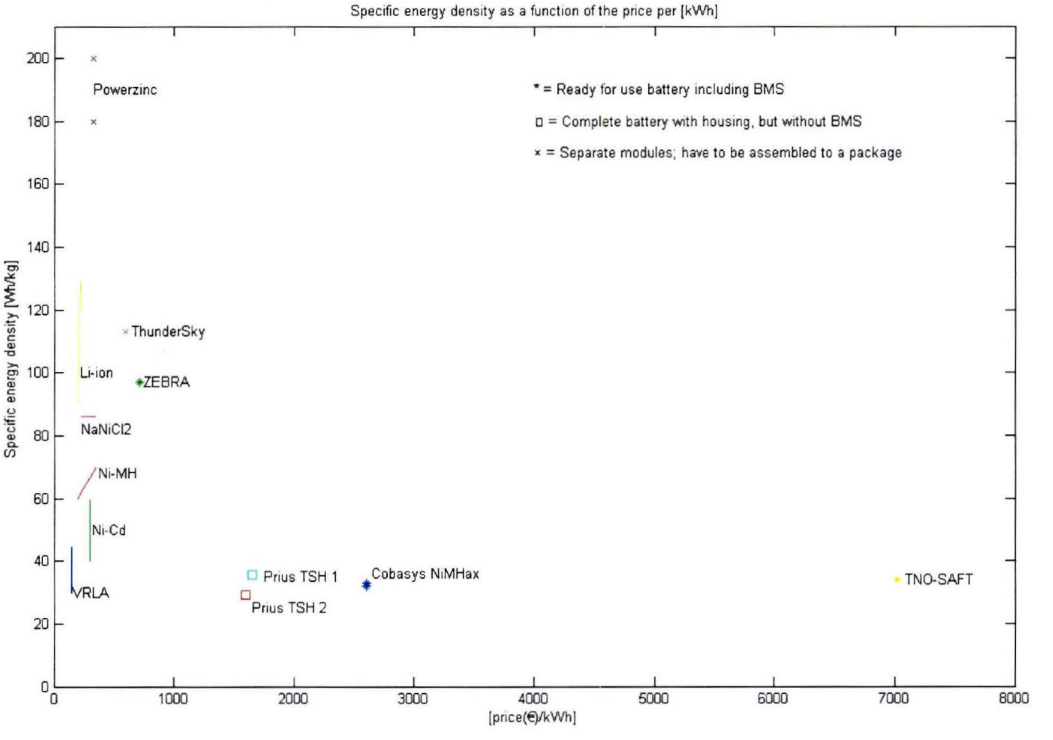

Figure 4.1.1: Specific energy density as a function of the price per [kWh]

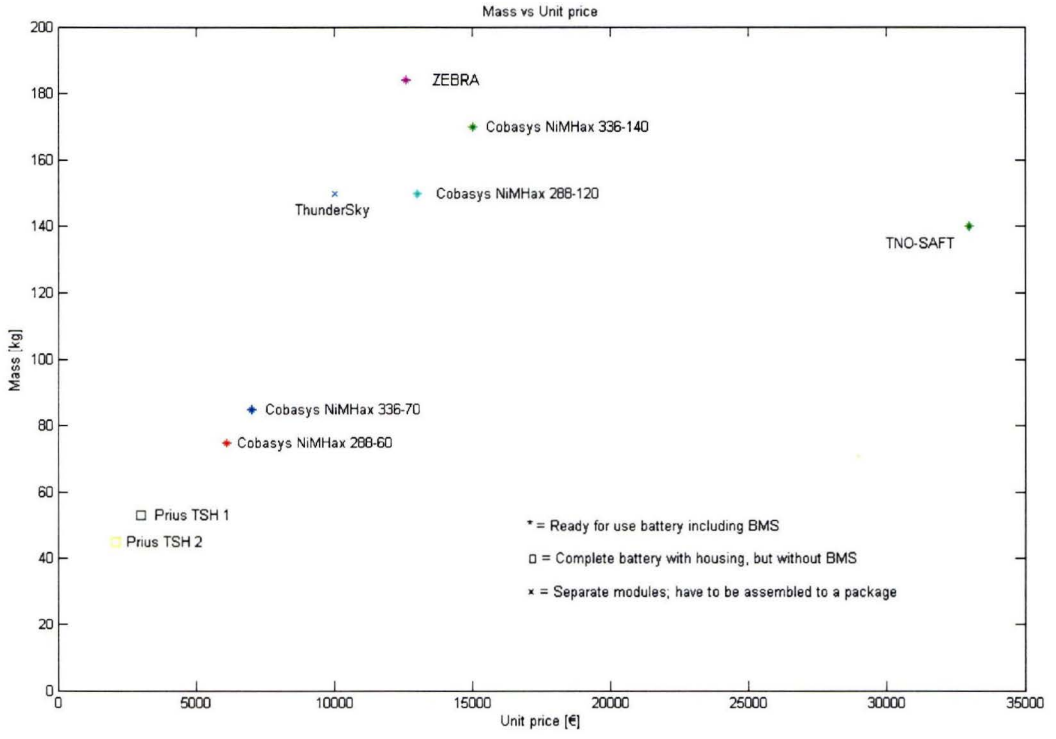

Figure 4.1.2: Mass versus price of a battery unit

The battery voltage has to correspond to the electric motors. The battery should be well commercially available and relatively low cost. The energy capacity should be proportional to the task of the vehicle as well as the power that can be delivered. For acceleration with 10 [m/s^2] the battery has to deliver a high peak power over a short period, which is not good for the battery life.

For the robot vehicle two NiMH-batteries from the Toyota Prius TSH 2, connected in parallel, will be used. For the power peaks and regenerative braking, a bank of super capacitor modules will be added. With this system the battery life is extended over a system without super capacitors.

§ 4.2 Super capacitors

Capacitors are used in all kinds of electric equipment since a long time. The capacitance of these capacitors is always expressed in [µF]. Since a few years super capacitors, also known as electrochemical double layer capacitors are sufficiently developed to be used in commercial applications. The capacity of super capacitors is a lot higher compared to the conventional capacitors and hence expressed in [F]. The difference between a battery and a super capacitor is in the energy and the power density. Super capacitors have a low energy density compared to batteries, but they can fully charge and discharge within a few seconds, so their power density is high compared to batteries. Super capacitors have a high efficiency, they can deliver and absorb high currents and work in a wide voltage

range. A benefit of super capacitors over batteries is the long cycle life and calendar life; they can be used for over 100.000 cycles with minimal change in performance. Super capacitors don't need any cycle strategies like with batteries and don't have a memory effect.

§ 4.2.1 System configurations

For the robot vehicle a system will be used where most of the energy is stored in the battery while the super capacitors will be used for the power peaks during accelerations and decelerations. The battery charges the capacitor bank that can then be discharged during accelerations. There are two basic configurations for the connection between a battery and a super capacitor bank:

Connection with a DC-DC-converter

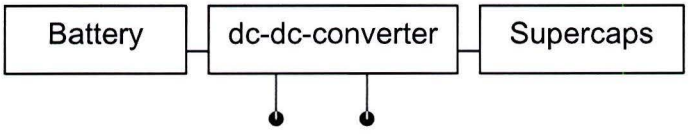

Figure 4.2.1: Battery and super capacitor bank connected with a dc-dc-converter

When discharging the super capacitors, their voltage drops. A dc-dc-converter is used to make the connection between the battery and super capacitors which have different voltages, see figure 4.2.1. This system ensures an optimal use of the battery and the super capacitors, but an extra dc-dc-converter has to be used, which contributes to the mass and volume of the system. Moreover the use of a dc-dc-converter results in extra energy loss, since the typical efficiency of a dc-dc-converter is between 85% and 90%.

Battery and super capacitor bank arranged in parallel

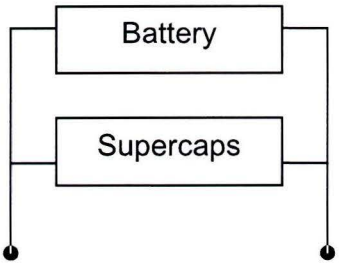

Figure 4.2.2: Battery and super capacitor bank arranged in parallel

With a parallel arrangement, see figure 4.2.2, the use of a dc-dc-converter can be saved. A drawback of this configuration is that the voltages of the battery and the super capacitor bank have to be the same. When discharging, the battery, which can only work

within a certain voltage range, limits the discharge of the super capacitors, so only a part of their energy can be used.

To save weight and volume, the parallel arrangement system will be used for the robot vehicle.

§ 4.2.2 Energy storage in super capacitors

The charge, Q [C], of a capacitor is given by the formula:

$$Q = C \cdot V \tag{4.1}$$

With:
C = capacitance [F]
V = voltage [V]

The energy, E [J], stored in a capacitor is:

$$E = \tfrac{1}{2} QV = \tfrac{1}{2} CV^2 \qquad [J] \tag{4.2}$$

In industry, the energy is often given in [kWh] instead of [J] and the capacity in [Ah] instead of [C]:

$$1[J] = 1[W \cdot s] = \frac{1}{3{,}6 \cdot 10^6}[kWh]$$

1 [F] = 1 [C V^{-1}] = 1 [AsV^{-1}]; 1 [Ah] = 3,6·10^3 [C]

The maximum current that can be supplied by a capacitor is given by the following formula:

$$I = \frac{V \cdot C}{T}$$

Where: T = discharge time [s]

Super capacitors are usually used in the range 50% State Of Charge (SOC) to 100% SOC, so this would be 1,25 [V] – 2,5 [V] for a normal single cell. Assuming a peak power of 55 [kW] during 2 [s] the energy required is 110 [kJ]. A cell with 2,5 [V] and 5000 [F], discharged from 100% SOC to 50% SOC can deliver

$$E_{capacitor} = \tfrac{1}{2} 5000\left(2{,}5^2 - 1{,}25^2\right) = 11{,}7[kJ]$$

This means ten of these cells can deliver the required energy. In practice this will not work, because the voltage of ten cells in series is 25 [V] and far below the battery voltage. So a number of cells have to be arranged in series and or parallel to reach the

desired voltage, instead of just looking at the required energy. The capacitance of a package capacitors arranged in parallel is given by:

$$C_{tot} = C_1 + C_2 + \ldots + C_n \tag{4.3}$$

The capacitance of a package capacitors arranged in series is given by:

$$\frac{1}{C_{tot}} = \frac{1}{C_1} + \frac{1}{C_2} + \ldots + \frac{1}{C_n} \tag{4.4}$$

To work properly the cells of a capacitor bank have to be balanced. In this way an equal contribution of each cell is ensured. In a system where a bank of super capacitors is connected to a battery, it is important that the battery can not overcharge the capacitors. When the voltage of the battery is above the voltage of the capacitor bank, the dielectricum or isolator inside the capacitors can get damaged and conductive. The battery from the Toyota Prius TSH 2 has a nominal voltage, V = 201,6 [V], but the maximum voltage is above this value. Exact data of the maximum voltage is not available, so based on data from other batteries it is assumed the maximum battery voltage is 252 [V].

Super capacitors are supplied by only a few companies. They can be purchased as single cells with a voltage of 2,5[V] to 2,7 [V] or in a module with voltages ranging from 15 [V] to 340 [V]. One company sells big cylindrical capacitors with voltages ranging from 14 [V] to 300 [V], but due to their volume they will not be used for the robot vehicle. In appendix D [Super capacitors] some companies that sell super capacitors are listed, together with some of their products.

The use of separate cells is not very practical, because around 90 cells would have to be assembled and balanced. The most practical solution is the use of super capacitor modules. For the energy system of the robot vehicle, a bank with Maxwell BPAK0350-modules will be used. The BPAK0350-module has a voltage, V = 15 [V] and a capacity, C = 58 [F]. Because the maximum battery voltage is 252 [V], a total of 17 super capacitor modules has to be used. The capacitance of this capacitor bank is calculated with formula 4.4 to be C = 3,4 [F]. For a voltage range of 220 [V] to 160 [V] the energy from the capacitor bank is calculated with formula 4.2:

$$E = \tfrac{1}{2} \cdot 3{,}4\left(220^2 - 155^2\right) = 41{,}4[kJ]$$

Would this energy be used in 2 [s], the delivered power from the capacitors is 20,7 [kW]. Each Toyota Prius TSH 2 battery delivers 21 [kW], so the energy system can deliver sufficient power for the drive and steering motors of the robot vehicle.

Chapter 5 Tires, wheels and drive line

The tires of the robot vehicle play an important role in the performance, because they are responsible for transferring the driving and steering forces onto the road surface. The tires are fitted on wheels and these wheels are directly connected to the drive line. This chapter will discuss the tires, wheels and the drive line.

§ 5.1 Tires

Conventional tires are made of a rubber mixture that is reinforced with various layers of plies. The tire is filled with air or another gas like nitrogen. The pressure of the gas inside the tire determines the spring stiffness together with the rubber characteristics. So a tire acts like a spring and there is only relevant damping in the sidewalls of the tire. This damping is relative low, about 50 [Ns/m] for a rolling tire.

There are two basic types in the construction of tires. The radial tire and the crossply or bias ply tire. Today almost all passenger cars are fitted with radial tires, but for racing the crossply tire is still in use.

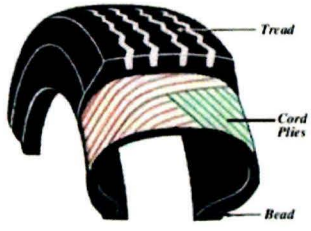

Figure 5.1.1: Crossply tire

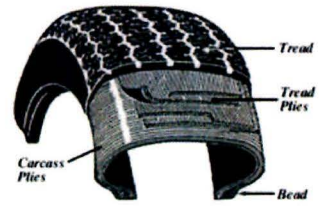

Figure 5.1.2: Radial tire

In a crossply tire, see figure 5.1.1, the reinforcement plies are located all over the tire. Superimposed layers of cord plies run from bead to bead. Each subsequent layer has its plies under another angle. This gives comparable rigidity between the tread and the side wall of the tire. In this way the tire is well capable of transferring forces in all directions.

The radial tire, see figure 5.1.2, has a separate carcass of plies that run from bead to bead. The tread is reinforced with other layers of plies. Usually at least one of these layers contains steel plies. This configuration separates the stiffness of the sidewalls from the tread, so it is possible to make the sidewalls more flexible compared to the tread. In this way the vertical tire characteristics can be improved. The radial tire has a longer life span compared to crossply tires.

Because of the high dynamic movements the robot vehicle has to make, crossply racing tires from "Cooper Avon tyres" will be used. The inside of the wheels should be used for the drive line to minimize the steering inertia and torque, so the driveline determines for a

great part the rim diameter. There are drive lines that fit inside a 13 [inch] wheel and drive lines that only fit in a 15 [inch] wheel, so for each wheel a tire is chosen. Since the tire diameter is a factor that determines the total height of the vehicle it is important to choose a tire with a minimal outer diameter for the rim used. In table 5.1.1 the two tires with their dimensions are listed. The spring stiffnesses of these tires are estimates, because no exact tire data is available for these tires.

Rim size [inch]	Tire type name	Rim choice [inch]	Outer diameter [mm]	Section width [mm]	Tread width [mm]	Spring stiffness [N/m]
13	7.5/19.5-13	6.0 - 8.5	480	218	193	$2{,}5 \cdot 10^5$
15	8.0/21.5-15	6.5 - 8.5	553	224	198	$2{,}7 \cdot 10^5$

Table 5.1.1: Tires with data

It is important that the tires have enough grip to be able to transfer all the forces to the road. The friction coefficient, μ, depends on a lot of factors, such as: tire compound, tire temperature, road surface, tire load, humidity, dust etc. For the above tires, no exact data is available, but there is data available from other tires with the same compound from where the coefficient of friction can be estimated, see figure 5.1.3.

Project:	**RC353STB**	**Size:**	**7.0/20.0-13**	**Camber:**	**1°**
Spec:	**10998**	**Tyre:**	**3 ply Pro Series**	**Pressure:**	**26 P.S.I.**
Tested:	**31/07/01**	**Rim:**	**6 x 13**	**Speed:**	**20 KPH**

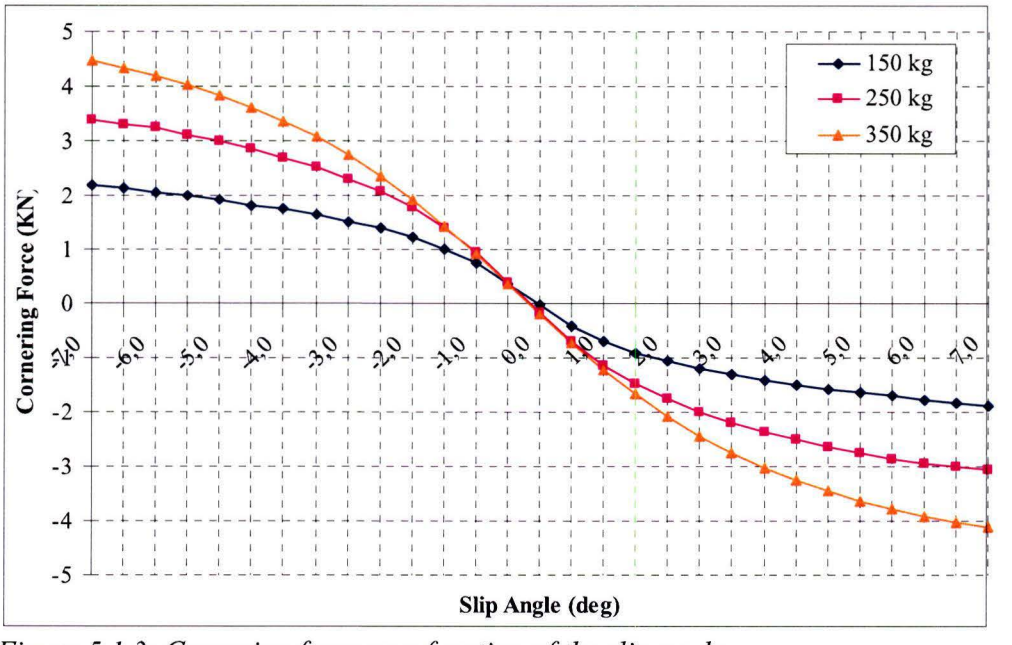

Figure 5.1.3: Cornering force as a function of the slip angle

The slip angle, α, is the angle between the direction of the wheel heading and the direction of wheel travel. The slip angle causes a lateral force. This lateral force F_{lat} divided by the vertical tire load, F_z gives the friction coefficient, μ:

$$\mu = \frac{F_{lat}}{F_z}$$

When a total vehicle mass of 600 [kg] is assumed and in cornering all the vertical load is divided between the outer two wheels, each wheel carries a load of 300 [kg]. The maximum cornering force at a slip angle of $\alpha = 7\ °$ is determined from figure 5.1.3 to be, $F_{corner} = 3900$ [N]

$$\mu = \frac{F_{corner}}{m \cdot g} = \frac{3900}{300 \cdot 9{,}81} = 1{,}3$$

The tire data from figure 5.1.3 is not from the tires that will be used and the data is from tires at working temperature, as it would be during a race. The robot vehicle has to perform while the tires have lower temperatures, so for safety a friction coefficient of $\mu = 1{,}1$ will be assumed.

The friction coefficient and the weight transfer, see appendix B [Weight transfer and the centre of gravity], determine the maximum vehicle acceleration together with the maximum motor torque. The total drive force for a required acceleration, F_{drive}, should not exceed the maximum friction force between the tires and the road, F_{fr}.

$$F_{drive} = F_{fr}$$
$$m \cdot a = \mu \cdot m \cdot g$$
$$a = \mu \cdot g$$

So with $\mu = 1{,}1$ the maximum acceleration would be $a = 10{,}8$ [m/s^2].
Due to weight transfer the normal force at the front wheels is lowered during acceleration, so the motors in these wheels can only supply as much power as the friction force allows. The motors in the rear wheels have to compensate for this to achieve the required acceleration. So the amount of weight transfer and hence the height of the centre of gravity and the wheel base determine the maximum motor torque together with the total vehicle mass and the required acceleration.

In figure 5.1.4 a diagram is displayed with the motor peak torque as function of the wheel diameter for various vehicle masses, assuming an acceleration of 10 [m/s^2] and two motors only supplying half the peak torque. In figure 5.1.5 is a same sort of diagram but now for various accelerations assuming a vehicle mass of 550 [kg].

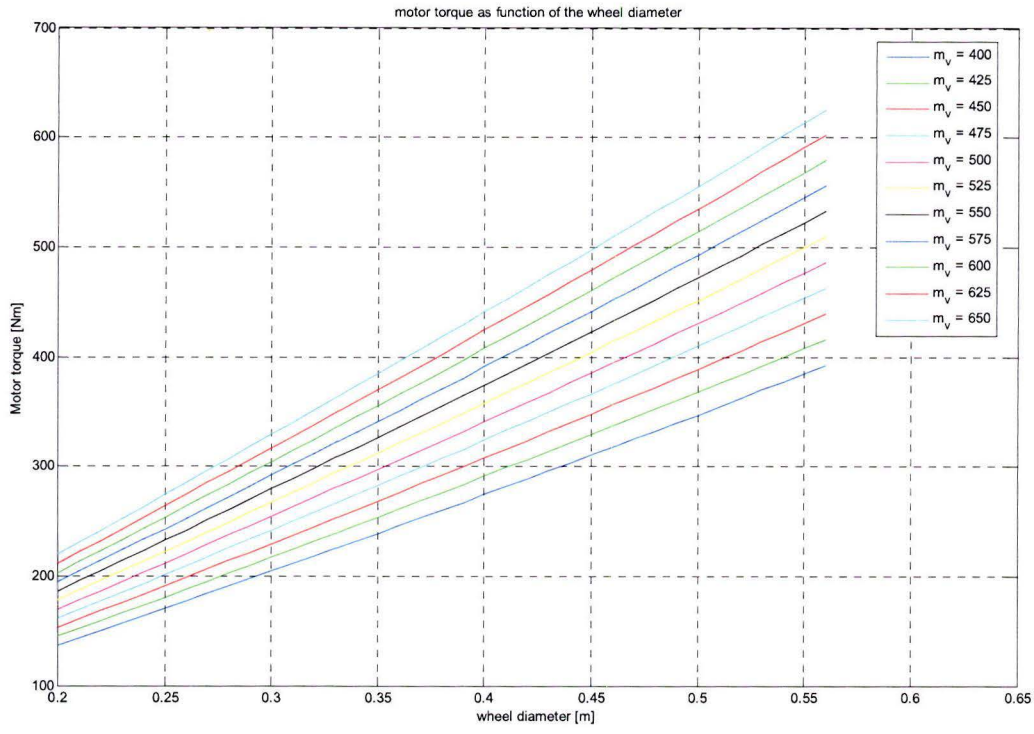

Figure 5.1.4: Motor torque as function of the wheel diameter for various vehicle masses

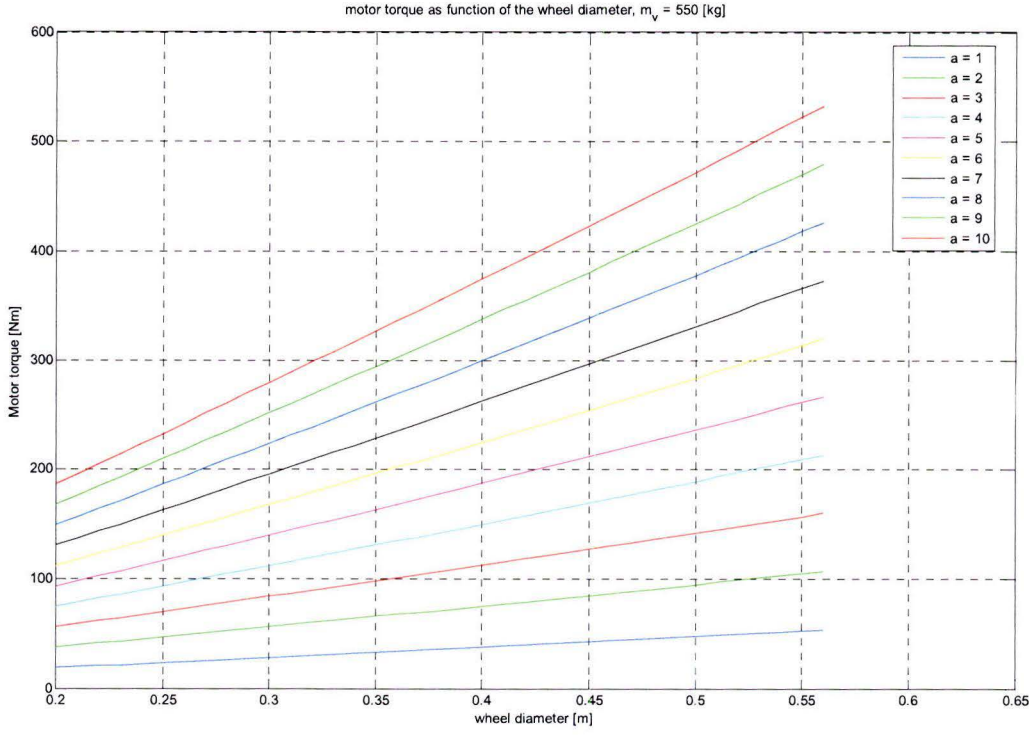

Figure 5.1.5: Motor torque as function of the wheel diameter for various accelerations

As can be seen in the above figures a drawback of a larger tire outer diameter is the high peak torque of the drive motors. A benefit of a larger outer tire diameter is that the vehicle has less problems with road irregularities.

§ 5.2 Wheels

The diameter and the width of the wheels are determined by the chosen tires. Since the total vehicle mass has to be as low as possible, the wheels should be made of a lightweight material. For now aluminium wheels will be used. In the future other materials like magnesium can be used, or the driveline and the rim can be integrated to reduce mass. In case the motor housing also functions as the rim one outer flange should be removable for the fitting of the tires. The contact surface of this flange with the motor housing should be sealed air tight with an o-ring. Balancing of the wheels can be done by rotating the wheel with its drive motor and detecting the unbalance with a separate accelerometer.

The rim used for the 13 [inch] tire has a width of 6,0 [inch] and the rim used for the 15 [inch] wheel has a width of 7.5 [inch]. These rims will be custom made by "Kodiak Motor Sports" or another specialized company.

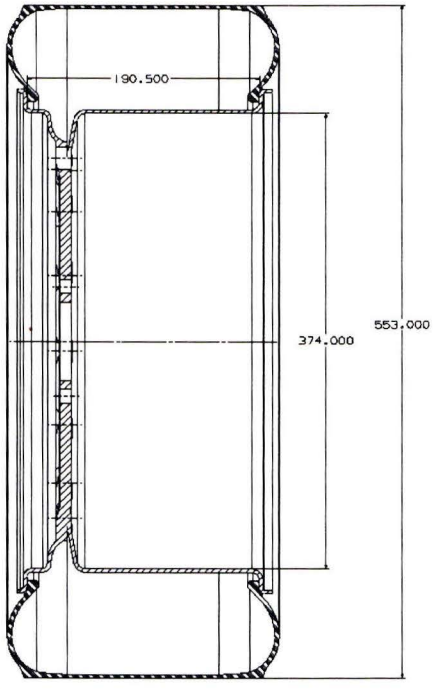

Figure 5.2.1: Cross section of a 15" wheel with tire

As can be seen in figure 5.2.1, the centre of the wheel is placed to one side of the wheel to get much space inside the wheel for the drive line. In this way the drive line can be

placed close to the steering axis to keep the inertia about this axis low, which results in a low steering torque and a small steering motor.

§ 5.3 Drive line

The drive line has to supply torque to each wheel to accelerate the vehicle to the required speeds. To minimize the inertia of the steered part of the wheel unit about the steering axis, the drive line should be located round or close to the steering axis and it should have a low mass.

Because the drive line is located in the part of the wheel unit that can be steered with an unlimited steering angle, the energy supply to the drive line has to go across a rotating connection. This can be done with electricity and hydraulics. It is also possible to go across the rotating connection with a rotational motion, but this would result in a relatively complex mechanical system. A hydro motor can have a high power density, but it is not suitable for large accelerations and a complete hydraulic system in the vehicle would be necessary. A hydraulic drive line could be used for a relative slow robot vehicle that has to carry heavy loads. Because of the high accelerations the robot vehicle has to make, a drive line with an electric motor will be used. A slipring will be used to go across the rotating parts.

Most electric motors deliver their peak power at high speeds, so a reduction is necessary to deliver sufficient torque to the wheels. A drawback of the use of a reduction is the added mass and volume. Besides this it can be difficult to fit the wheel bearings in this drive line, except for the configuration where the bearing in the reduction box are used as wheel bearings. Most commercial reduction boxes are made for a long life span and little effort is made to reduce mass. The most compact solution for a drive line with a reduction box would be to make a custom reduction box combined with the proper wheel bearings right beside or around the electric motor depending on the shape of the motor. When a frameless motor is used, the motor and the reduction can be built in the same housing resulting in an even more compact drive line. For the controllability of the drive line it is important that the reduction has minimal play.

When a custom reduction is built, it is possible to build in a mechanical energy buffer in the form of a flywheel. At standstill or at low speeds, the flywheel can be loaded with energy. When a large acceleration is required, the stored energy can be used. The efficiency of this energy buffer can be high because there is no conversion of energy necessary.

Two main motor types are suitable for a drive line without a reduction. The axial flux motor, where the direction of the flux is parallel to the mechanical motor axis, has at least a 4 times lower mass compared to an asynchronous motor with a comparable power. This motor type is used in the drive line of Moving Base 2. The other motor type is the switched reluctance motor. In this motor the current is controlled switched on and off in

the various motor windings. This motor has a big constant torque and power area in the torque-speed characterization.

In appendix E [Drive motors] is a list with some motors divided in motors that would need a reduction and direct drive motors. The best drive motor for a 13 [inch] wheel is the frameless motor Megaflux MF0255075C from Emoteq. However this company has no drive electronics for this motor with a DC power input and no other suitable driver is found. A custom built driver is expensive compared to an off the shelf one, so another motor will be used.

Because of the low mass and volume, the motor EW3530 from PML Flightlink is chosen. This motor is a complete unit with built in wheel bearings. It comes in a short version, SA and a longer version, LA. For now the SA version will be used, because the LA version is more expensive. A drawback of the use of this motor is that it only fits in a 15 [inch] wheel.

The EW3530SA motor has a mass of 14,5 [kg] and a peak torque of 550 [Nm]. With the outer tire diameter D = 553 [mm] the maximum driving force is F_{drive} = 1989 [N]. Due to weight transfer, see appendix B [Weight transfer and the centre of gravity] two wheels can only transfer 681 [N] to the road assuming a friction coefficient, μ = 1,3. At maximum acceleration the maximum driving force that can be transferred to the road is: $F_{drive,tot}$ = 5341 [N], which requires a maximum total vehicle mass of 534 [kg].

Chapter 6 Suspension

For the handling of a wheeled vehicle it is important that all wheels have good contact with the road. In this way they are able to transfer the forces that determine the movement of this vehicle and less energy is lost. A vehicle with more than three wheels should have a connection between the wheels that allows vertical movements of the wheels so they can follow road irregularities and retain good contact with the road. The deformation of the tires and the frame that connects the wheels can compensate for small irregularities in the road. However, since rolling tires act like a spring and have little damping, small irregularities can cause vertical accelerations that can result in poor tire road contact. The vertical forces and accelerations increase with increasing vehicle speed.

A suspension system can increase the performance of a vehicle and reduce vertical forces due to accelerations, therefore the four wheeled robot vehicle will be equipped with a suspension system. The suspension system has to allow vertical wheel movement and prevent all other movements with respect to the main frame of the vehicle. The shock absorber in the suspension system reduces vertical accelerations by temporary storing energy in a spring and converting kinetic energy into heat in a damper.

§ 6.1 Wheel travel and guiding

Independent suspension systems in passenger cars are directly connected to the stub axle beside the wheel. For driven wheels, this stub axle contains the wheel bearings and a coupling for connection with the drive shaft. For electric driven vehicles, equipped with wheel motors, the same independent suspension systems are used. However, all these suspension systems have a limited steering angle, because the suspension members are located beside the wheel. The suspension of the robot vehicle has to be designed to allow an unlimited steering angle as desired.

The maximum vertical wheel movement is dependent on the suspension system. In most passenger cars the vertical wheel movement is chosen with comfort in mind. Springs with a relatively low spring rate are used. Those springs need a relatively long spring travel, which influences the ride height of the vehicle.

The wheel travel of the robot vehicle is mainly determined by the height of the centre of gravity. In the space between the main frame and the road is no mass, so the ride height directly influences the height of the centre of gravity. The static ride height is the sum of the minimal ground clearance and the wheel travel from static to maximum load. The height of the centre of gravity and therefore the wheel travel should be as low as possible to minimize weight transfer. Since road holding and performance is most important for the robot vehicle and it will be operated on well paved and asphalted roads, a wheel travel of 50 [mm] is chosen. Of this total wheel travel, about 1/3, 17 [mm], will be static wheel travel.

The suspension has to be adjustable with respect to the main frame to compensate for the inaccuracies of the production of this frame and other components. The spring rate and damping factor should be adjustable for different loads and applications and the vertical wheel movement should not significantly influence the movement in the horizontal plane. Furthermore it is important that the weight of the suspension has a low contribution to the total mass, the centre of gravity and the inertia with regard to the yaw axis of the vehicle.

With this in mind, some concepts have been devised.

1. Linear guidance with linear ball bearings and a connection link

   The wheel carrying arm has got a tube above the wheel with a smooth outer surface that is guided in a bigger tube with a linear ball bearing, see figure 6.1.1 and 6.1.2. A connection link between the inner and outer tube, prevents the rotation about the axes of the tubes. The outer tube can be supported on bearings in the main frame for the steering of the wheel. The shock absorber can be placed inside the inner tube, or with the use of a rocker beside it. With the last option there is more freedom of choice for the shock absorber.

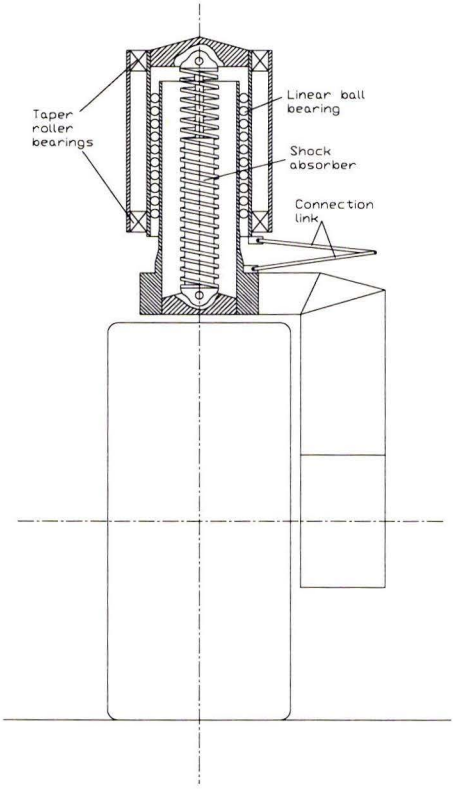

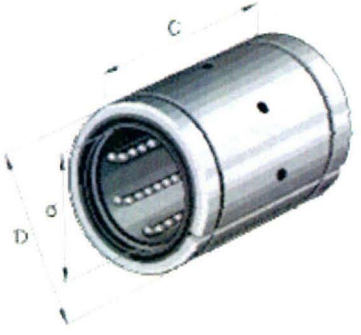

Figure 6.1.1: Linear ball bearing

Figure 6.1.2: Wheel carrying arm guided in linear ball bearings, schematic, partially cross-cut

The largest linear ball bearing of the standard range has an inner diameter of 50 [mm]. To reach the desired bending stiffness, the inner tube would need a considerable wall thickness, which adds a lot of mass to the wheel unit. A larger linear ball bearing will have to be custom built and have a price tag accordingly. Moreover surface finish of the inner tube is an important factor in the smoothness of guidance of the system.

2. Linear guidance with cylindrical rollers in a tube with triangular cross section

Two tubes with triangular cross section telescope, with cylindrical rollers between them, see figure 6.1.3. Two roller units are fixed and one is used for pre-tensioning.

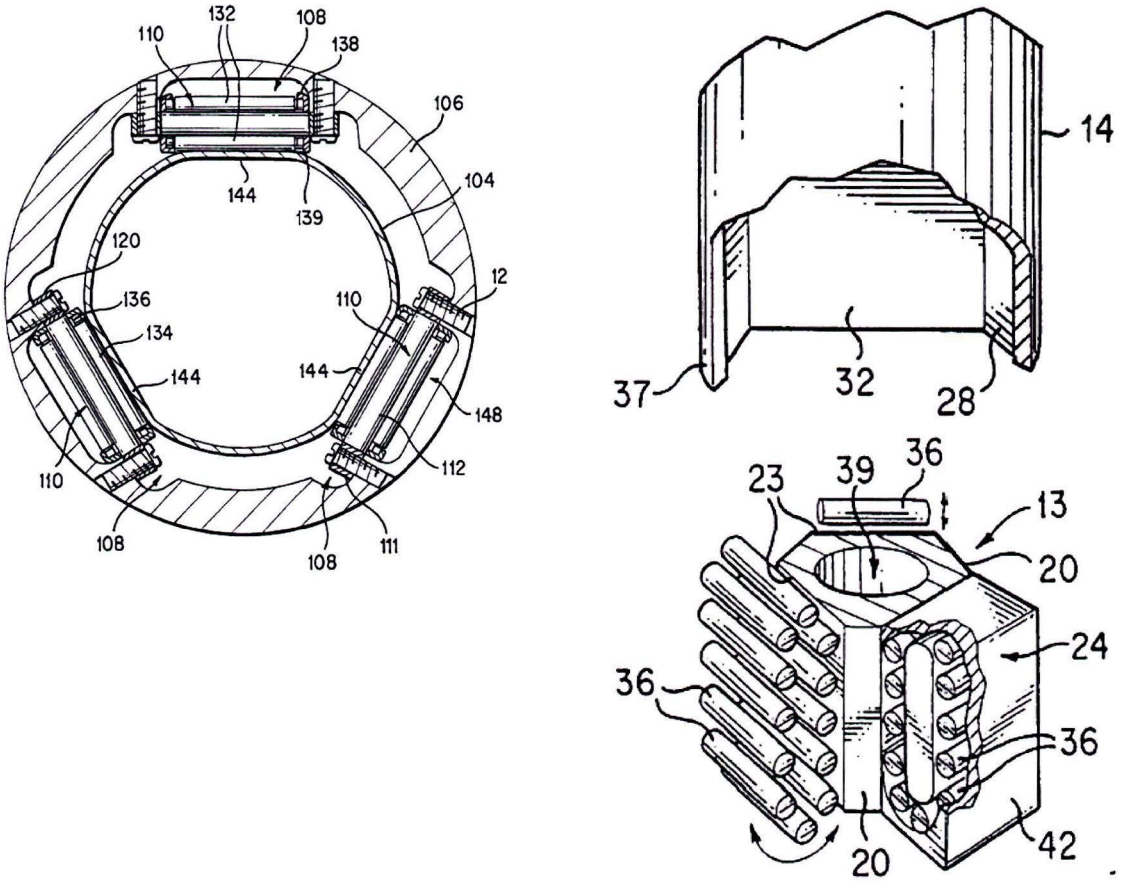

Figure 6.1.3: Top view (left) and isometric view of two different linear guidance systems with rollers

The inner tube is part of the wheel carrying arm and the outer tube is supported on bearings in the main frame for steering. Like concept one, the shock absorber can

be placed inside the inner tube, or with the use of a rocker beside it. Because of the triangular cross section of the tubes, there is no need for a connection link between the tubes to transfer rotation. Like in concept one, the smoothness of the three surfaces on the inner tube determines for a great part the smoothness of guidance.

Such a system is used in an application where the forces and moments are relatively low compared to the robot vehicle. For the use of this concept, twelve roller units would be used for each wheel unit. Therefore this system would become too complex and expensive.

3. Suspension in the wheel carrying arm with a trailing arm

The wheel carrying arm consists of two parts that are connected with each other by a hinge. The lower part is connected to the wheel. Between the two is a shock absorber, see figure 6.1.4.

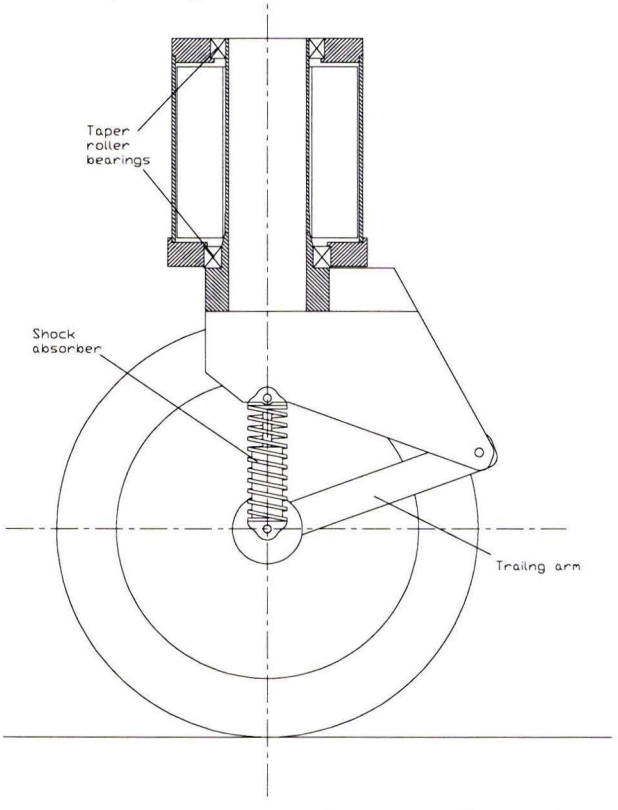

Figure 6.1.4: Wheel carrying arm with a trailing arm, schematic, partially cross-cut

For the wheel travel of 50 [mm] and the requirement that no part sticks out of the turning radius of the wheel, the length of the trailing arm causes a large horizontal movement with each vertical wheel movement. The hinge in the trailing arm has to be strong and stiff enough to transfer the large steering torque.

4. Double wishbone above the wheel

The wheel carrying arm is supported in two bearings above the wheel. From each bearing two rods connect the wheel unit to the main frame see figure 6.1.5.

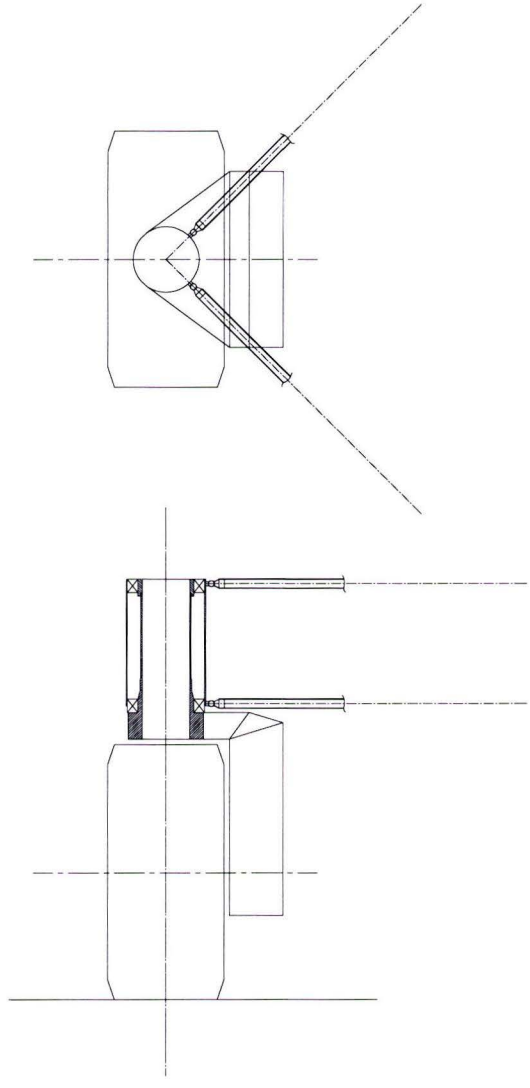

Figure 6.1.5: Top and side view of the double wishbone suspension, schematic, partially cross-cut

The top and bottom rods guide the wheel carrying arm in vertical direction and each rod pair at the lower and upper bearing prevent the movement in the horizontal plane. A push or a pull rod has to be connected to the outer tube of the wheel carrying arm to transfer the vertical forces to the shock absorber.

The double wishbone above the wheel is chosen for the robot vehicle, because it is adjustable, has a relatively low mass of which the greater part can be placed in various positions and it contributes to a low yaw inertia of the total vehicle.

§ 6.2 Double wishbone suspension

The double wishbone construction can be implemented in various ways, but for all constructions it is important that the connection provides a stiff connection between the wheel unit and the main frame. Besides it is important that the connection members have enough strength and resistance to buckling for high load situations.

The connection members should be as long as possible, because this length, together with the wheel travel, determines the shortening of the connection members. The longer the connection members, the less is their influence on the movement of the wheel in the horizontal plane. For further calculations it will be assumed that the length of the connection members is 500 [mm].

For the hinge points three possibilities will be considered.

1. Leaf springs: The benefit of leaf springs is that they have no play and there is no friction in the hinge.
   In appendix F [Leaf springs] the dimensions of a leaf spring hinge are calculated.
2. Rod ends: Rod ends can handle higher loads with respect to their turning capability, but will always have friction and the possibility of play after some time.
3. Rubber bearings: These types of hinges are used for passenger car, because they are cheap and isolate the bodywork from high frequent vibrations. Due to the rubber in the hinge, the stiffness is lower compared to the previous two hinge types.

Because the robot vehicle will be used in an automotive environment and the stiffness of rod end hinges is higher than rubber bearings, rod ends will be used for the hinges of the wishbone suspension.

§ 6.2.1 Placement of the suspension rods

The positioning of the suspension rods determines the vertical wheel movement and the vehicle behaviour. The centre lines of the upper and lower rod of a rod pair intersect. The line from this intersection to the centre of the tire road contact crosses the roll centre in the middle of the vehicle see figure 6.2.1.

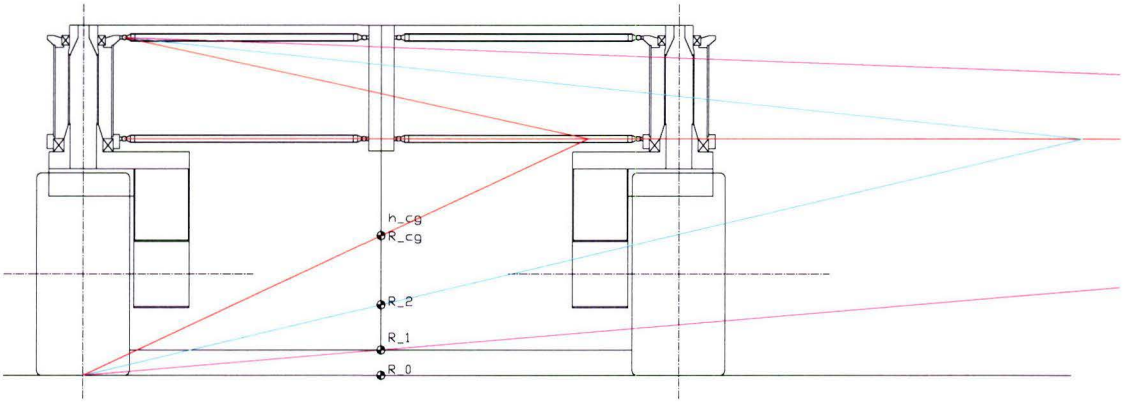

Figure 6.2.1: Schematic side view of the vehicle, with four different roll centre versions

The distance between the roll centre and the centre of gravity determines the initial roll moment for cornering actions. During cornering, the orientation of the suspension rods is different from the initial situation, as is the roll moment. The higher the roll centre, the bigger the angle between the suspension rods will be, resulting in a small distance between the connection points at the main frame. This means the connection is not stiff and forces at the main frame will be high. In the case when the two rods are parallel and horizontal the intersection point is at infinity and the roll centre will be located at the road, R_0. This configuration will be used, because in this way the vertical wheel movement is along a straight line and a stiff connection between the wheel unit and the main frame is realized. Another advantage of this configuration is the absence of the jacking effect [Dixon].

§ 6.2.2 Anti rotation system

The suspension rods are placed under an angle of 90° seen from above, see figure 6.2.2, where the green lines represent the centre lines of the suspension rods. In this way the rods can have a maximum length and the connection is stiff compared to configurations with a smaller angle. The hinge points at the wheel unit are located at a distance from the pole of the centre lines. The rotation of the wheel unit around this pole has to be fixed. This will be done with a conical tube connected to the wheel unit and a rod perpendicular to this tube that connects the tube to the main frame. Due to the wheel travel and the shortening of the connection rod, a little bump steer is present, but this is very small so

that it can be neglected. Moreover this bump steer can be corrected by the steering motor. The conical tube will bend due to the steering torque and the connection with the main frame. The amount of bending of this tube is calculated for the maximum possible steering torque with the FEA-program ALGOR, see appendix G [Conical tube anti rotation system].

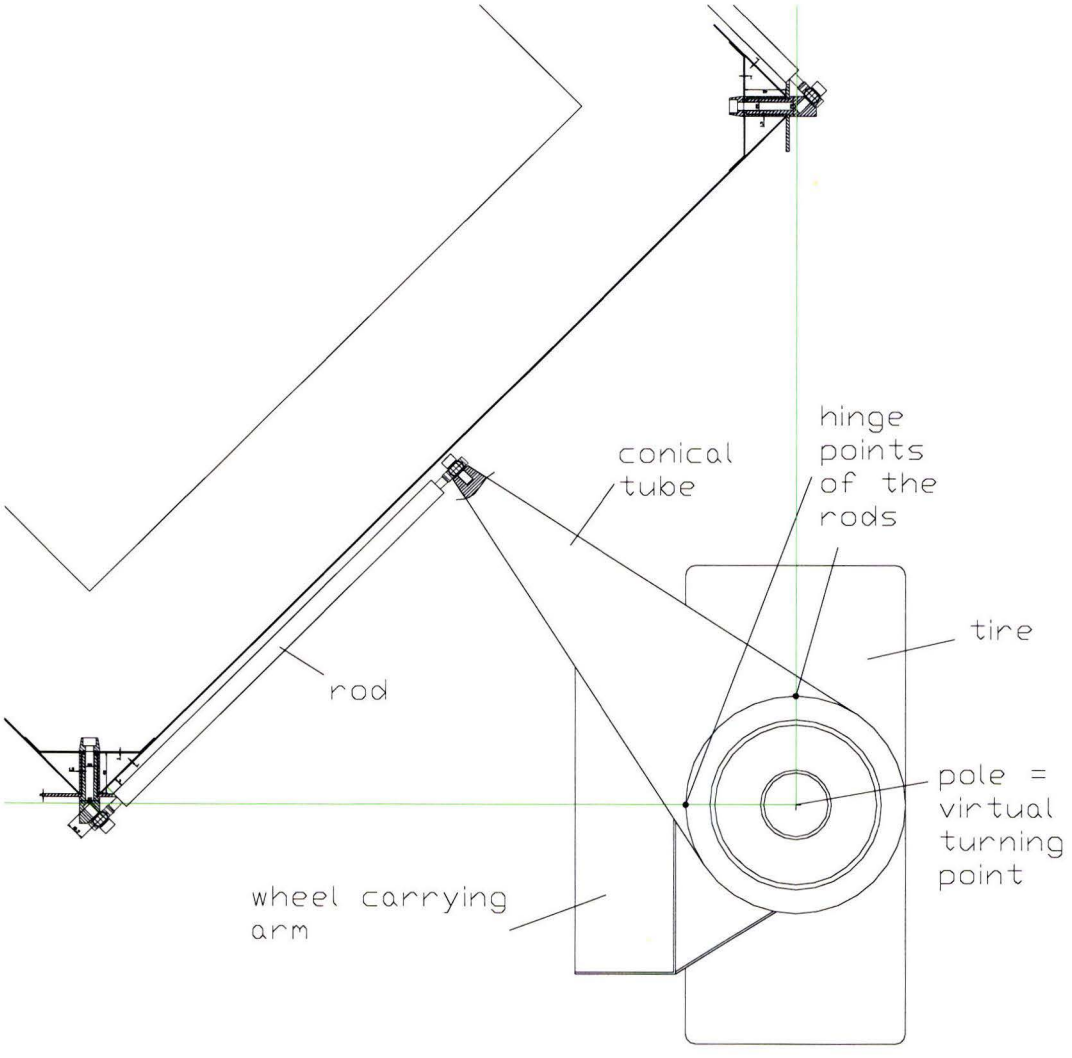

Figure 6.2.2: Anti rotation system

§ 6.2.3 Configuration of the suspension system

The vertical forces acting on the tires have to be transferred from the wheel unit to a shock absorber located at the main frame. This can be done in various ways. A push rod or a pull rod can be used, as well as various types and placements of rockers. In most race cars for example a push rod is used, because this rod helps to transfer the lateral tire forces to the frame of the race car. So the push rod relieves the lower wishbone of part of the heavy load it has to transfer. For the robot vehicle the wishbones are above the wheel. The angle of a push rod with the horizontal will be relatively small, which results in high forces in the horizontal plane acting on the main frame. These forces have to be supported by the frame and can transferred by means of a rocker, which ads mass to the top of the main frame. With a pull rod on the other hand, the shock absorber and the rocker can be placed at a lower point in the main frame, which helps to lower the centre of gravity. A drawback of the use of a pull rod is the added load to the wishbones although the angle of the pull rod with the horizontal is relatively large resulting in a small horizontal force component.

In appendix H [Suspension configuration concepts] some concepts for the suspension configuration are described. From these concepts configuration 3, "Pullrod with horizontal shock absorber" is chosen, see figure 6.2.3. This concept uses relatively few parts from which most can be placed near the bottom of the main frame to keep the centre of gravity low. The pullrod is connected to the top of the wheel unit and to the rocker in the shock absorber unit. The centre line of the pullrod crosses the lower corner of the main frame, so the forces can be well transferred to the main frame. The shock absorber unit consists of a U-profile with the shock absorber and the rocker mounted inside. Because the shock absorber unit is placed on the outside of the main frame it is accessible for quick adjustments.

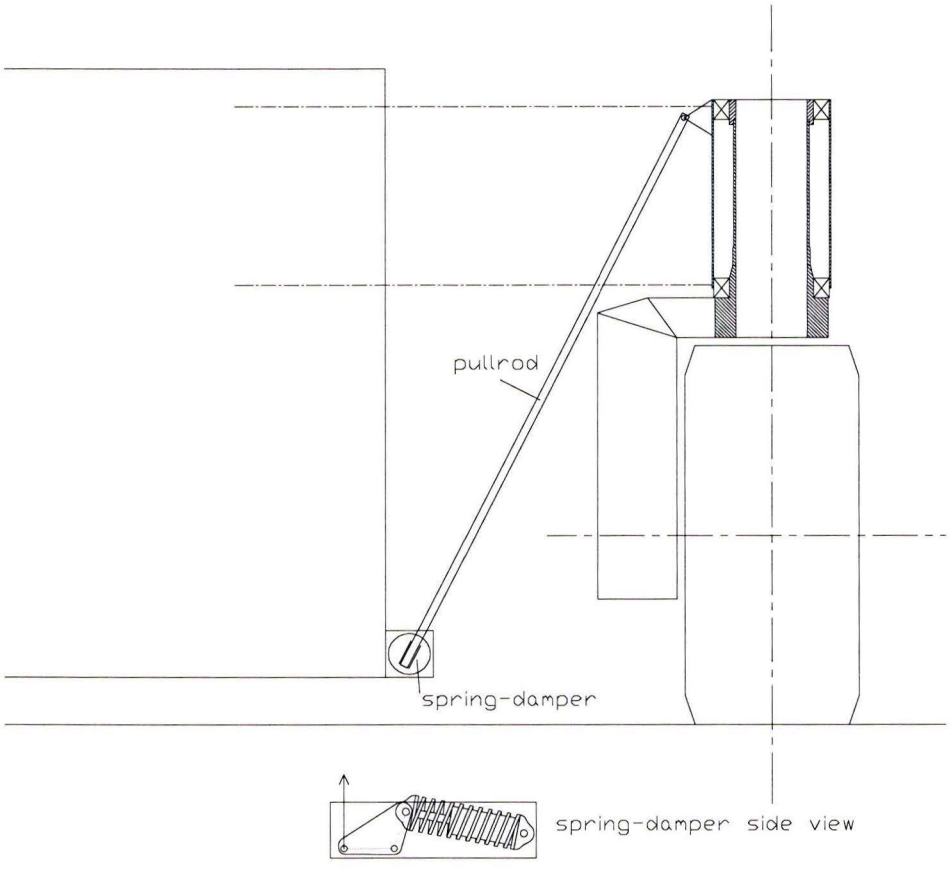

Figure 6.2.3: Suspension configuration

§ 6.2.4 Forces on the suspension rods

For determination of the dimensions of the suspension rods and the rod ends, the forces acting on them have to be known. For maximum braking and maximum cornering, where almost all forces act on two wheels, the forces in the suspension rods will be determined. Because of the symmetry in the vehicle, the forces in the suspension rods will be comparable in both situations.

The maximum lateral force that acts in the tire-road contact is assumed to be $F_W = 3000$ [N], see figure 6.2.4. At the same time there is a vertical force, F_n, acting on the tire. This vertical force acts against the mass-force of the wheel unit and the vertical component of the force in the pull rod, F_p. The sum of all forces and the sum of all moments around the hinge of the lower suspension rod are zero.

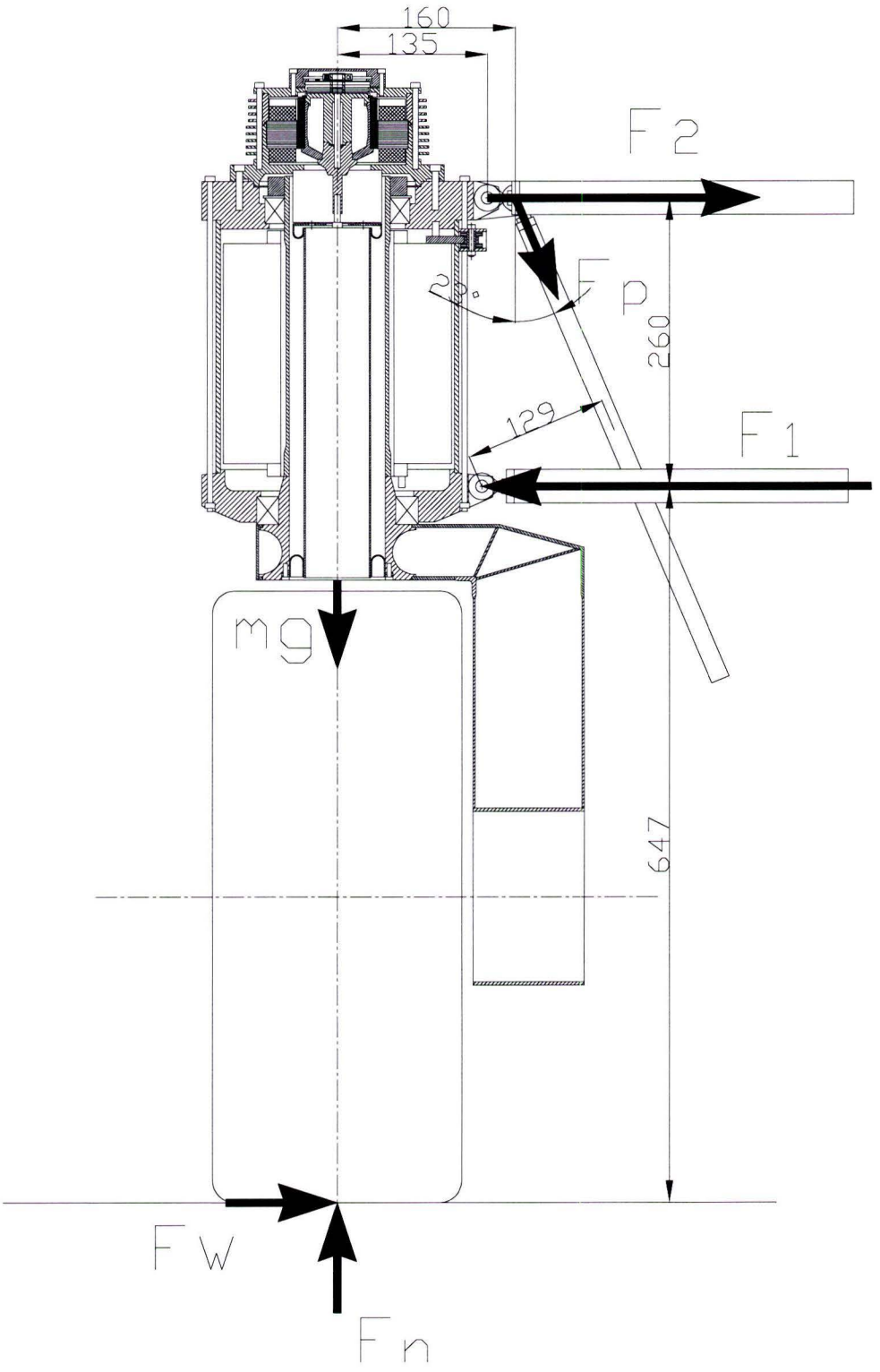

Figure 6.2.4: Forces acting on the suspension

Force equilibrium:

$$F_1 = F_w + F_2 + F_p \sin(23^\circ) \quad (6.1)$$

$$F_n = mg + F_p \cos(23^\circ) \quad (6.2)$$

The force in the pull rod is determined by the mass of the main frame with its components and is assumed to be $F_p = 2500$ [N]. The mass of a wheel unit is about m = 60 [kg], so with formula (6.2) the normal force is:

$$F_n = 60 \cdot 9{,}81 + 2500\cos(23^\circ) = 2890[N]$$

Equilibrium of moments about the hinge point of the lower suspension rod:

$$0{,}647F_w + 0{,}135mg = 0{,}135F_n + 0{,}26F_2 + 0{,}129F_p \quad (6.3)$$

Substitution of known variables in (6.3) gives:

$$0{,}647 \cdot 3000 + 0{,}135 \cdot 60 \cdot 9{,}81 = 0{,}135 \cdot 2890 + 0{,}26F_2 + 0{,}129 \cdot 2500 \Rightarrow$$
$$F_2 = 5030[N]$$

Force F_1 can now be calculated with formula (6.1):

$$F_1 = 3000 + 5030 + 2500\sin(23^\circ) = 9007[N]$$

Due to the length of the suspension rods, the push forces are the most critical, because they can cause buckling. The formulas for buckling can be found in appendix I [Buckling]. For a range of tube diameters and wall thicknesses the buckling forces are calculated with MATLAB. In figure 6.2.5 and 6.2.6 are two diagrams with respectively the buckling force and the mass as a function of the diameter for various wall thicknesses for steel tubes. In figure 6.2.7 and 6.2.8 are the same diagrams, but now for aluminium.

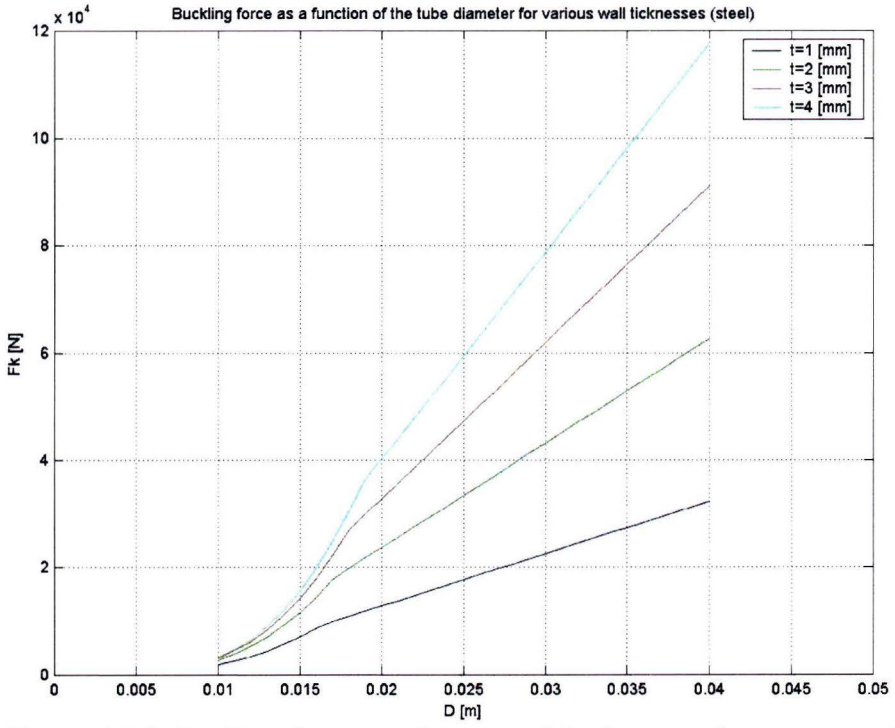

Figure 6.2.5: Buckling force as a function of the diameter for various wall thicknesses of steel tubes.

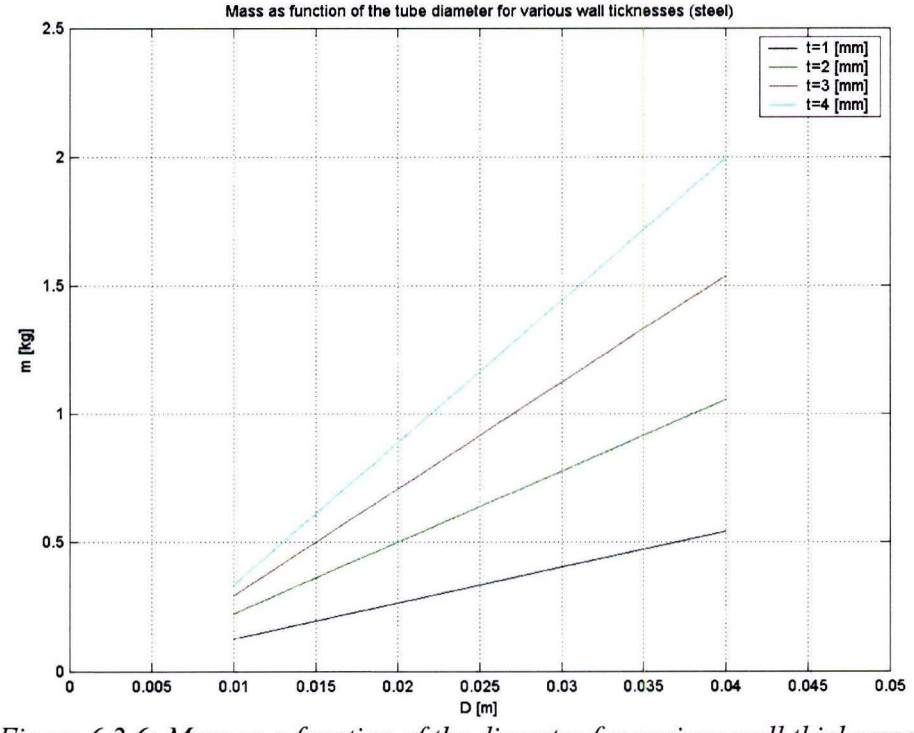

Figure 6.2.6: Mass as a function of the diameter for various wall thicknesses of steel tubes.

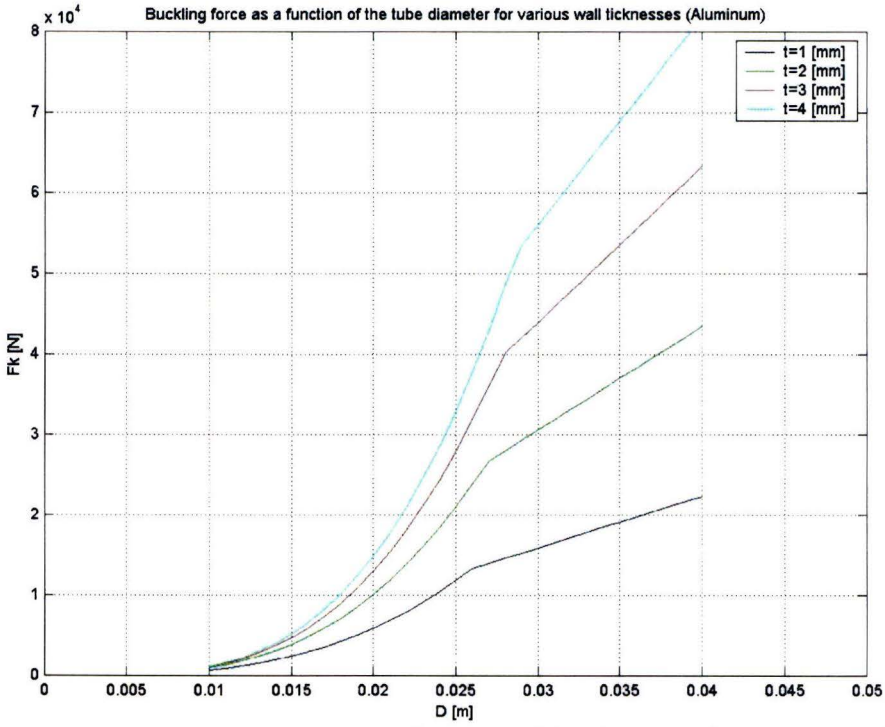

Figure 6.2.7: Buckling force as a function of the diameter for various wall thicknesses of aluminium tubes.

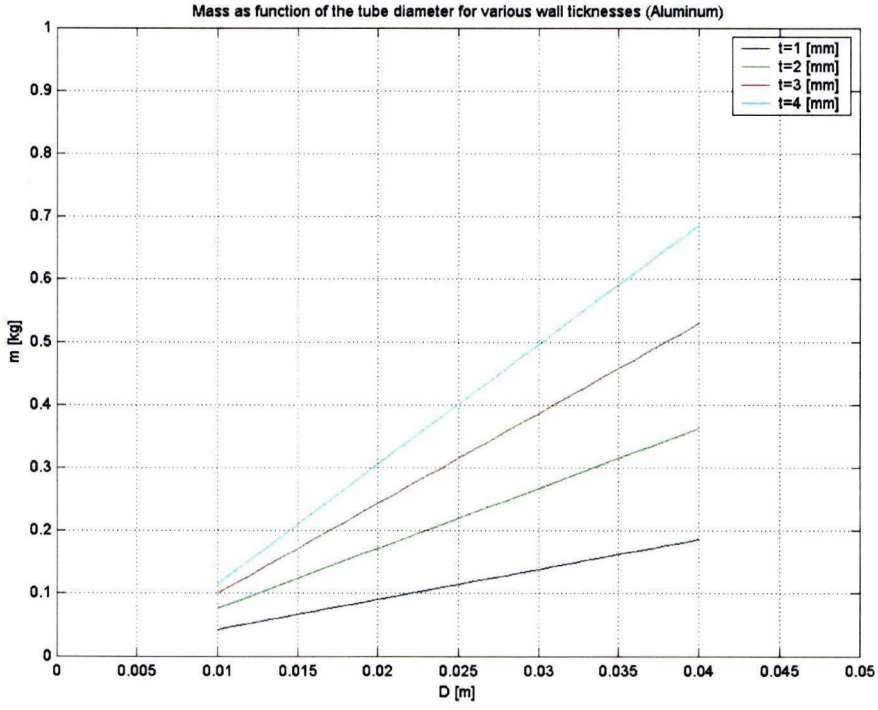

Figure 6.2.8: Mass as a function of the diameter for various wall thicknesses of aluminium tubes.

From the above figures it can be seen that the aluminium tubes are more resistant to buckling with respect to their mass compared to the steel tubes, so an aluminium tube will be used. From figure 6.2.7 and 6.2.8 a suitable aluminium tube can be determined. The tube with a diameter 30 [mm] and a wall thickness of 3 [mm] will be used. At each end a steel insert is attached by means of thread and glue. The inserts have thread for the rod ends. The rod ends that will be used are "Fluro GAXSW 10 MS". In figure 6.2.9 is a drawing of one end of a rod assembly.

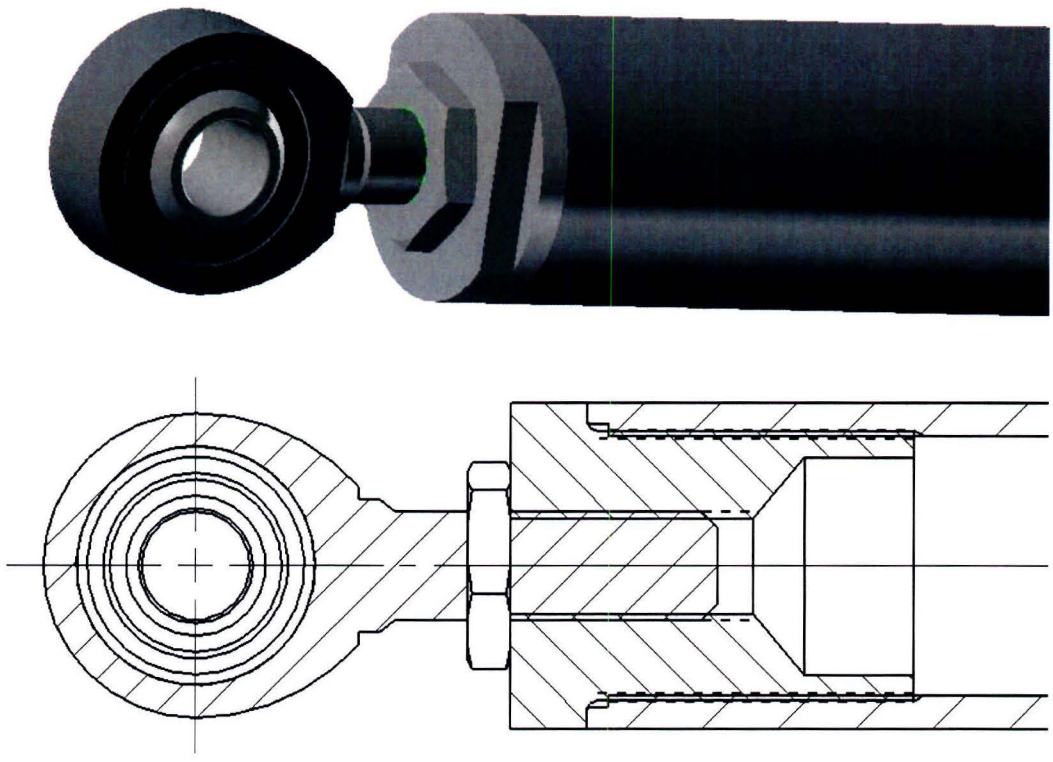

Figure 6.2.9: One end of a rod assembly in 3D and cross section

The stiffness of a rod assembly will be approximated by the stiffness of the aluminium tube with length l = 458 [mm]. The area of the cross section is:

$$A = \frac{\pi}{4}\left(D^2 - d^2\right) = 2{,}54 \cdot 10^{-4}\left[m^2\right]$$

The stiffness is:

$$c = \frac{EA}{l} = \frac{7 \cdot 10^{10} \cdot 2{,}54 \cdot 10^{-4}}{0{,}458} = 3{,}89 \cdot 10^{7}\left[N/m\right]$$

§ 6.2.5 Determination of the spring stiffness

For a given wheel travel in a static situation, a certain force is required from the shock absorber to keep the vehicle at the desired height. In driving situations, higher forces and more wheel travel may be needed. If a linear spring characteristic is assumed, the spring stiffness can be calculated by taking the static situation and a situation where almost the maximum wheel travel available is reached and dividing the difference in force by the difference in wheel travel of the two points.

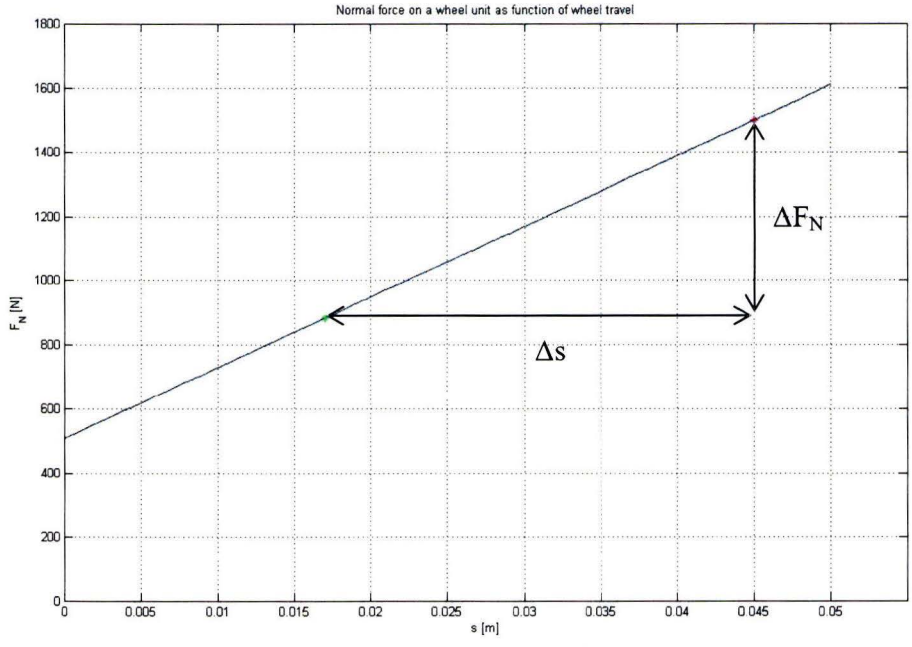

Figure 6.2.10: Normal force on a wheel unit as function of the wheel travel

In the static situation a quarter of the mass of the main frame with components (600-4*60 = 390) has to be supported by the shock absorber of one wheel unit. This is 90 [kg], so the vertical force on this wheel unit is 883 [N], see figure 1. The static wheel travel is 17 [mm] as is determined in paragraph 6.1. The vertical suspension force during a deceleration of 13 [m/s^2] is around 1500 [N]. In this situation the maximum wheel travel should almost be reached and is set to 45 [mm], so there is 10 % of the 50 [mm] wheel travel left. The required suspension stiffness at the wheel is:

$$C_{wheel} = \frac{\Delta F_N}{\Delta s_{wheel}} = \frac{1500 - 883}{0{,}045 - 0{,}017} = 2{,}2 \cdot 10^4 [N/m]$$

The pullrod is placed under an angle of 23° with the vertical, so the required stiffness at the rocker becomes:

$$C_{rocker} = \frac{C_{wheel}}{\cos^2(23^\circ)} = 2{,}6 \cdot 10^4 [N/m]$$

The required stiffness is of the same order as the stiffness of springs used on motorcycles, see appendix J [Comparison of various motor cycle rear shocks]. The spring deflection is chosen to be comparable to the deflection of a motorcycle spring and is set to 36 [mm]. The ratio of the rocker is

$$i_{rocker} = \frac{spring\_deflection}{wheel\_travel} = \frac{0{,}036}{0{,}05} = 0{,}72$$

This ratio is chosen so that an existing spring-damper can be used: Showa GD05-50

The spring stiffness calculated with the rocker ratio is:

$$C_{spring} = \frac{C_{rocker}}{i^2_{rocker}} = \frac{2{,}6 \cdot 10^4}{0{,}72^2} = 5{,}01 \cdot 10^4 [N/m]$$

Since the spring stiffness of the spring-damper Showa GD05-50 is $5{,}03 \cdot 10^4$ [N/m], this one will be used.

The damping parameter will be determined with the quarter car model in the next paragraph. Since this value is the damping value at the wheel unit it has to be multiplied by

$$\frac{1}{i^2_{total}} = \frac{1}{i^2_{pullrod}} \cdot \frac{1}{i^2_{rocker}} = \frac{1}{\cos^2(23^\circ)} \cdot \frac{1}{0{,}72^2}$$

§ 6.3 Quarter car model

The behaviour of the robot vehicle can be modelled with a quarter car model. As explained in the name, this model represents a quarter of the vehicle, so the suspension of one wheel unit is considered. This model can be used to set a good value for the damping of the shock absorbers. The schematic representation of this model is shown in figure 6.3.1.

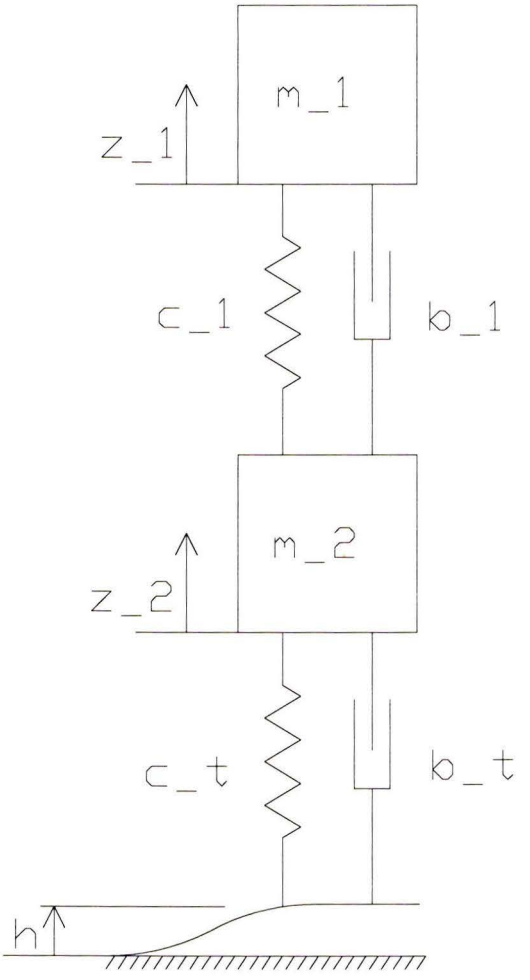

$m_1 = 90$ [kg]

$c_1 = 2{,}2 \cdot 10^4$ [N/m]

b_1 = to be determined

$m_2 = 60$ [kg]

$c_t = 2{,}7 \cdot 10^5$ [N/m]

$b_t = 50$ [Ns/m]

Figure 6.3.1: Quarter car model

The equations of motion for this system are:

$$m_1\ddot{z}_1 = -c_1(z_1 - z_2) - b_1(\dot{z}_1 - \dot{z}_2) \tag{6.4}$$

$$m_2\ddot{z}_2 = c_1(z_1 - z_2) + b_1(\dot{z}_1 - \dot{z}_2) - c_t(z_2 - h) - b_t(\dot{z}_2 - \dot{h}) \tag{6.5}$$

$$\ddot{z}_1 = -\frac{c_1}{m_1} z_1 + \frac{c_1}{m_1} z_2 - \frac{b_1}{m_1} \dot{z}_1 + \frac{b_1}{m_1} \dot{z}_2 \tag{6.6}$$

$$\ddot{z}_2 = \frac{c_1}{m_2} z_1 - \frac{(c_1 + c_t)}{m_2} z_2 + \frac{b_1}{m_2} \dot{z}_1 - \frac{(b_1 + b_t)}{m_2} \dot{z}_2 + \frac{c_t}{m_2} h + \frac{b_t}{m_2} \dot{h} \tag{6.7}$$

In matrix form:

$$\begin{bmatrix} \dot{z}_1 \\ \ddot{z}_1 \\ \dot{z}_2 \\ \ddot{z}_2 \end{bmatrix} = \begin{bmatrix} 0 & 1 & 0 & 0 \\ -\frac{c_1}{m_1} & -\frac{b_1}{m_1} & \frac{c_1}{m_1} & \frac{b_1}{m_1} \\ 0 & 0 & 0 & 1 \\ \frac{c_1}{m_2} & \frac{b_1}{m_2} & -\frac{(c_1 + c_t)}{m_2} & -\frac{(b_1 + b_t)}{m_2} \end{bmatrix} \cdot \begin{bmatrix} z_1 \\ \dot{z}_1 \\ z_2 \\ \dot{z}_2 \end{bmatrix} + \begin{bmatrix} 0 & 0 \\ 0 & 0 \\ 0 & 0 \\ \frac{c_t}{m_2} & \frac{b_t}{m_2} \end{bmatrix} \cdot \begin{bmatrix} h \\ \dot{h} \end{bmatrix} \tag{6.8}$$

The normal tyre load is given by:

$$F_N = (m_1 + m_2)g + m_1 \ddot{z}_1 + m_2 \ddot{z}_2 > 0 \tag{6.9}$$

This normal tyre load is built up out of the static and the dynamic tyre load.

$$F_{N,static} = (m_1 + m_2)g \tag{6.10}$$

$$F_{N,dynamic} = m_1 \ddot{z}_1 + m_2 \ddot{z}_2 \tag{6.11}$$

For road holding it is best to have a low dynamic tyre load, because the normal tyre load determines, together with the friction coefficient, the amount of driving and lateral force that can be transferred to the road. Equation (6.9) rewritten for the acceleration of m_1, the main frame, gives:

$$\ddot{z}_1 > -\frac{(m_1 + m_2)}{m_1} g - \frac{m_2}{m_1} \ddot{z}_2 \tag{6.12}$$

From equation (6.9) it is clear the main frame, m_1 should have a minimum acceleration for road holding. In contrary to this is the fact that the vertical accelerations of the main frame have a negative effect on the electronic and other parts in the frame. And, in case the robot vehicle would be adapted to move people, this acceleration is a direct measure for the comfort these people experience. In passenger cars the vertical acceleration of the car body is minimized by keeping the unsprung mass low compared to the sprung mass, the car body.

For the robot vehicle design considerable effort has been put into lowering the mass of the wheel units, since this is unsprung mass. Because of the wheel motor, slipring and steering system, the mass of the wheel unit is nevertheless relatively high. The high dynamic movements of the robot vehicle require good road holding properties. Therefore

the suspension will be configured for good road holding. In situations where more comfort is desired, the suspension setting can be altered and the performance should be reduced accordingly. In case sensitive sensors, a camera or other equipment should be connected to the frame, these parts can be put on a platform with suspension that is designed for this purpose. Springs with low stiffness should be used to isolate the platform from the rest of the vehicle. For quick adaptation of the platform for different equipment, the use of air springs can be considered.

This quarter car model consists of two masses and hence it has two eigenfrequencies. These two eigenfrequencies are close to the eigenfrequencies of the separate masses with their springs and dampers. The eigenfrequencies of the separate masses are:

$$f_1 = \sqrt{\frac{c_1}{m_1}} \cdot \frac{1}{2\pi} = 2{,}5[Hz]$$

$$f_2 = \sqrt{\frac{c_t}{m_2}} \cdot \frac{1}{2\pi} = 10{,}7[Hz]$$

Without damping, the system would swing up when excited in one of the eigenfrequencies. Since the damping in the tyre is very small, the damper in the shock absorber is for a great part responsible for the vehicle behaviour. With an extreme high damping coefficient the two masses will act like one mass on the tyre stiffness and with an extreme low damping coefficient the damper has little effect and the system will still swing up resulting in a high dynamic tyre load and poor handling. There exists an optimum damping coefficient for ride comfort and an optimal damping coefficient for minimal dynamic tyre load and thus optimal handling. The response of the system to an ISO road profile is calculated with Matlab for various damping coefficients, see appendix K [Quarter car model].

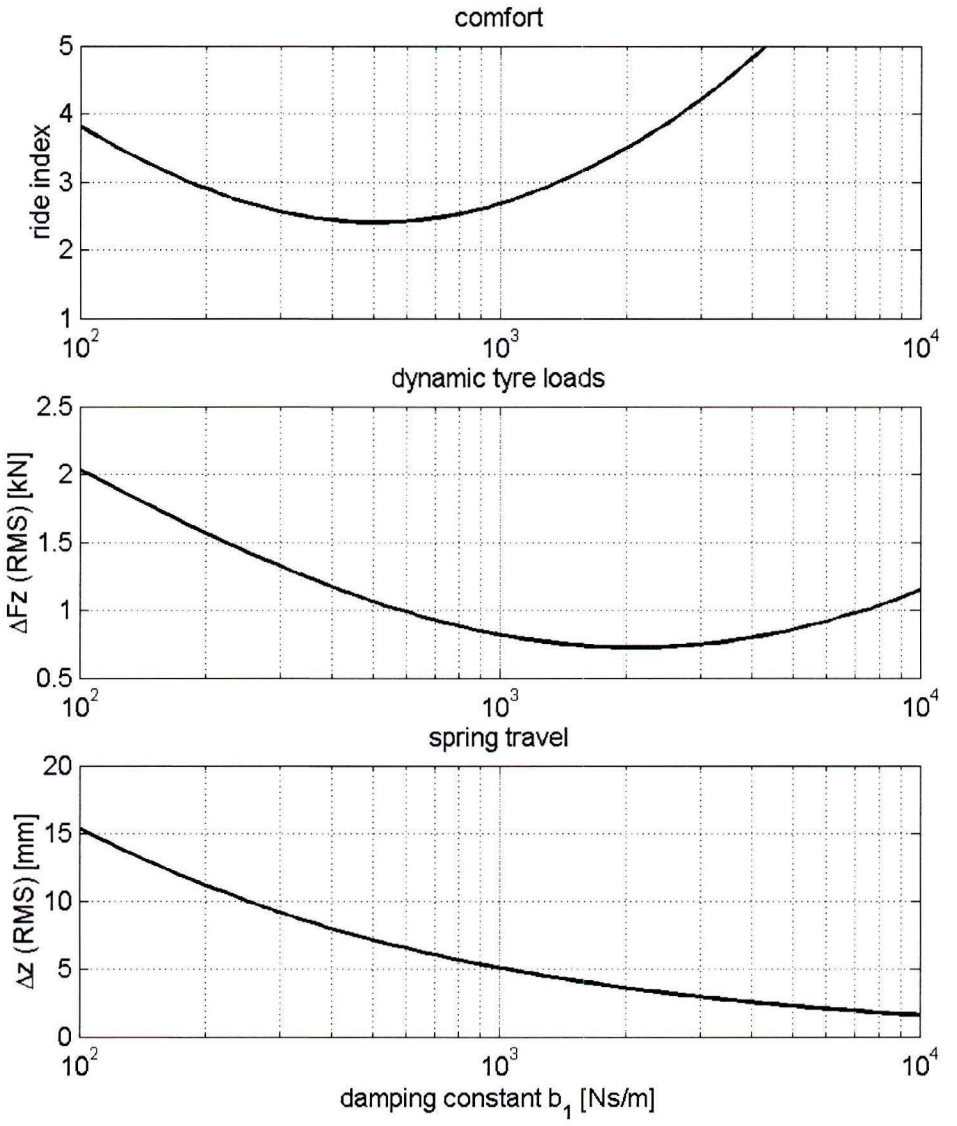

Figure 6.3.2: Ride comfort, dynamic tyre load (RMS) and spring travel (RMS) as function of the damping constant, for road class C (average) and a vehicle speed of 7 [m/s].

From figure 6.3.2 and 6.3.3 it can be seen there is an optimum damping coefficient for comfort and another for dynamic tyre loads. It can also be seen the spring travel decreases with an increasing damping coefficient. For ISO road profiles in simulation, average values of the height of bumps are used. This is why the Root Mean Square (RMS) results are shown. The peak values that can occur on this road profile are 3 times the root mean square value. For the two situations the optimal damping coefficient for minimal dynamic tyre load and thus for best handling is $b_1 = 2000$ [Ns/m], so this value will be used.

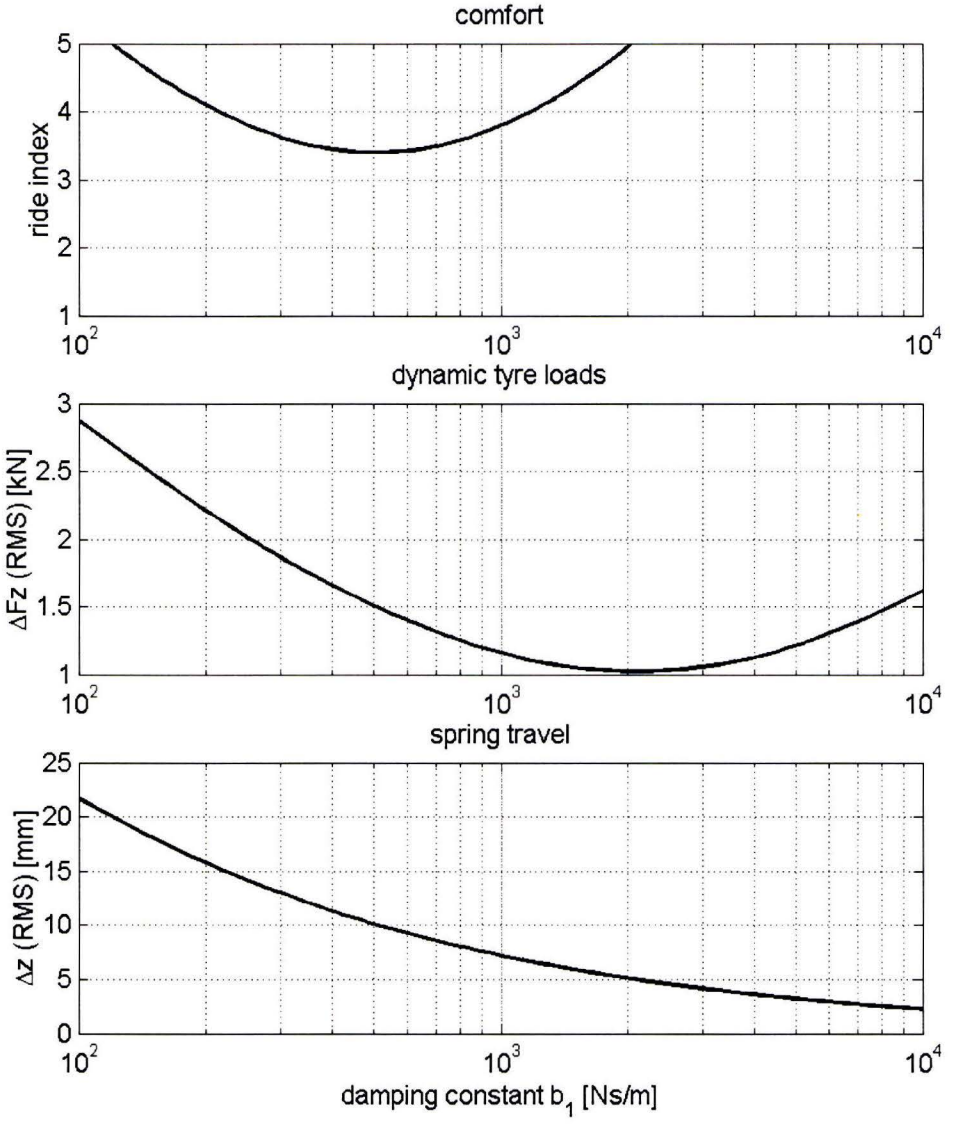

Figure 6.3.3: Ride comfort, dynamic tyre load (RMS) and spring travel (RMS) as function of the damping constant, for road class C (average) and a vehicle speed of 14 [m/s].

The displacement response of this system to inputs over a frequency range is shown in figure 6.3.4. In this figure two resonance peaks can be seen at 1,9 [Hz] and 9,8 [Hz] corresponding to the two system eigenfrequencies. In figure 6.3.5 the response of the system to a step input of 10 [mm] can be seen.

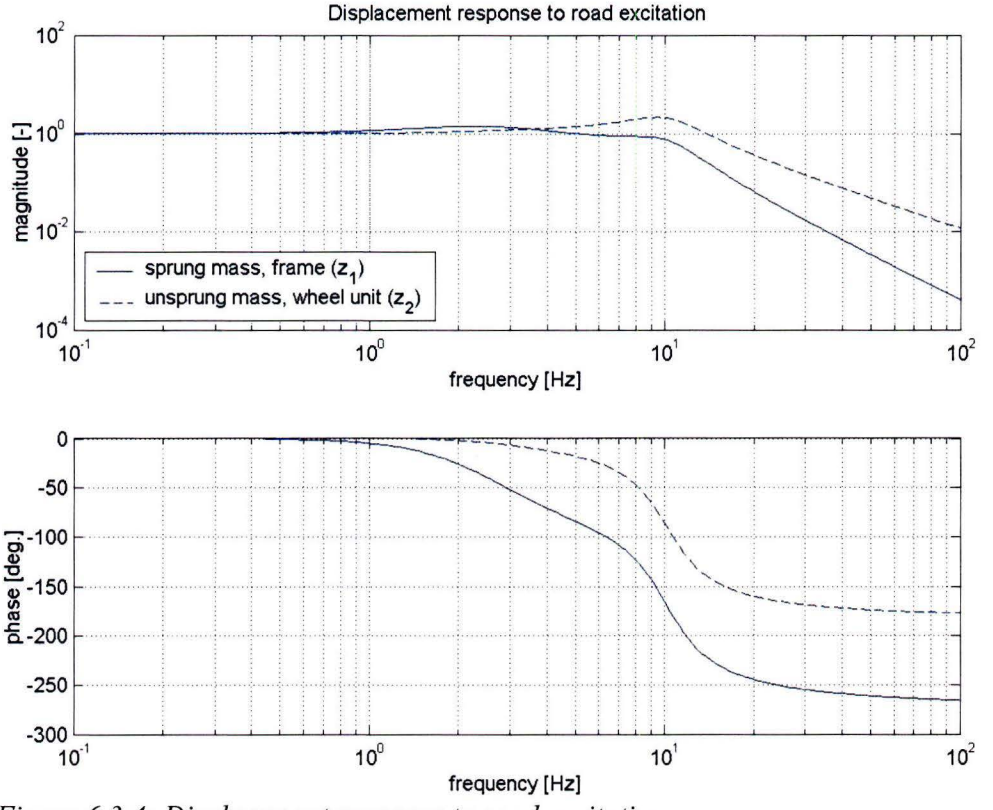

Figure 6.3.4: Displacement response to road excitations

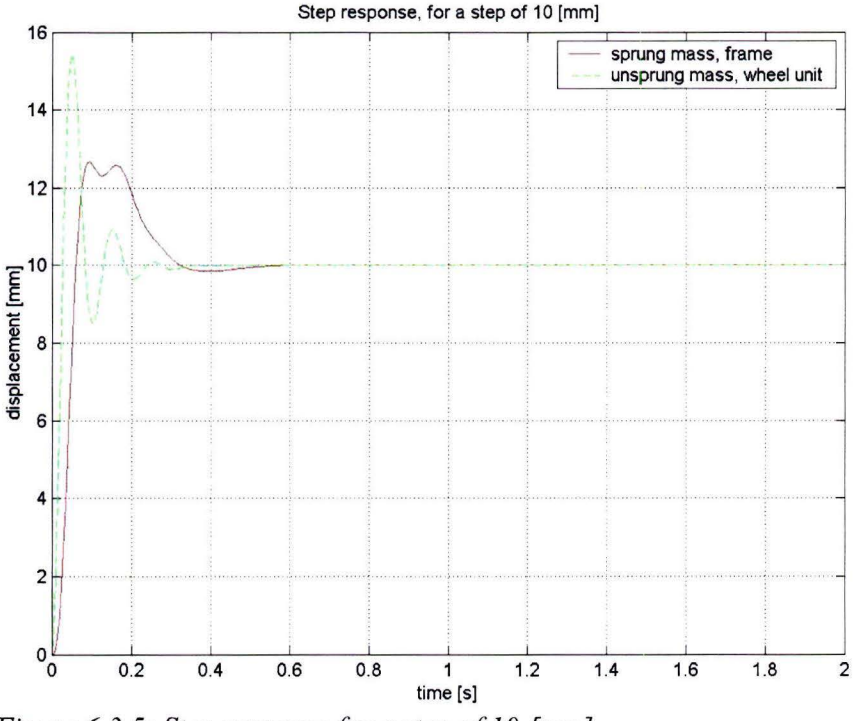

Figure 6.3.5: Step response for a step of 10 [mm]

§ 6.4 Anti roll system

Passenger cars and other road vehicles have a defined driving direction; hence front and rear wheels can be defined. To prevent excessive vehicle body roll in cornering an anti roll system is added to the suspension system of these vehicles. The system that is used in most vehicles consists of a torsion bar that connects the front wheels and a torsion bar that connects the rear wheels. The robot vehicle can move in all directions in the horizontal plane, so it has no defined front or rear wheels. Because of this, the anti roll system for the robot vehicle has to be adaptable to the driving direction.

A modular anti roll system is added to the shock absorber module. This system, see figure 6.4.1 and 6.4.2, consists of an aluminium housing that will be connected to the rocker of the shock absorber module. In this housing is a piston between two sets of Belleville springs. This piston is coupled to a piston rod of a hydraulic cylinder which is mounted to the frame. The two chambers of the hydraulic cylinder, with equal volume per length, are directly coupled with a pipe. In this pipe is an electro-mechanical valve which can be used to block the connection between the two chambers and thus locking the hydraulic piston. When the hydraulic piston is locked, the stiffness of the Belleville springs shunts the shock absorber. This minimizes the wheel travel, so less roll is possible.

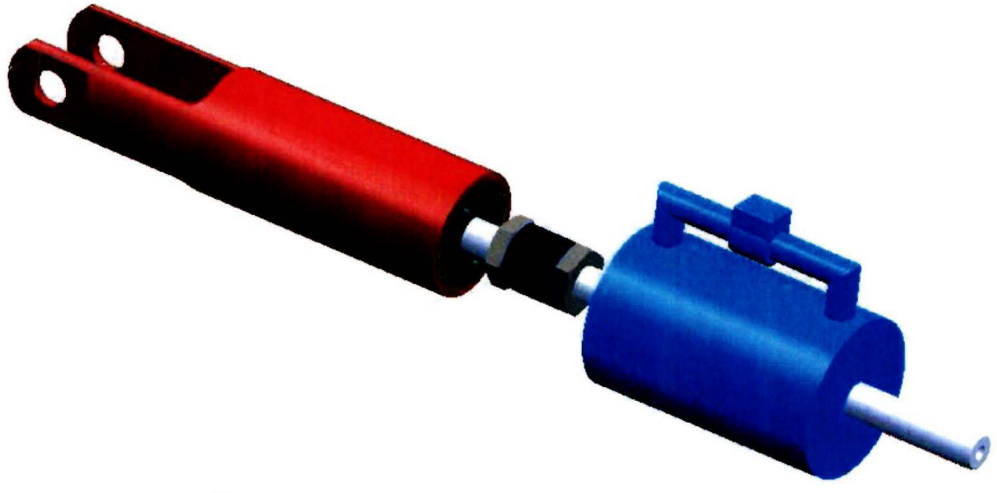

Figure 6.4.1: Anti roll system

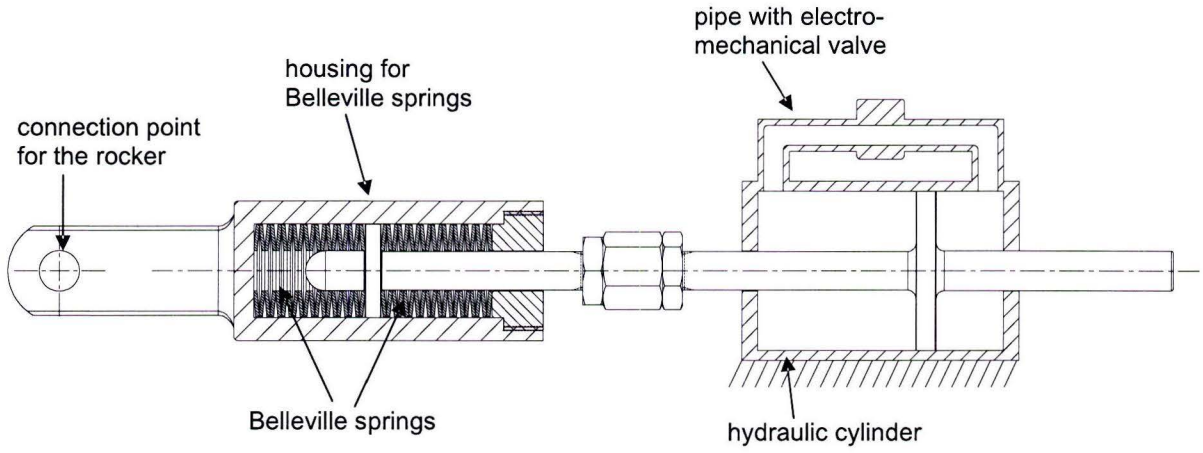

Figure 6.4.2: Anti roll system, section view

The stiffness of the Belleville springs is determined in the same way as in paragraph 6.2.5. The maximum wheel travel with the anti roll system engaged is set to 10 [mm]. This stiffness at the wheel is:

$$C_{wheel,anti\_roll} = \frac{\Delta F_N}{\Delta s_{wheel}} = \frac{1500-883}{0{,}01} = 6{,}2 \cdot 10^4 [N/m]$$

And hence at the rocker:

$$C_{rock,anti\_roll} = C_{wheel,anti\_roll} \frac{1}{\cos^2(23^\circ)} \cdot \frac{1}{0{,}72^2} = 1{,}4 \cdot 10^5 [N/m]$$

This spring stiffness is the sum of the stiffnesses of the shock absorber, as determined in § 6.2.5, and the Belleville springs:

$$C_{belleville} = C_{rock,anti\_roll} - C_{shock} = 9{,}0 \cdot 10^4 [N/m]$$

This stiffness is made with 20 Belleville springs, with D = 23 [mm] and d = 10,2 [mm], placed in series.

The hydraulic cylinder with the electro-mechanical valve can also be used as an extra damper. In this way skyhook damping can be used to improve the dynamic behaviour of the robot vehicle.

Chapter 7 Steering

§ 7.1 Requirements for the steering system

Each wheel unit of the mobile robot will be steered by an electric motor in combination with a reduction. This electric motor has to deliver a certain amount of torque, T to overcome the friction between the tire and the road and to give the wheel unit a certain angular acceleration and speed. Since the friction between the tire and the road is only significant at standstill or at low vehicle speeds, the required torque at speeds above 10 km/h is dictated by the desired steering action.

An extreme steering action could be needed when the mobile robot is driving towards a test vehicle with the maximum velocity of 50 [km/h] and has to make an evasive manoeuvre to avoid a collision, see figure 7.1.1.

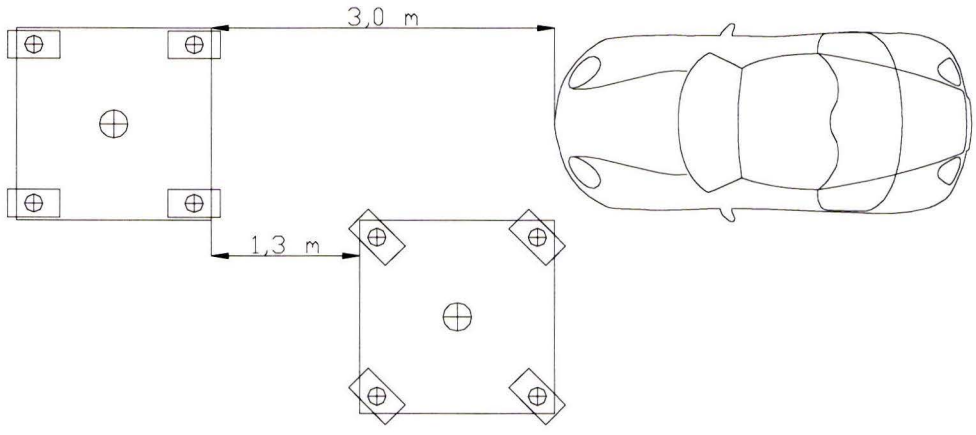

Figure 7.1.1: The mobile robots avoids a collision with the test vehicle

It is assumed that the critical distance from where the mobile robot should be able to avoid a collision is at 3 [m] from the test vehicle. If all four wheels would steer 45° it would take one length of the mobile robot, that is 1,7 [m], to avoid the test vehicle. This means that the wheels should be steered within the distance of 1,3 [m]. At 50 [km/h] the mobile robot covers 13,9 [m] every second, so the distance of 1,3 [m] is covered in t = 0,09 [s]. Actually the vehicle is already moving sideways before the steering angle of $\varphi = 45^{\circ}$ is reached. This means there is more time for the steering action. For the calculations it is assumed the available time is t = 0,1 [s]. The required angular acceleration, $\dot{\omega}$ is calculated as follows:

$$\varphi = \tfrac{1}{2}\dot{\omega}t^2$$
$$\frac{2\pi}{8} = \tfrac{1}{2}\dot{\omega}(0{,}1)^2 \Rightarrow \dot{\omega} = 157\left[rad/s^2\right] \qquad (7.1)$$

The torque required for this angular acceleration depends on the inertia of the steered parts of the wheel unit about the steering axis, $J_{z,total}$.

$$T_{steer,inertia} = J_{z,total} \cdot \dot{\omega} \qquad (7.2)$$

The static steering torque due to the friction between the tire and the road can be calculated with the following formula [Dixon].

$$T_{RSt} = \frac{\mu F_v^{1,5}}{3 p_i^{0,5}} \qquad (7.3)$$

with: p_i = tire pressure
μ = coefficient of friction (1,1)
F_v = normal force

The static steering torque can change in time because all the variables in the formula can change in time. The normal force, F_v can change due to weight transfer. The coefficient of friction changes with the temperature of the tires, the slip angle and the road surface. The tire pressure changes with temperature and it is important in servicing of the robot vehicle that the tire pressure is checked before operating the vehicle.

§ 7.1.1 Steering system of Moving Base 2

In chapter 2 the outline of the steering system of the current Moving Base is discussed. The maximum torque delivered by the steering motor is T_{motor} = 4,58 [Nm], so with the reduction i = 1/59 the output torque is T_{out} = 270 [Nm]. The inertia of the total steering system is 2,0 [kgm^2] what results in a maximum angular acceleration of $\dot{\omega}_{max}$ = 135 [rad/s^2] In the control system the maximum steering speed is set to n_{steer} = 1,24 [turns/s].

§ 7.2 Steering system of the mobile robot

§ 7.2.1 Steering concept 1: External motor with a two stage reduction

The first concept for the steering system consists of a housed electromotor beside the steering axis with a two stage reduction. The electric motor is connected to a reduction box by means of a pulley on the motor shaft and a synchronous belt to a second pulley at the input shaft of the reduction box, see figure 7.2.1.

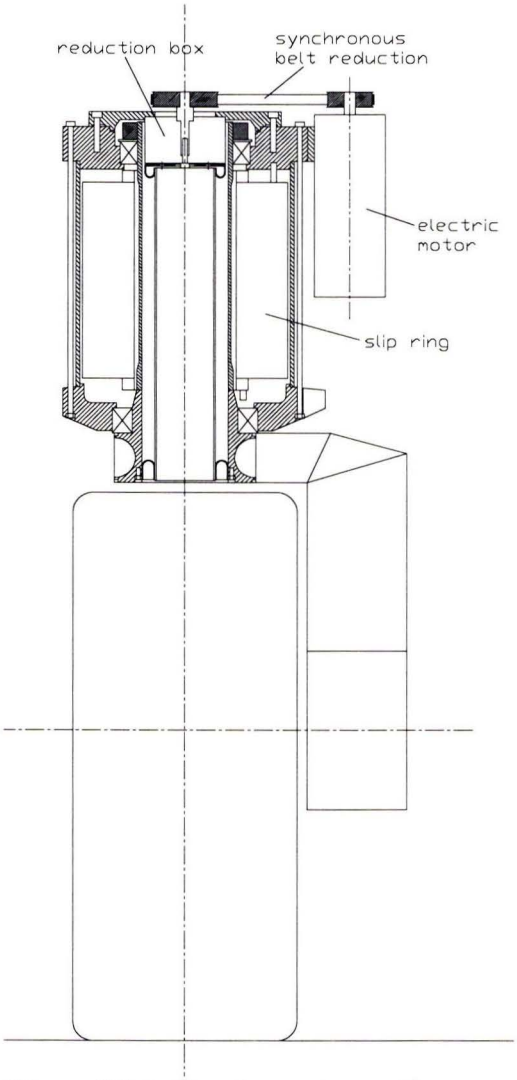

Figure 7.2.1: Steering system with a two stage reduction, schematic

With this configuration it is easy to change the steering motor to another type with other specifications. The motor is not enclosed by the construction, so it can be cooled easily. Besides, this configuration has little contribution to the total height of the vehicle. For the

controlling of the steering system it is important that there is no or very little play in the transmission and that the transmission provides a stiff connection between the motor and the wheel carrying arm. The synchronous belt is the least stiff part of the transmission, but it is in the faster part of the transmission, so the effect at the output of the reduction box is minimal. From this steering system a model is made, see figure 7.2.2.

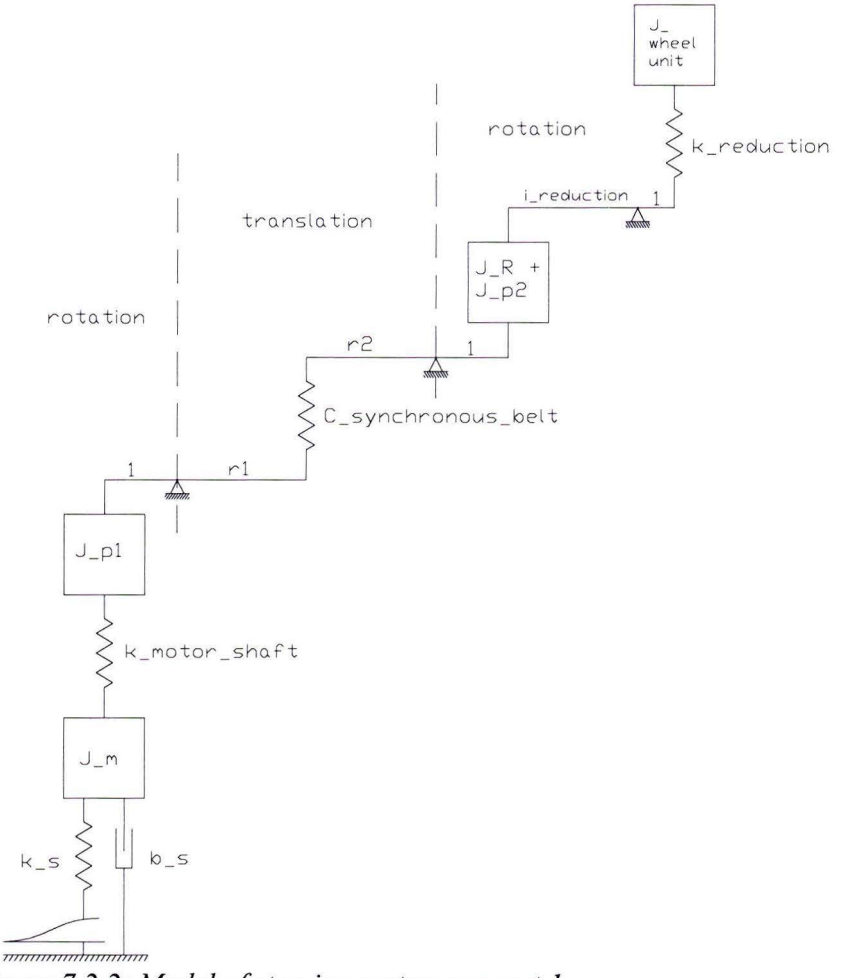

Figure 7.2.2: Model of steering system concept 1

Following all the parts of the model will be briefly explained:

J_{wheel_unit}	This is the inertia of the wheel carrying arm with drive motor and connecting parts.
$k_{reduction}$	The stiffness of the reduction box
$i_{reduction}$	The ratio of the reduction box
$J_R + J_{p2}$	The inertia of the reduction box and the inertia of belt pulley 2
r_2	The radius of pulley 2
$C_{synchronous\_belt}$	Stiffness of the synchronous belt
r_1	The radius of pulley 1

J_{p1}	The inertia of pulley 1
k_{motor_shaft}	The stiffness of the shaft of the electric motor
J_m	The inertia of the rotor of the electric motor
k_s	The servo stiffness provided by the control electronics
b_s	The servo damping provided by the control electronics

This model can be reduced to a model without reductions seen from the output of the system, that is J_{wheel_unit}. The reduced model together with the reduced values is shown in figure 7.2.3.

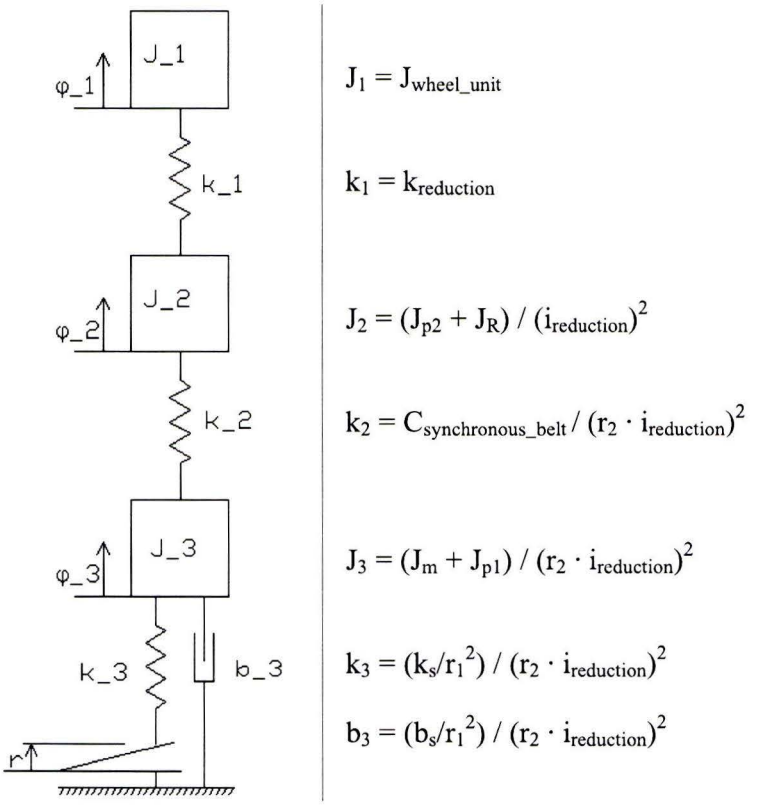

Figure 7.2.3: Reduced model of steering system concept 1

From this reduced model it can be seen that the inertia's of the electric motor and the synchronous belt pulleys have a large effect on the total steering system, because they are divided by the square of the reduction ratios, from which $i_{reduction} = 1/37$. Standard aluminium synchronous belt pulleys have inertias that are too high for the system to work properly. To reduce the total inertia, plastic fibre reinforced pulleys have to be used.

§ 7.2.2 Steering concept 2: Frameless motor connected to the reduction

The second concept consists of a frameless motor that is directly connected to the input shaft of the reduction box. The bearings of the reduction box also function as the bearings for the electric motor. In this way a relative compact steering system can be made, see figure 7.2.4.

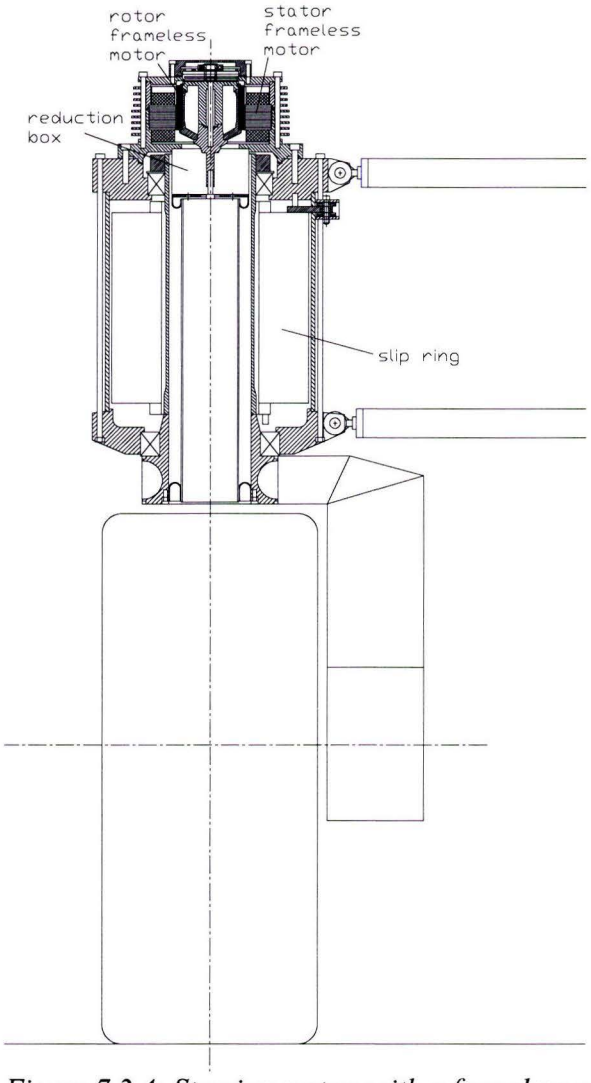

Figure 7.2.4: Steering system with a frameless motor, schematic

Because of the direct connection of the frameless motor to the reduction, there is only the lost motion of the reduction, which is less than 1,5 [arcmin] and there is a stiff connection between the motor and the wheel carrying arm. The housing of the frameless motor

should be constructed to allow sufficient heat transfer from the motor to the surrounding air.

Concept two is chosen, because of the direct and stiff connection between the motor and the wheel carrying arm and because this steering system is most compact.

§ 7.3 Construction and parts of the steering system

The inertia's of the parts at the input side of the reduction have to be divided by the square of the reduction ratio, as could be seen with steering concept one. To reduce this effect, either the inertia's of these parts can be reduced or the reduction ratio can be reduced. Reducing the reduction ratio also lowers the output torque for the same motor, so a compromise has to be made.

For the reduction the "Spinea Twinspin TS80" is chosen. This is a lightweight and compact reduction with a high load capacity, see appendix L [Specifications Moving Base version D] and appendix M [Spinea Twinspin TS80]. The reduction ratio is i = 1/37, so based on the data from the current Moving Base, the electric motor has to be capable of providing a torque, T = 7 [Nm]. The frameless motor that will be used for the steering system is "Bayside Motion K127100_ED1". This motor has a high peak torque and acceptable dimensions, see appendix L [Specifications Moving Base version D]. The drive for this electric motor is "Emoteq Hathaway BDT 33015", see appendix L [Specifications Moving Base version D]. In figure 7.3.1 is a detailed drawing of the steering system.

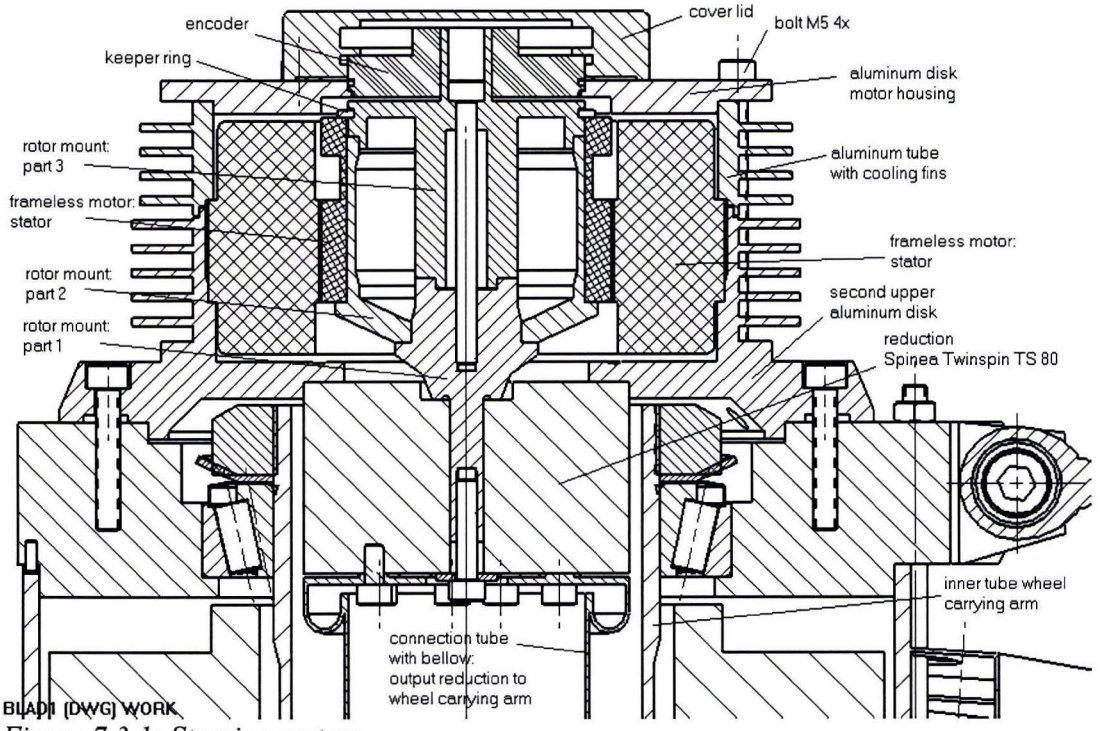

Figure 7.3.1: Steering system

The reduction is mounted to the "second upper aluminium disc" and is partly inside the inner tube of the wheel carrying arm. This reduces the total height of the vehicle. The stator of the frameless motor is also mounted to the "second upper aluminium disc" and is clamped with another aluminium tube and "aluminium disc motor housing" with four M5 bolts. This motor housing has fins for the cooling of the motor.

The steel "rotor mount part 1" is mounted to the input shaft of the reduction with a peg and a M5 bolt from the other side of the reduction. Onto this part the "rotor mount part 2" is placed together with the rotor of the frameless motor, which is mounted with glue. Then "rotor mount part 3" is mounted onto part 1 and part 2 with a long M5 bolt. A keeper ring is used for safety.

The encoder from "Netzer Precision", see appendix L [Specifications Moving Base version D] is connected to "rotor mount part 3" and its housing is clamped to the aluminium disk of the motor housing with a cover lid.

The output flange of the reduction is connected to the wheel carrying arm with a tube with a bellow at each side. In this way only the rotation is transferred and the connection is not over determined. The torsional stiffness of this connection tube is calculated in appendix N [Calculation of the torsional stiffness of the connection tube in the steering system]

§ 7.4 Cooling fins for the frameless motor

Due to the internal resistance of the motor, part of the electric energy will be converted into heat. This heat production has a negative effect on other components because of expanding of materials and the change in viscosity of lubricants. And of course the motor itself can get damaged if it gets to hot. To improve the heat transfer from the motor the housing will be equipped with cooling fins.

The length of the cooling fins is 15 [mm] and is mainly determined by the rest of the construction. Cooling fins are most efficient when the thickness is about one tenth of the length. Because of the application of the vehicle and ease of production, the thickness of the fins will be 2 [mm]. The spacing between the fins should be big enough, because it is not desired that the fins absorb heat from the surrounding fins by radiation or convection. This would reduce the efficiency of the cooling fins.

To find a proper value for the spacing between the fins, the boundary layer of airflow over a cooling fin is examined, see figure 7.4.1.

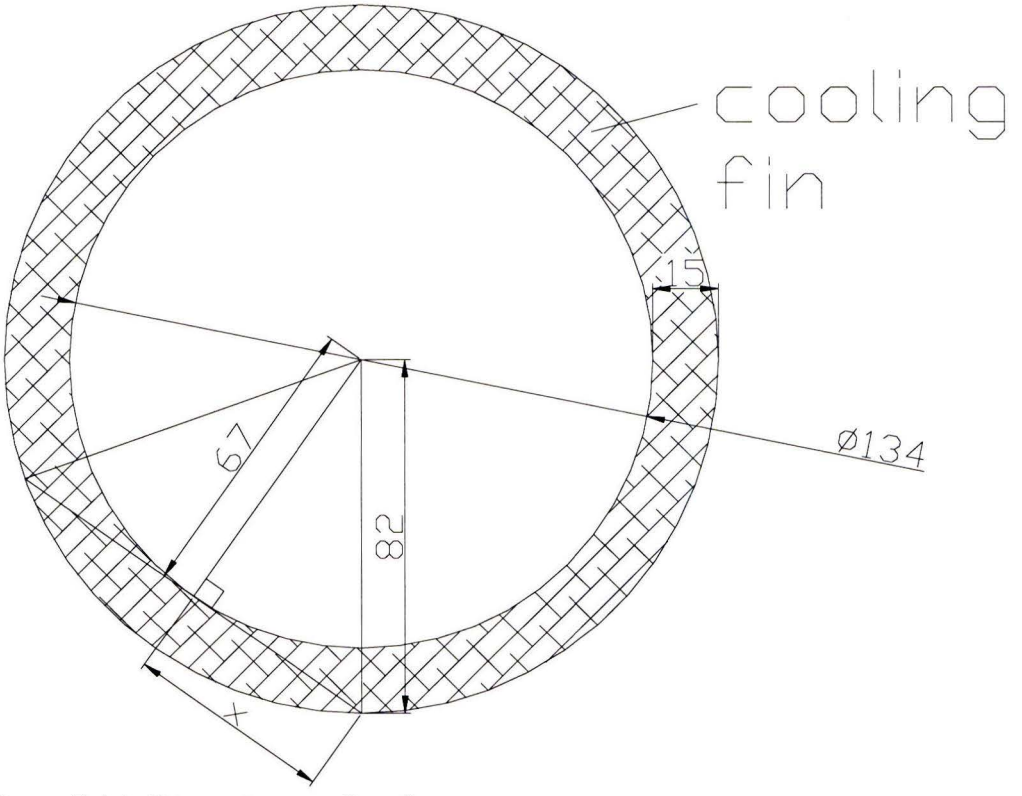

Figure 7.4.1: Dimensions cooling fin

$x = \sqrt{82^2 - 67^2} = 47[mm]$, so the maximum flow length is approximately 94 [mm]

For air at 27 °C applies: $\rho = 1{,}177$ [kg/m^3] and $\nu = 15{,}68 \cdot 10^{-6}$ [m^2/s]

For an average speed of 20 [km/h], that is 5,5 [m/s], the velocity of the airflow is $V_\infty =$ 5,5 [m/s]. The Reynolds number for this situation is:

$$\mathrm{Re}_L = \frac{V_\infty L}{\nu} = 3{,}3 \cdot 10^4 < 5 \cdot 10^5$$

Since $\mathrm{Re}_L < 5 \cdot 10^5$ the flow is laminar. With this information the maximum boundary layer thickness, δ can be calculated.

$$\delta = \frac{5x}{\sqrt{\mathrm{Re}_x}} = \frac{5x}{\sqrt{\left(\frac{V_\infty x}{\nu}\right)}} = 8{,}4 \cdot 10^{-3}\sqrt{x} = 2{,}6 \cdot 10^{-3}[m]$$

The boundary layers of two fins grow to each other, but the length of 94 [mm] is not applicable to the whole fin area. So the spacing between two fins is chosen to be 4 [mm]

The heat production in the motor depends on the load, but for the calculation a constant torque of 7,3 [Nm] is assumed. The current used to produce this torque is 13 [A]. With the internal resistance of the motor, R = 1,19 [Ω], the voltage drop can be calculated:

$$V = R \cdot I = 15{,}47 \text{ [V]}$$

The power that is converted to heat is:

$$P = V \cdot I = 201 \text{ [W]} = 201 \text{ [J/s]}$$

With the thermal resistance of the motor, $R_{th} = 0{,}7$ [°C/W], the motor temperature without cooling is:

$$T_w = P \cdot R_{th} = 140{,}7 \text{ [°C]}$$

For comparison the heat transfer by convection for a housing without cooling fins will be calculated. The cylinder has a diameter, D = 134 [mm] and a length, L = 60 [mm]. The area available for convection is, $A = \pi DL = 2.52 \cdot 10^{-2}$ [m^2]. For the average convection heat transfer coefficient between the cylinder and the surrounding air a value of, $h_c = 5$ [W/m^2K] is assumed. The temperature of the surrounding air is, $T_\infty = 20$ [°C]. The transferred heat by conduction is [Jana]:

$$q_c = h_c \cdot A(T_w - T_\infty) = 15 \text{ [W]}$$

Following the heat transfer by convection for a housing with cooling fins is calculated.

Collection of data:

$L = 15$ [mm]	Length of a fin
$2\delta = 2$ [mm]	Fin thickness
$L_{sp} = 4$ [mm]	Spacing between two fins
$N = 9$	Number of fins
$L_c = L + \delta = 16$ [mm]	Corrected fin length
$R_1 = 67$ [mm]	Radius from centreline to the fin root
$R_2 = 82$ [mm]	Radius from centreline to the fin tip
$R_{2c} = R_2 + \delta = 82 + 1 = 83$ [mm]	Corrected radius
$T_w = 140{,}7$ [°C]	Wall temperature
$T_\infty = 20$ [°C]	Temperature of the surrounding air
$\overline{h_c} = 5$ [W/m^2K]	Average convection heat transfer coefficient
$k_{Al} = 200$ [W/mK]	Thermal conductivity of aluminium
$A_p = 2\delta L_c = 3{,}2 \cdot 10^{-5}$ [m^2]	Fin profile area
$A_s = 2\pi(R_{2c}^2 - R_1^2) = 1{,}5 \cdot 10^{-2}$ [m^2]	Fin surface area

With the use of the following two factors:

$$\frac{R_{2c}}{R_1} = 1{,}24$$

$$L_c^{1/2}\left(\frac{\bar{h}_c}{kA_p}\right)^{1/2} = 0{,}057$$

and the efficiency diagram, figure 2.38 in [Jana], the fin efficiency is determined to be $\eta_e = 0{,}98$. The heat transferred by convection through the cooling fins is:

$$q_f = N\eta_e \bar{h}_c A_s (T_w - T_\infty) = 79{,}4[W]$$

From the area of the cylinder wall between the cooling fins is also heat transferred. This area is:

$$A_{sw} = \pi \cdot 134 \cdot 10^{-3}\left(10 \cdot 4 \cdot 10^{-3}\right) = 1{,}68 \cdot 10^{-2}[m^2]$$

The heat transfer through this area is:

$$q_f = \bar{h}_c A_{sw} (T_w - T_\infty) = 10{,}1[W]$$

The total heat transferred from the motor housing is:

$$q_{tot} = q_f + q_w = 89{,}5[W]$$

From the results of both calculations it can be seen that the heat transfer with cooling fins is six times better compared to a housing without cooling fins.

§ 7.5 Modelling of the steering system

From this steering system also a model is made, see figure 7.5.1.

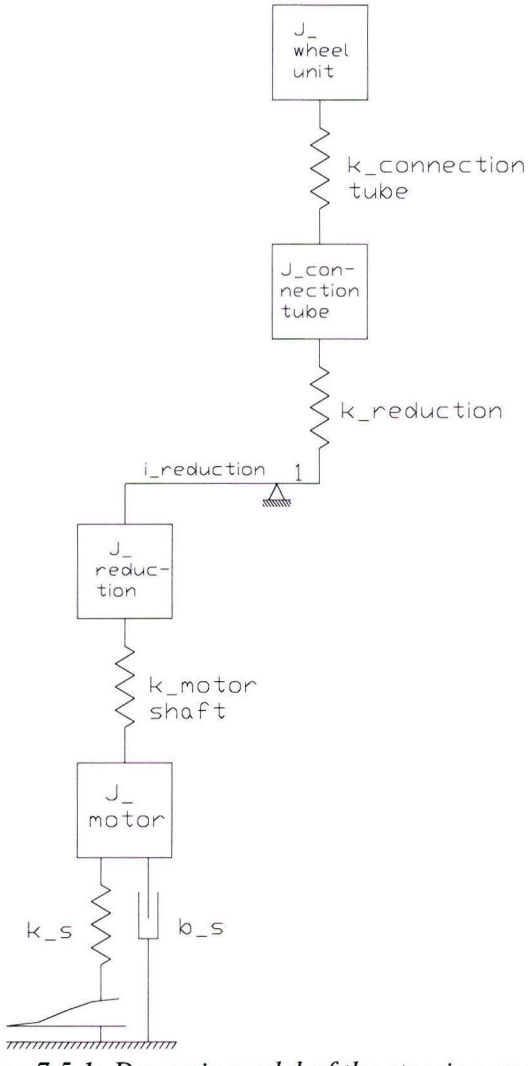

Figure 7.5.1: Dynamic model of the steering system

Following all the parts of the model will be briefly explained:

$J_{wheel\_unit} = 0{,}64$ [kgm^2]	This is the inertia of the wheel carrying arm with drive motor and connecting parts. This value is determined with the CAD model in Unigraphics.
$k_{connection\_tube} = 4{,}1 \cdot 10^4$ [Nm/rad]	The stiffness of the connection tube
$J_{connection\_tube} = 4{,}13 \cdot 10^{-4}$ [kgm^2]	The inertia of the connection tube
$k_{reduction} = 2{,}96 \cdot 10^4$ [Nm/rad]	The stiffness of the reduction box

$i_{reduction} = 1/37$	The ratio of the reduction box
$J_{reduction} = 0{,}027 \cdot 10^{-4}$ [kgm^2]	The inertia of the reduction box
$k_{motor\_shaft} = 4{,}12 \cdot 10^{4}$ [Nm/rad]	The stiffness of the shaft of the electric motor
$J_{motor} = 3{,}45 \cdot 10^{-4}$ [kgm^2]	The inertia of the rotor of the electric motor with the connection parts
k_s	The servo stiffness provided by the control electronics
b_s	The servo damping provided by the control electronics

This model can be reduced to a model without the reduction, seen from the output of the system, that is J_{wheel_unit}. The reduced model together with the reduced values is shown in figure 7.5.2.

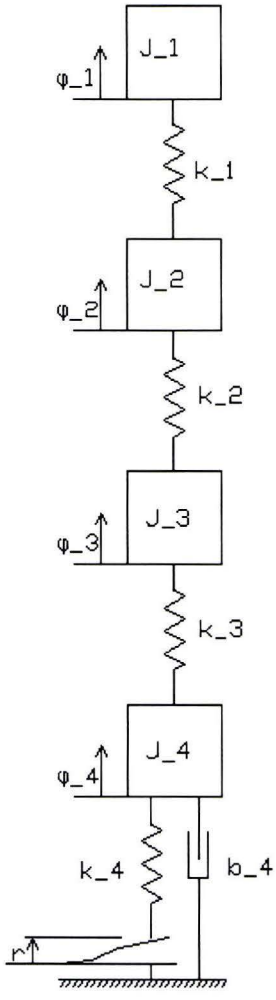

$J_1 = J_{wheel\ unit}$ $= 0{,}64$ [kgm^2]

$k_1 = k_{connection\ tube}$ $= 4{,}1 \cdot 10^{4}$ [Nm/rad]

$J_2 = J_{connection\ tube}$ $= 4{,}13 \cdot 10^{-4}$ [kgm^2]

$k_2 = k_{reduction}$ $= 3 \cdot 10^{4}$ [Nm/rad]

$J_3 = J_{reduction} / (i_{reduction})^2$ $= 3{,}7 \cdot 10^{-3}$ [kgm^2]

$k_3 = k_{motor\ shaft} / (i_{reduction})^2$ $= 5{,}6 \cdot 10^{7}$ [Nm/rad]

$J_4 = J_{motor} / (i_{reduction})^2$ $= 0{,}47$ [kgm^2]

$k_4 = k_s / (i_{reduction})^2$

$b_4 = b_s / (i_{reduction})^2$

Figure 7.5.2: Reduced model of the steering system

The inertia of the connection tube is low compared to the inertia of the wheel carrying arm, see appendix N [Calculation of the torsional stiffness of the connection tube in the steering system]. The motor shaft has a high torsional stiffness compared to the stiffness of the reduction. The reduction also has a relative small inertia. Therefore these three factors will be neglected, so the model can be reduced to the model in figure 7.5.3.

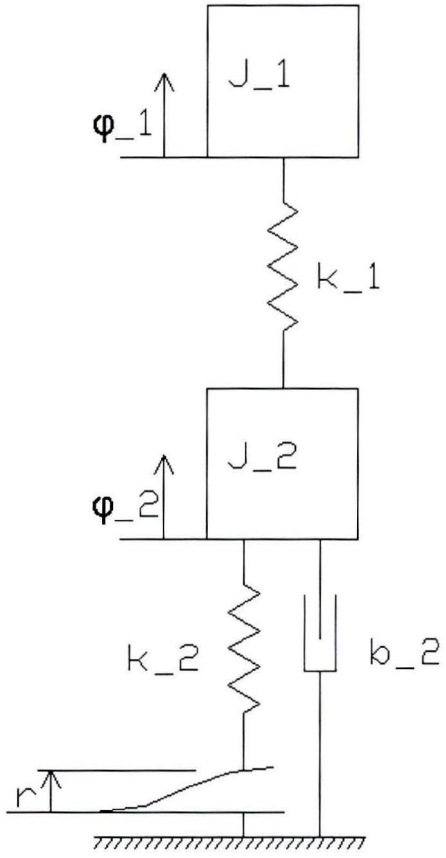

$J_1 = J_{\text{wheel unit}} = 0{,}64\ [\text{kgm}^2]$

$$\frac{1}{k_1} = \frac{1}{k_{reduction}} + \frac{1}{k_{connectiontu\_tube}} \Rightarrow$$

$k_1 = 1{,}7 \cdot 10^4\ [\text{Nm/rad}]$

$J_2 = J_{\text{motor}} / (i_{\text{reduction}})^2 = 0{,}47\ [\text{kgm}^2]$

$k_2 = k_s / (i_{\text{reduction}})^2$

$b_2 = b_s / (i_{\text{reduction}})^2$

Figure 7.5.3: Further reduced model

The equations of motion for the reduced model of figure 7.5.3 are:

$$J_1\ddot{\varphi}_1 = -k_1(\varphi_1 - \varphi_2)$$
$$J_2\ddot{\varphi}_2 = k_1(\varphi_1 - \varphi_2) - k_2(\varphi_2 - r) - b_2\dot{\varphi}_2$$

$$\ddot{\varphi}_1 = \frac{-k_1}{J_1}\varphi_1 + \frac{k_1}{J_1}\varphi_2$$
$$\ddot{\varphi}_2 = \frac{k_1}{J_2}\varphi_1 - \frac{(k_1 + k_2)}{J_2}\varphi_2 - \frac{b_2}{J_2}\dot{\varphi}_2 + \frac{k_2}{J_2}r$$

In matrix form:

With:
$$x_1 = \varphi_1$$
$$x_2 = \dot{\varphi}_1$$
$$y_1 = \varphi_2$$
$$y_2 = \dot{\varphi}_2$$

$$\begin{bmatrix} \dot{x}_1 \\ \dot{x}_2 \\ \dot{y}_1 \\ \dot{y}_2 \end{bmatrix} = \begin{bmatrix} 0 & 1 & 0 & 0 \\ \frac{-k_1}{J_1} & 0 & \frac{k_1}{J_1} & 0 \\ 0 & 0 & 0 & 1 \\ \frac{k_1}{J_2} & 0 & \frac{-(k_1+k_2)}{J_2} & \frac{-b_2}{J_2} \end{bmatrix} \cdot \begin{bmatrix} x_1 \\ x_2 \\ y_1 \\ y_2 \end{bmatrix} + \begin{bmatrix} 0 \\ 0 \\ 0 \\ \frac{k_2}{J_2} \end{bmatrix} \cdot [r]$$

The response of this system to a parabolic set-up can be determined with the program Matlab, see appendix O [Model steering system]. The servo stiffness is based on equal eigenfrequencies of the two inertia's:

$$\omega_1 = \omega_2 \Rightarrow \sqrt{\frac{k_1}{J_1}} = \sqrt{\frac{k_2}{J_2}} \Rightarrow$$
$$k_2 = J_2 \frac{k_1}{J_1}$$

The servo damping is determined by the formula:

$$b_2 = 2\varsigma\sqrt{k_2}(J_1 + J_2)$$

Where the relative damping, $\varsigma = 0.7$ is the most optimal value for a parabolic set-up [4007]. The response of the steering system for a steering action of 90° in 0,2 [s] is plotted in figure 7.5.4. It can be seen that the response is accurately following the input signal. The calculated positional error for this steering action is 0,25 degrees.

From the steering model it can be seen that the total inertia with respect to the steering axis is: $J_{z,total} = 1{,}18$ [kgm^2]. With formula (7.2) the steering torque needed for the evasive manoeuvre becomes: $T_{steer} = 185$ [Nm]

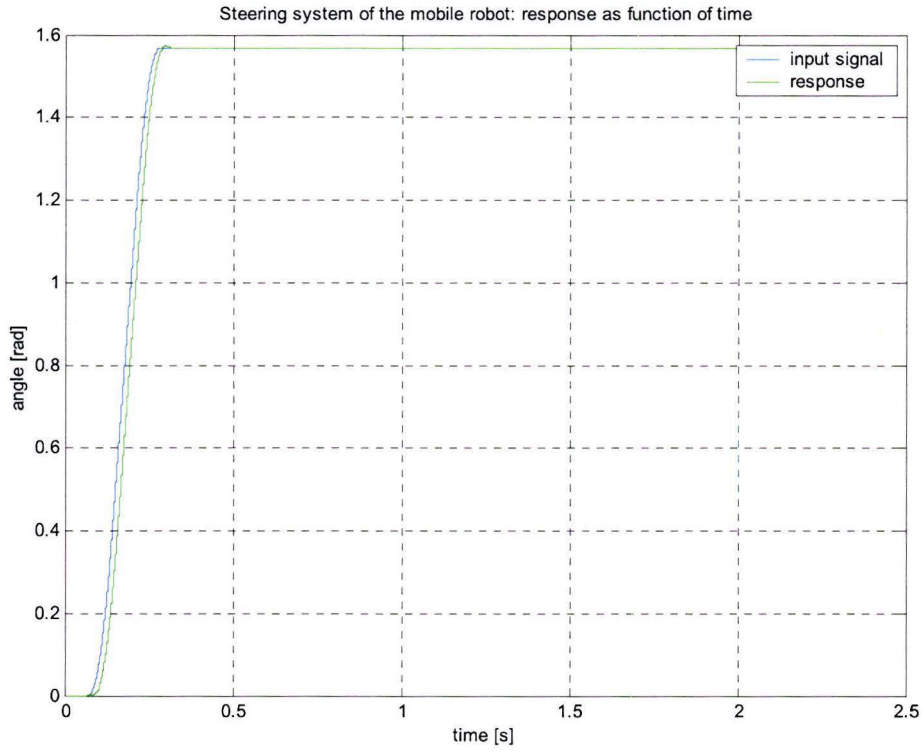

Figure 7.5.4, Response of the steering system to a parabolic set-up

The static steering torque due to the tire road contact will be calculated with formula (7.3). The normal force on a wheel unit in normal conditions is assumed to be $F_v = 1500$ [N]. The tire pressure and coefficient of friction are respectively: $p_i = 1 \cdot 10^5$ [Pa] and $\mu = 1{,}1$. The static steering torque is:

$$T_{RSt} = \frac{\mu F_v^{1,5}}{3 p_i^{0,5}} = 67{,}4[Nm]$$

Since the electric motor produces a nominal torque of 7 [Nm], the output torque can be:

$$T_{out} = \frac{T_{in}}{i}\eta = \frac{7}{1/37}0{,}9 = 233[N]$$

where η is the efficiency of the reduction. This output torque is sufficient for the calculated steering situations. If the mobile robot is loaded with a mass, more torque may be necessary, which can be temporarily delivered, because the motor can produce a peak torque of 21 [Nm].

Chapter 8 Construction

§ 8.1 Wheel carrying arm

The function of the wheel carrying arm is, as explained in its name, to support the wheel and connect it with the bearings located at the ends of the suspension rods. It has to provide a stiff connection, fit in a limited space and add little mass to the total vehicle.

§ 8.1.1 Design of the wheel carrying arm

The wheel carrying arm can be like a fork, as is common use for two wheeled vehicles, or it can be one sided like stub axles on passenger cars. Since the drive motor is located completely inside the wheel, with a fork shaped wheel carrying arm, the motor would have to be detached in order to change the wheel, or the wheel carrying arm would have to be taken apart. Because of this, a one sided wheel carrying arm will be used.

The space for the wheel carrying arm beside the wheel is limited to the turning radius of the wheel, see figure 8.1.1. This limit is set, because the wheel carrying arm should not determine the required space for the steering of the wheel unit.

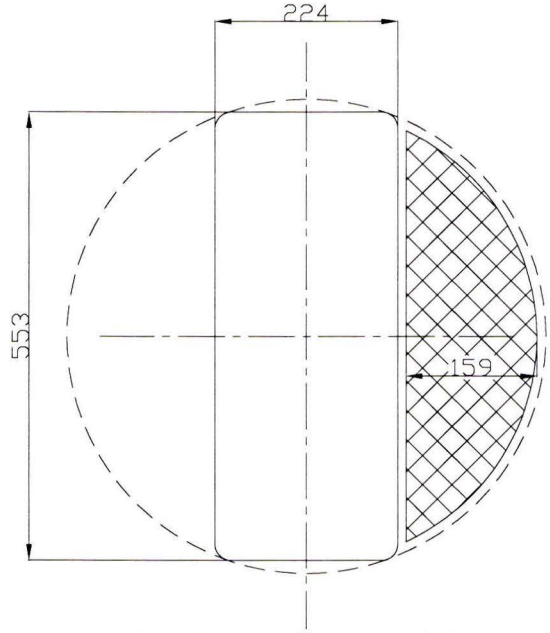

Figure 8.1.1: Top view of a tire with the turning radius dashed and the available space beside the wheel crosshatched

Above the wheel, less space is available, because the height of the wheel carrying arm above the wheel directly contributes to the total vehicle height.

The available space and the material should be used in an optimal way. The wheel carrying arm will be loaded with forces that cause bending moments. If a beam with rectangular cross section, loaded with a bending moment, M, is considered, the stress, σ, in the beam is not equally distributed over the height, see figure 8.1.2.

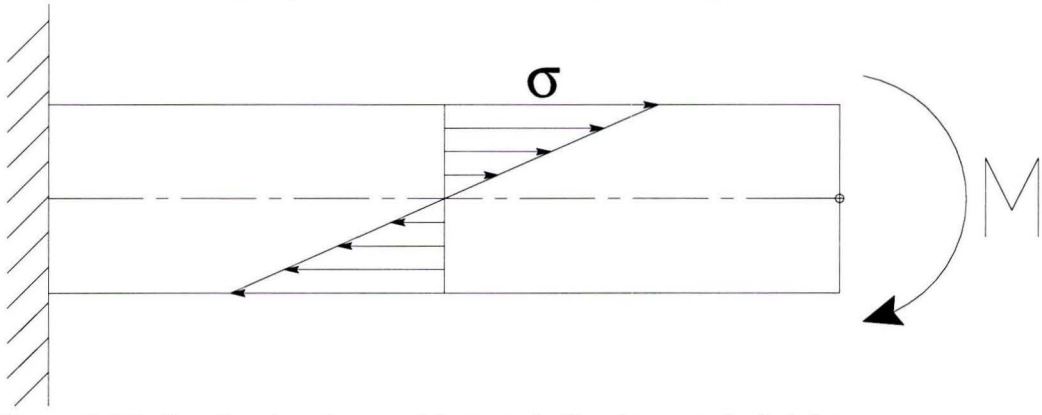

Figure 8.1.2: Bending in a beam with stress indication over its height.

The material around the centre line of the beam has a low contribution in resisting the bending moment. So for an optimal use of the material, all material should be located at the outer fibre of the beam, like in a tube with rectangular cross section. The wheel carrying arm will be hollow with most material located at the outer surface of the construction. It will be built up out of steel because steel has advantages over aluminium for this type of construction, see appendix P [Steel versus aluminium in construction].

Beside the wheel, a part of the wheel carrying arm has a rectangular cross section that fits well in the available space, see figure 8.1.3.

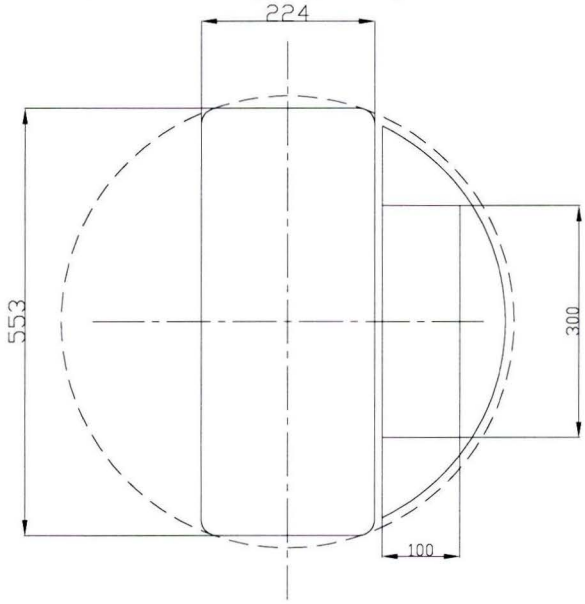

Figure 8.1.3: Top view of a tire with the rectangular cross section of part of the wheel carrying arm

The wheel carrying arm should have a small height in the part above the wheel, because the height of this part contributes to the total vehicle height. In contradiction with this demand is the fact that the bending stiffness in a tube increases with h^3 where h is the height of the tube. To make a choice for the height and the material thickness of the hollow construction, tubes with rectangular cross section and various heights and wall thicknesses are compared. The width of the tube is 300 [mm], the length is 150 [mm] and a moment of 1300 [Nm] is applied. The deflection of the tube results in a deflection of the wheel in the tire road contact, see figure 8.1.4.

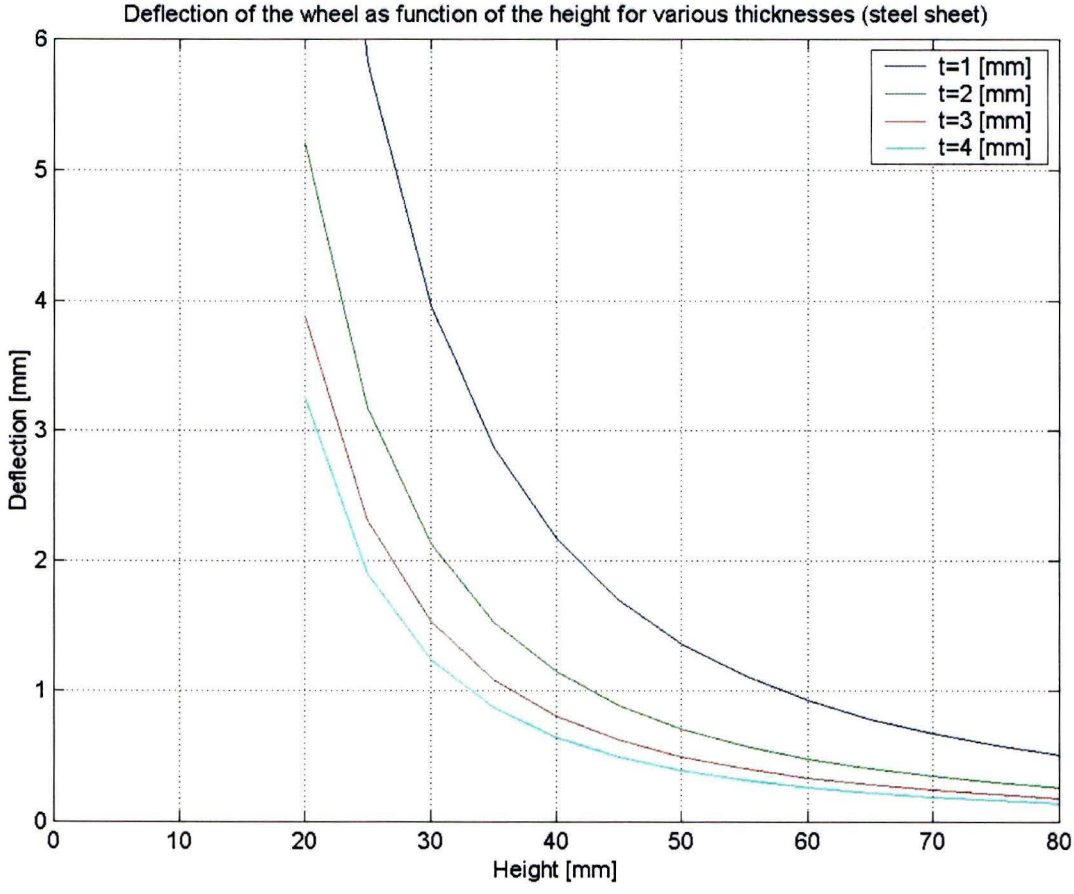

Figure 8.1.4: Deflection of the wheel in the tire road contact due to bending of a tube as function of the height for various wall thicknesses.

With this information the height is set to h = 50 [mm] with a wall thickness t = 3 [mm]. In figure 8.1.4 it can be seen the deflection of the wheel for the applied moment is 0,5 [mm], what is an acceptable value.

The wheel carrying arm will have a bend, because it has to create a connection from beside the wheel to the centre line above the wheel. The bending moment will increase towards this bend, so the wheel carrying arm will have a tapered form, with the widest part at the bend.

Beside the wheel and at its centre line is a steel tube that is machined on a lathe. It has grooves on either side for the fitting of steel sheets, see figure 8.1.4. The first steel sheet with thickness, t = 2 [mm] is formed as can be seen in figure 8.1.4 and is welded to the steel tube.

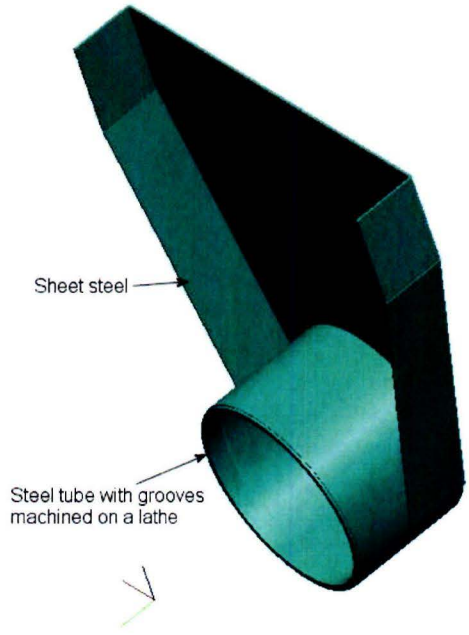

Figure 8.1.4: Wheel carrying arm: steel tube with first piece sheet steel

A piece of sheet steel that is almost equal to the first piece is welded to the other end of the tube and to the other sheet steel part, see figure 8.1.5.

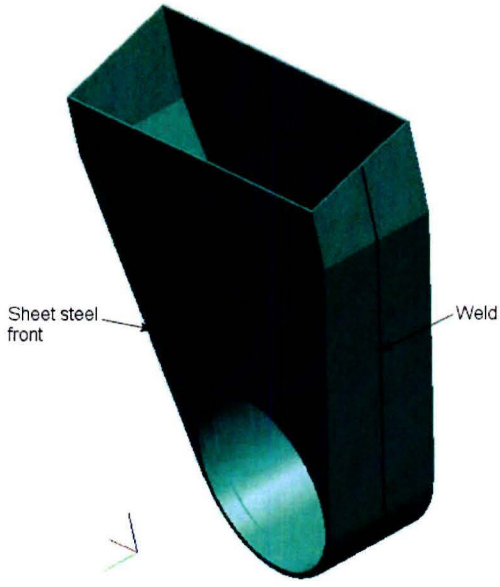

Figure 8.1.5: Wheel carrying arm: steel tube with two pieces sheet steel

To the top of the second steel sheet an angle iron, with dimensions 25 x 25 x 4 [mm], is welded. The sides of this angle iron are machined to create a fluent transition from the iron angle to the steel sheet. The angle iron has a larger thickness compared to the sheet steel and allows the welding of two partition sheets to it without considerably weakening the inner angle of the wheel carrying arm, see figure 8.1.6. Besides, the weld of the sheet steel to the angle iron is in an area where the stress is relatively low. The partition sheets are made out of one steel sheet, with thickness t = 2 [mm], that is formed. The ends of the partition sheets on the long side are square toothed. These square teeth fit in pockets in the steel sheet that will be put on top of the wheel carrying arm and are welded once they are in place, see figure 8.1.7.

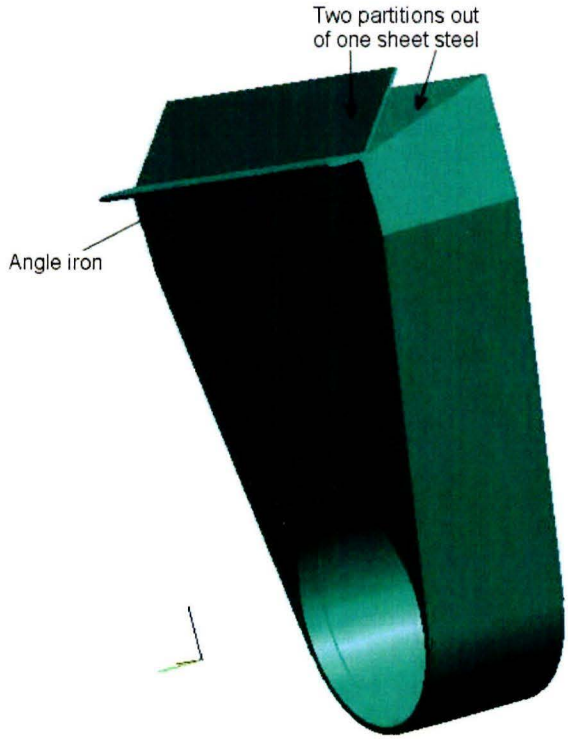

Figure 8.1.6: Wheel carrying arm: steel tube with two pieces sheet steel, angle iron and two partitions

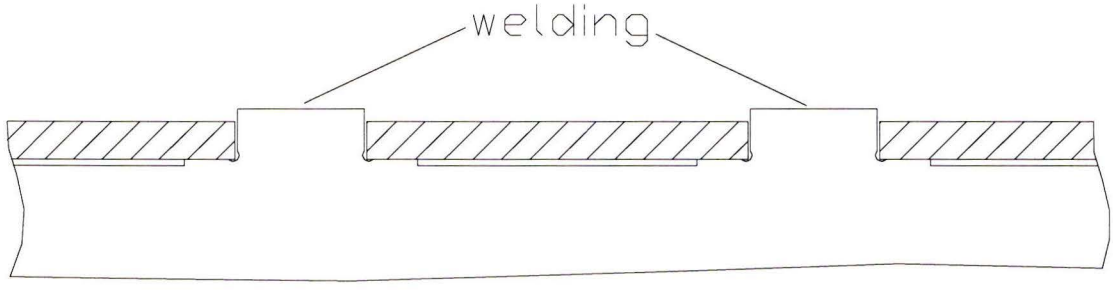

Figure 8.1.7: Square toothed plate end with sectioned top sheet

A formed piece of sheet steel, with thickness t = 3 [mm], that is located above the tire, is welded to the angle iron, see figure 8.1.8. In this piece of sheet steel a hole is made for the connection with a machined cylinder that is welded to it. For extra support of the machined cylinder a partition sheet is welded to the steel sheet.

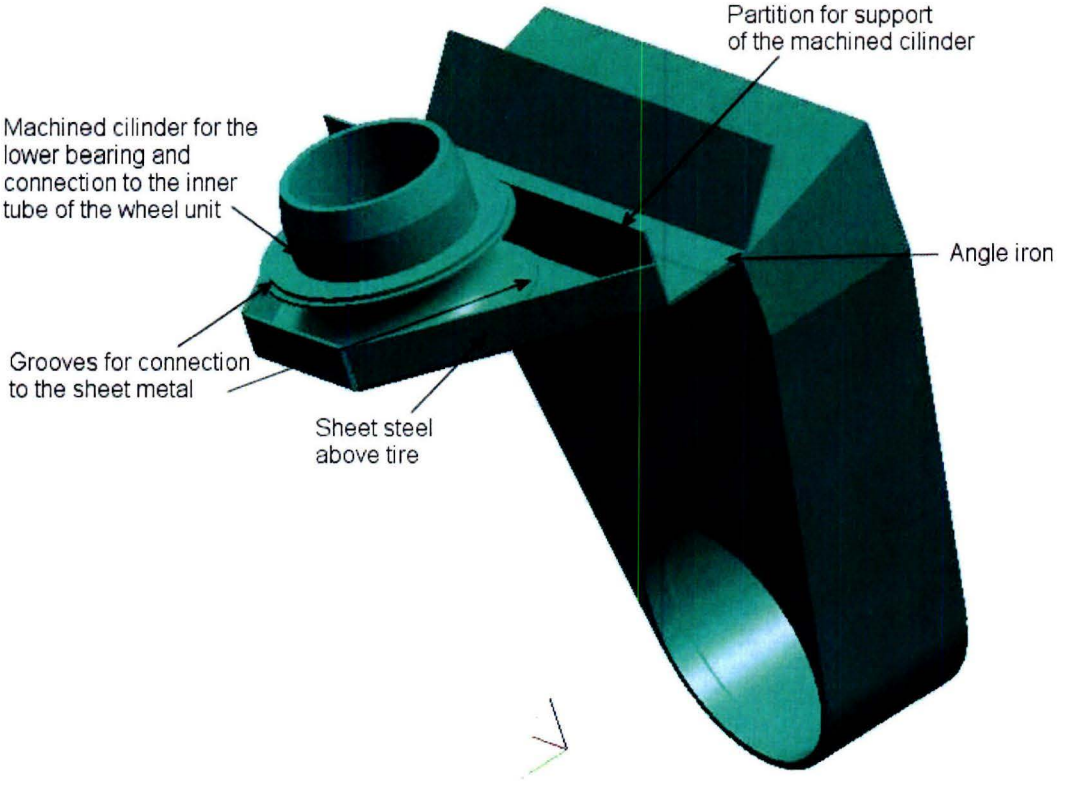

Figure 8.1.8: Wheel carrying arm: steel tube with two pieces sheet steel, angle iron, two partitions, lower sheet steel above the tire, machined cylinder and a partition for support of the cylinder.

The top steel sheet, with thickness t = 3 [mm], is also formed and has slots for the fitting of the three partition sheets, see figure 8.1.9. This sheet also has a hole for the connection with the machined cylinder. The square teeth of the partition sheets are welded from the outside to the top steel sheet as well as the machined cylinder.

To the top of the machined cylinder the inner tube is welded, see figure 8.1.10. The inner tube has a thickness t = 5 [mm] at the location of the weld, to reduce the stress in and around the welds. The machined cylinder is conical at the top, with an angle of 14 degrees with the vertical, for a fluent transition to the tube. The overall inner diameter of this tube is d = 86 [mm] and the wall thickness t = 3 [mm]. The top of the tube has a thickness t = 4,5 [mm] for the fitting of the tapered roller bearing with inner diameter d = 95 [mm]. To the top of the cylinder also thread is cut, for a nut that is used for securing and adjusting of the bearing assembly. After critical welds are inspected and the seatings for the bearings are re-machined the wheel carrying arm is finished. A cross section of the wheel carrying arm can be seen in figure 8.1.11.

Figure 8.1.9: Wheel carrying arm: steel tube with two pieces sheet steel, angle iron, two partitions, lower sheet steel above the tire, machined cylinder, a partition for support of the cylinder and the top steel sheet.

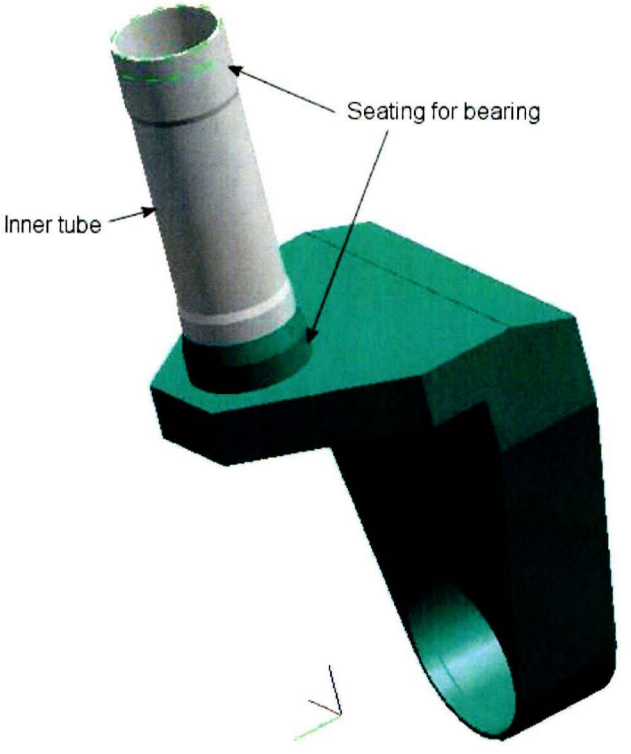

Figure 8.1.10: Wheel carrying arm complete with the inner tube welded to the machined cylinder.

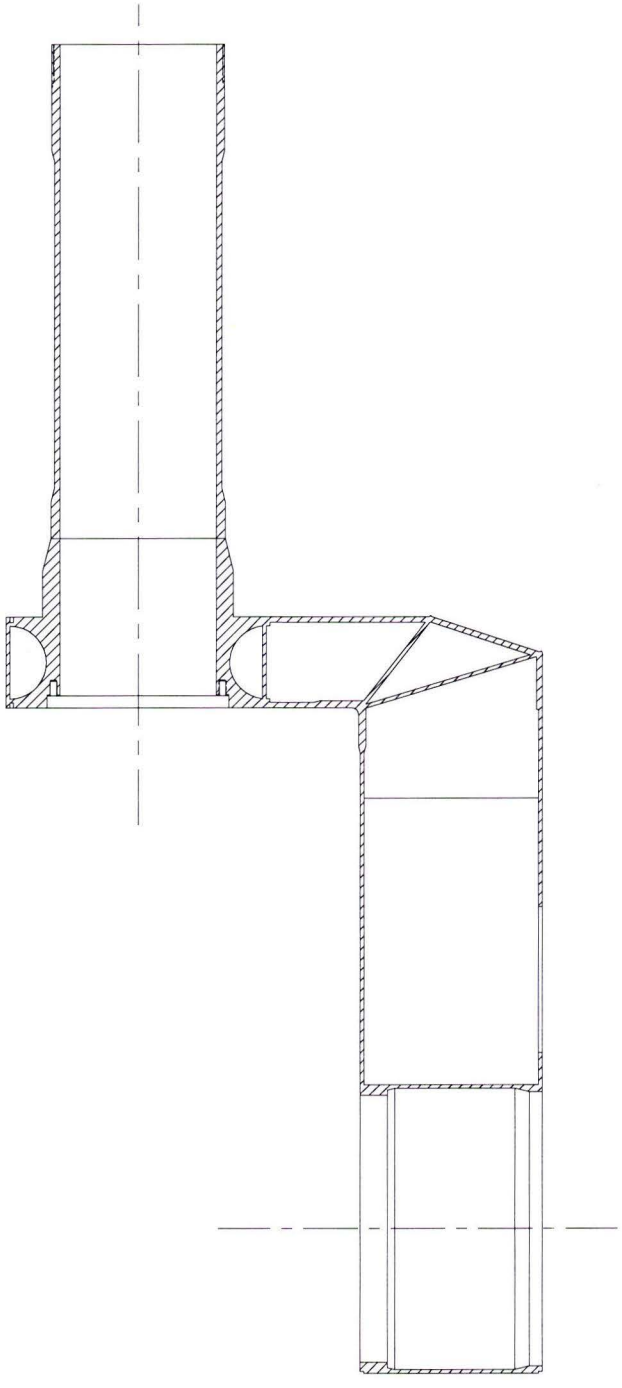

Figure 8.1.11: Cross section view of the wheel carrying arm

The wheel carrying arm is analyzed for some load situations to find out the stress distribution in the construction and the stiffness of the various parts, see appendix Q [Forces acting on the wheel carrying arm]. At the end of this appendix the total stiffness of the suspension for lateral loads is approximated.

§ 8.1.2 Connection of the wheel motor and the wheel

For the connection of the drive motor and the wheel to the wheel carrying arm an adapter is used. The tube of the wheel carrying arm beside the wheel has a flange at the side of the wheel, see figure 8.1.11. This flange is used to clamp the aluminium adapter to the wheel carrying arm, see figure 8.1.12

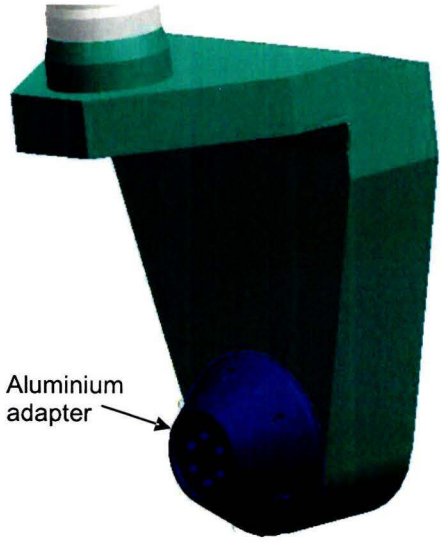

Figure 8.1.12: Wheel carrying arm with adapter

The wheel motor is directly mounted to this adapter with 6 M12x25 screws, see figure 8.1.13.

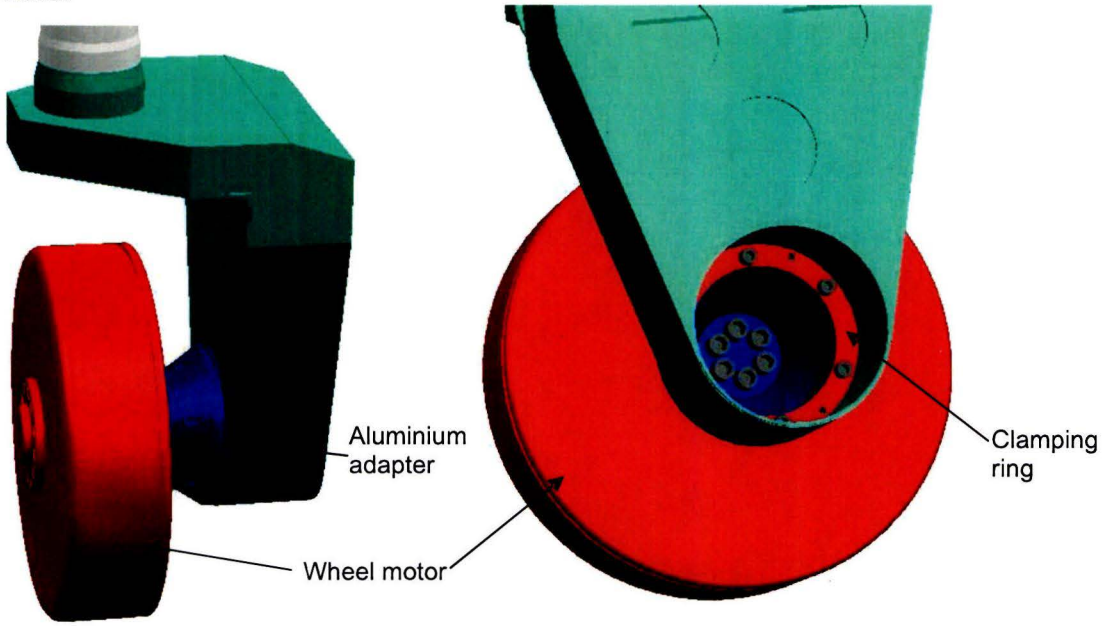

Figure 8.1.13: Wheel motor mounted to the adapter and the ring for clamping of the adapter (right view)

The ring for the clamping of the adapter can be seen in the right view of figure 8.1.13. The adapter is clamped with 6 M8x40 screws. The back of the wheel carrying arm is covered with an aluminium disc, see figure 8.1.14. This disc closes the tube and helps to keep the tube in its form. The disc is fixed with 3 M6x95 screws to the clamping ring.

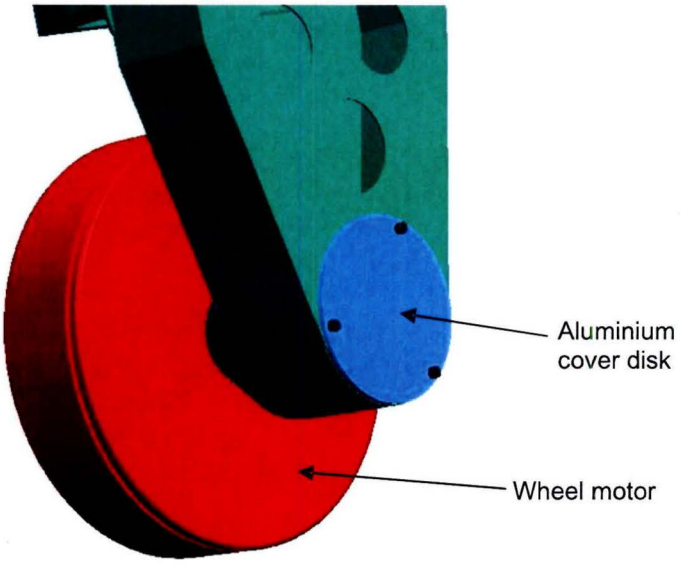

Figure 8.1.14: Wheel carrying arm with adapter, clamping ring, wheel motor and cover disc

The wheel motor is a complete unit for the drive of the vehicle and it also contains the wheel bearings. Because of this, the wheel with the tire can be directly mounted to the wheel motor, see figure 8.1.15.

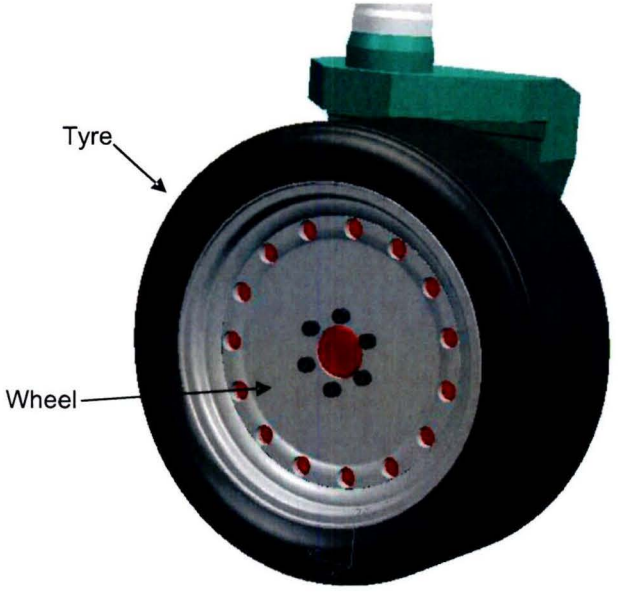

Figure 8.1.15: Wheel carrying arm with adapter, clamping ring, wheel motor, cover disc and wheel with tire

The wheel motor centre of gravity is placed close (distance r) to the steering axis of the wheel unit to minimize the inertia around this axis. Because the wheel motor is the part with the largest mass in the wheel unit and the inertia increases with r^2, the position of the wheel motor is important for minimizing the inertia around the steering axis.

§ 8.2 Construction of the wheel unit

The rest of the construction of the wheel unit is described in this paragraph, starting from the wheel carrying arm with the wheel assembled like in figure 8.1.15. Together with the figures in this paragraph it may be useful to look at the cross section drawing of the wheel unit in appendix R [Wheel unit].

A tapered roller bearing together with a Nilos sealing ring is placed on the machined cylinder of the wheel carrying arm, see figure 8.2.1. A tapered roller bearing assembly is used because it is adjustable and can handle the forces in axial and radial direction. This tapered roller bearing has the lowest mass, m = 1,15 [kg] for the bearing range with inner diameter d = 105 [mm]. More information about the Nilos sealing ring can be found in appendix S [Nilos rings for tapered roller bearings].

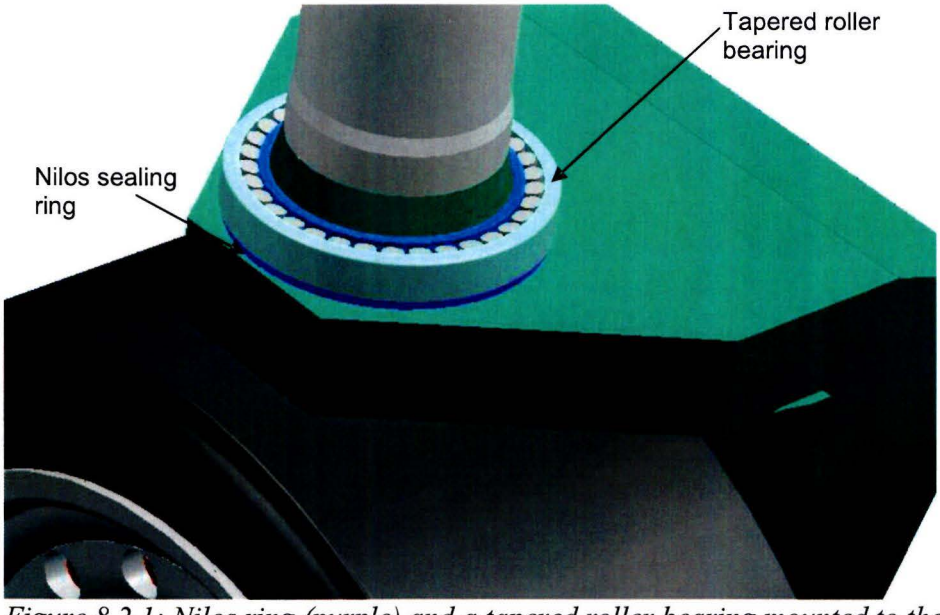

Figure 8.2.1: Nilos ring (purple) and a tapered roller bearing mounted to the wheel carrying arm

On top of the tapered roller bearing the "milled lower aluminium disc" is mounted. This disc has an edge for the fitting of the outer tube of the wheel unit and a little pin (red) that is used for the angle orientation of the tube to the disc, see figure 8.2.2. This disc also has connection points for two suspension rods.

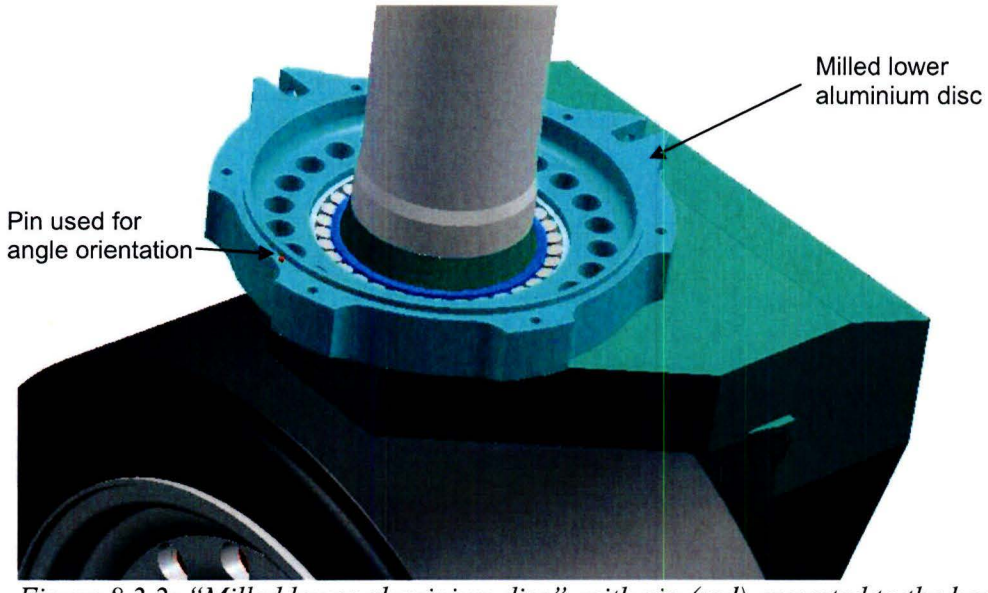

Figure 8.2.2: "Milled lower aluminium disc", with pin (red), mounted to the bearing

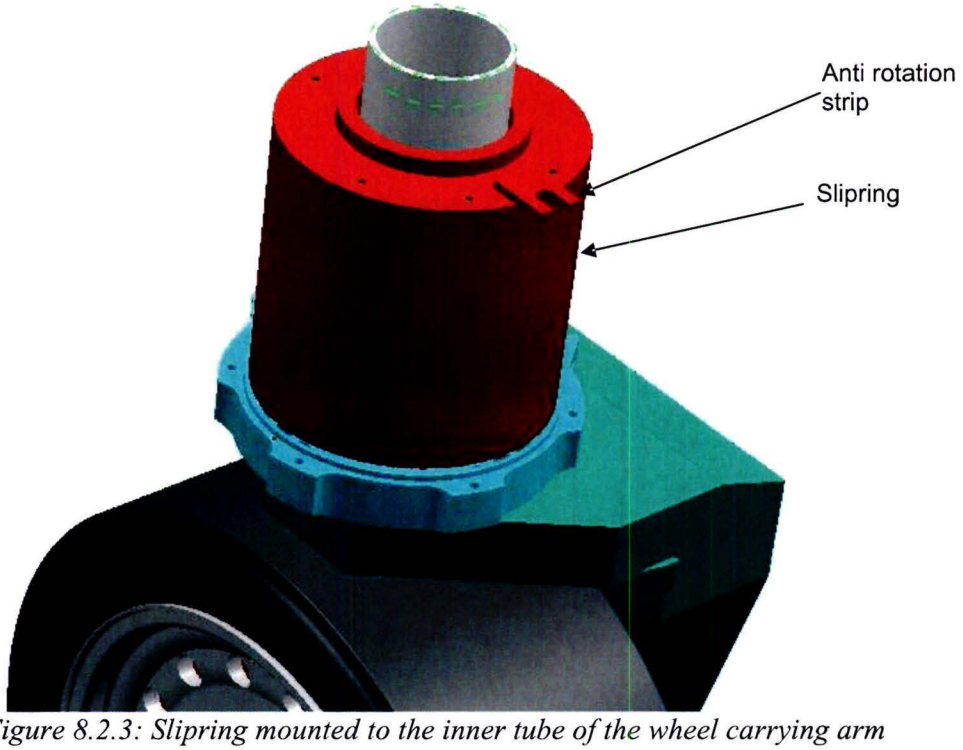

Figure 8.2.3: Slipring mounted to the inner tube of the wheel carrying arm

The slipring, which is used for the transfer of energy and data from the non-rotating part of the wheel unit to the rotating part of the wheel unit, is attached to the inner tube of the wheel carrying arm. The outer part of the slipring has to be fixed in rotation about the vertical axis to the non-rotating part of the wheel unit. This is done with the metal strip

that is attached to the top of the slipring, see figure 8.2.3. The rotation fixation will be further discussed hereunder.

The "aluminium outer tube" is placed over the slipring and fits to the "milled lower aluminium disc", see figure 8.2.4. Its angle orientation is determined by a pin that fits in a groove in the outer tube. The conical tube that is used in the anti rotation system of the suspension, as described in chapter 6, is directly welded to the "aluminium outer tube"

For the rotation fixation of the slipring, the "aluminium outer tube" has a hole with a tube with rectangular cross section welded to it, see figure 8.2.4 and 8.2.5. The metal strip from the slipring fits in this rectangular tube with play on each side. The strip is held in place by a plastic cylinder with a metal tube inside it, which is clamped to the rectangular tube. The rectangular tube is covered by a plastic cover that allows inspection of the rotation fixation system. In case the slipring fails and locks up or due to another cause, the rotation fixation can break. To detect failure, micro switches can be used. These micro switches can trigger a safety system to shut down the power in case the slipring fails.

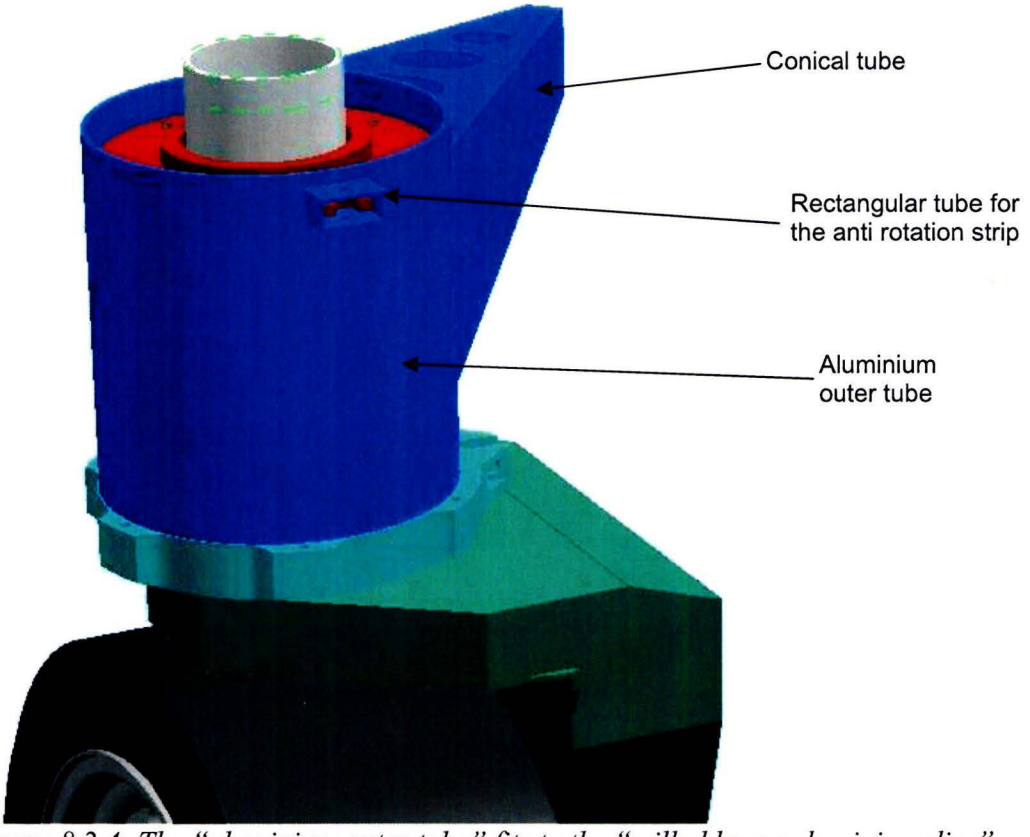

Figure 8.2.4: The "aluminium outer tube" fits to the "milled lower aluminium disc"

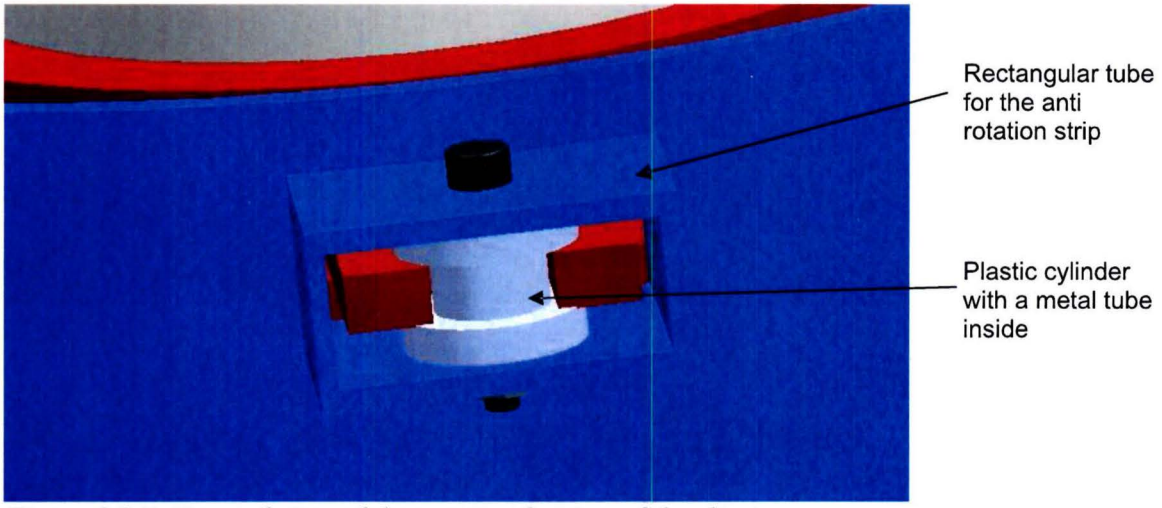

Figure 8.2.5: Zoomed view of the rotation fixation of the slipring

On top of the "aluminium outer tube" the "milled upper aluminium disc_01" is mounted, see figure 8.2.6. This disc also has an edge for the fitting to the tube and a little pin is used for the angle orientation like with the "milled lower aluminium disc". Two suspension rods can be mounted to this disc as well as the pull rod that connects the wheel unit to the shock absorber. Both discs and the tube are secured with 6 rods with nuts. The second tapered roller bearing is mounted to the "milled upper aluminium disc_01" and the "inner tube" of the wheel carrying arm.

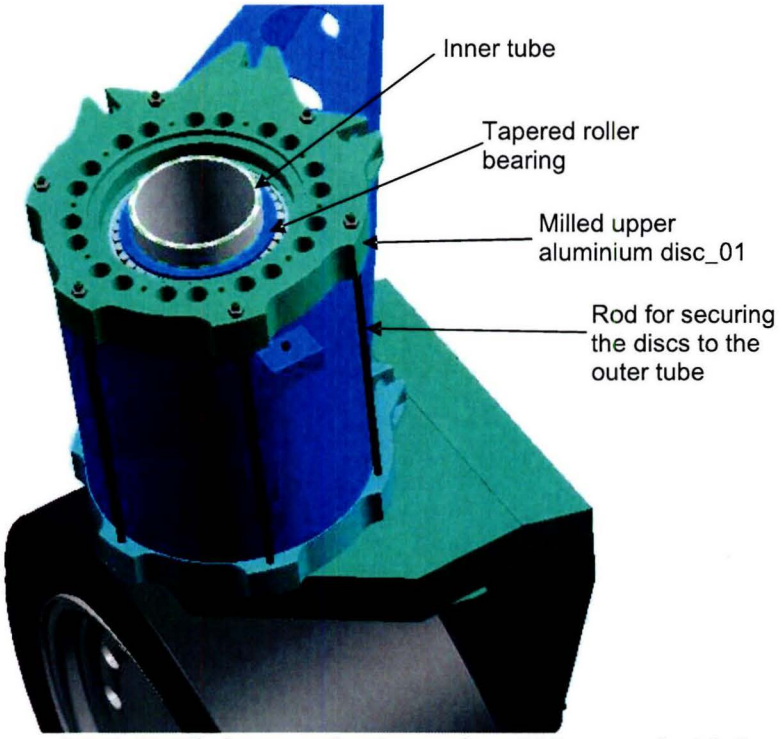

Figure 8.2.6: "Milled upper aluminium disc_01" secured with 6 rods with nuts

This tapered roller bearing will also be sealed with a Nilos ring. The bearing assembly is fixed and can be adjusted with a nut together with a keeper ring, see figure 8.2.7.

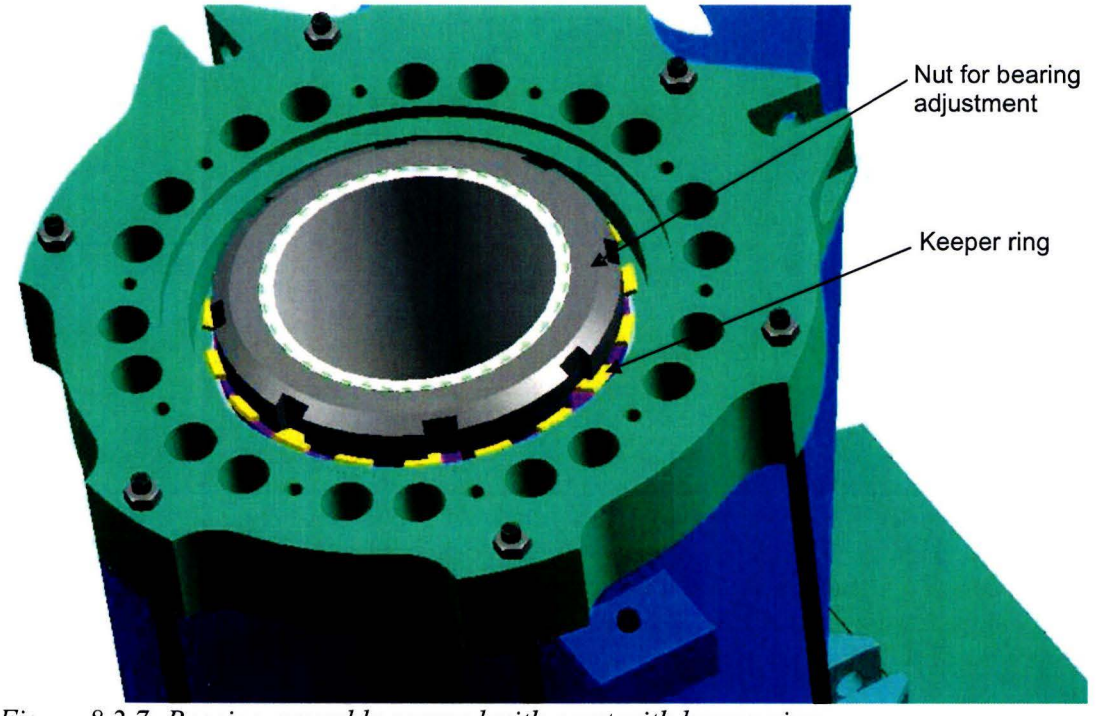

Figure 8.2.7: Bearing assembly secured with a nut with keeper ring

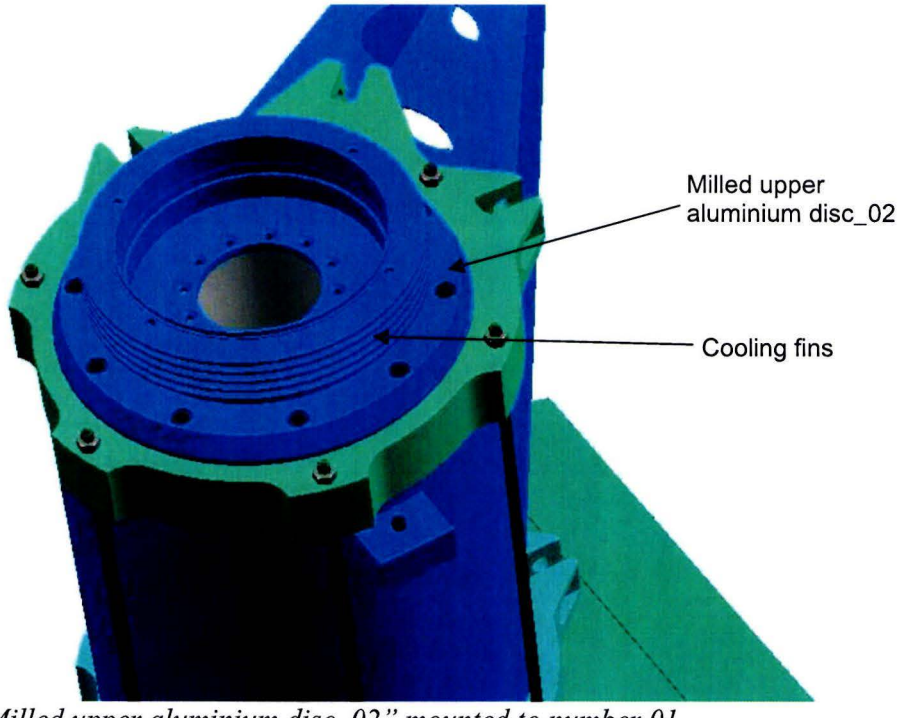

Figure 8.2.8: "Milled upper aluminium disc_02" mounted to number 01

The "milled upper aluminium disc_02" is mounted to the "milled upper aluminium disc_01" with 10 M6x35 screws, see figure 8.2.8. This number of screws is necessary, because the steering torque is transferred through the connection of these parts. The "milled upper aluminium disc_02" provides the mounting point for the reduction of the steering system and is part of the housing of the steering motor. Therefore the upper part of this disc has fins for the cooling of the electric steering motor.

For the next part of the construction of the wheel unit, a subassembly of part of the steering system is made. The "rotor mount_01" is connected to the input of the reduction, Spinea Twinspin TS80, and secured with an M5x25 screw, see figure 8.2.9

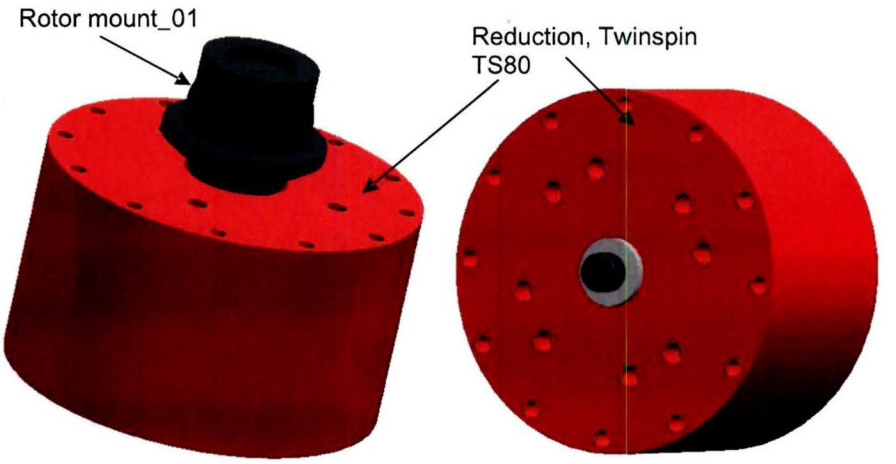

Figure 8.2.9: "Rotor mount_01" connected to the input of the reduction

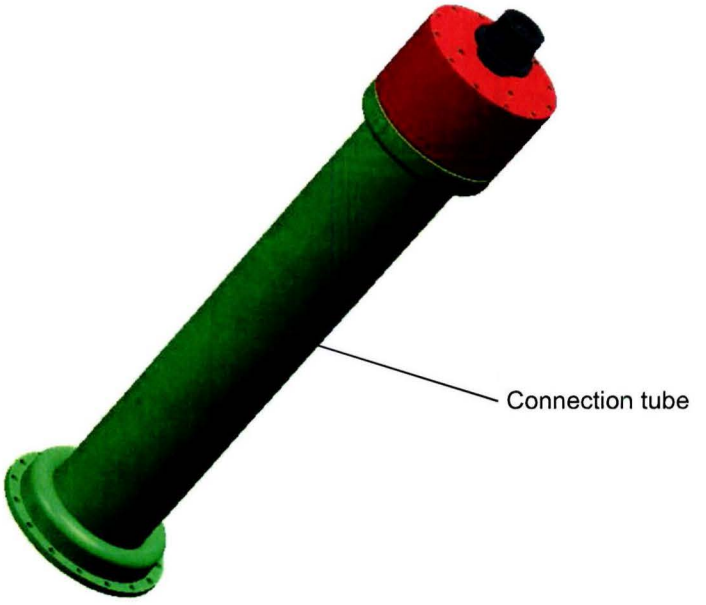

Figure 8.2.10: "Connection tube" mounted to the output side of the reduction

The "connection tube", that is used to connect the reduction with the wheel carrying arm, is attached to the output flange of the reduction from the inside of the tube with 8 M5x10 screws. This subassembly is mounted from the bottom of the wheel carrying arm with the wheel motor taken off. The reduction is mounted to the "milled upper aluminium disc_02" and the connection tube is attached to the "machined cylinder" of the wheel carrying arm, see figure 8.2.11 and 8.2.12.

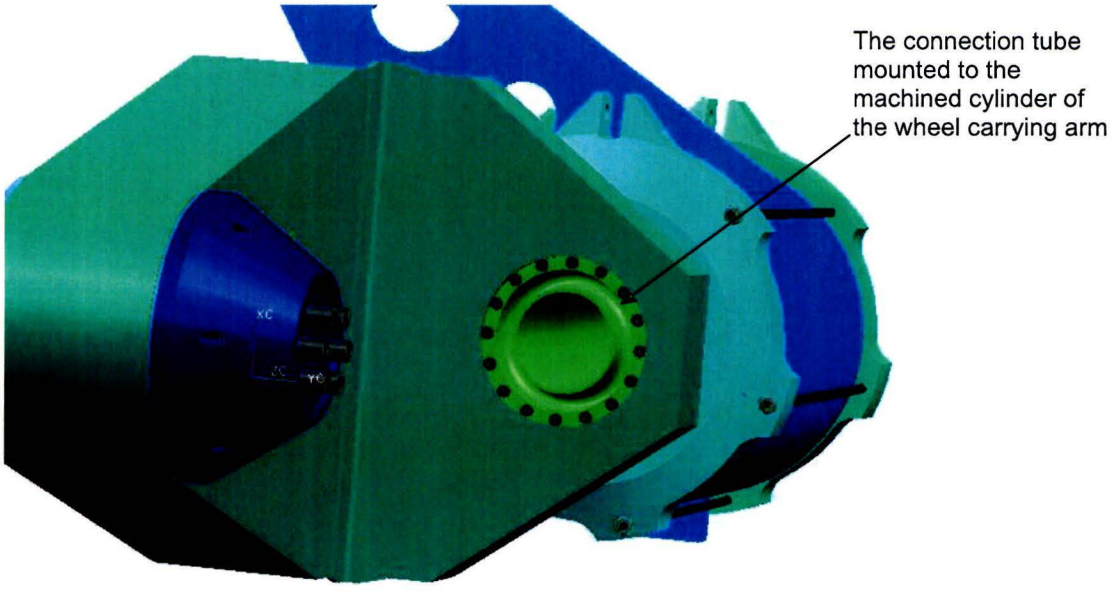

Figure 8.2.11: Subassembly of the steering system mounted from the bottom of the wheel carrying arm to the "machined cylinder"

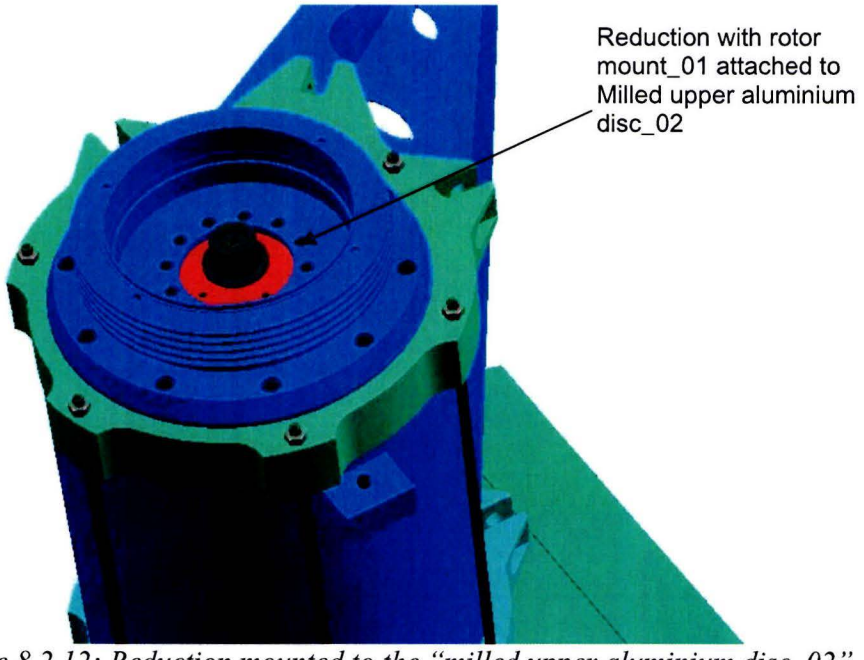

Figure 8.2.12: Reduction mounted to the "milled upper aluminium disc_02"

The stator of the frameless motor is mounted to the "milled upper aluminium disc_02". The rotor of the frameless motor, together with "rotor mount_02" is fitted to "rotor mount_01", see figure 8.2.13.

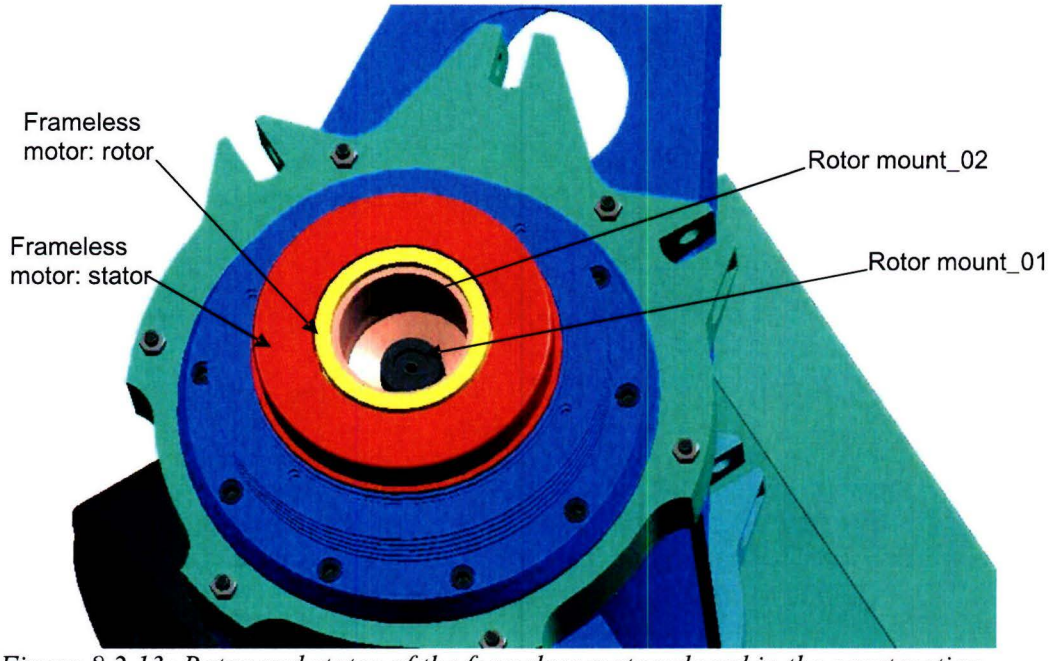

Figure 8.2.13: Rotor and stator of the frameless motor placed in the construction

The steering motor assembly is further built up with the "aluminium tube with cooling fins" that is placed over the stator and with "rotor mount_03" that is secured with an M5x65 screw. A keeper ring is used to secure the rotor of the frameless motor to the rotor mounts.

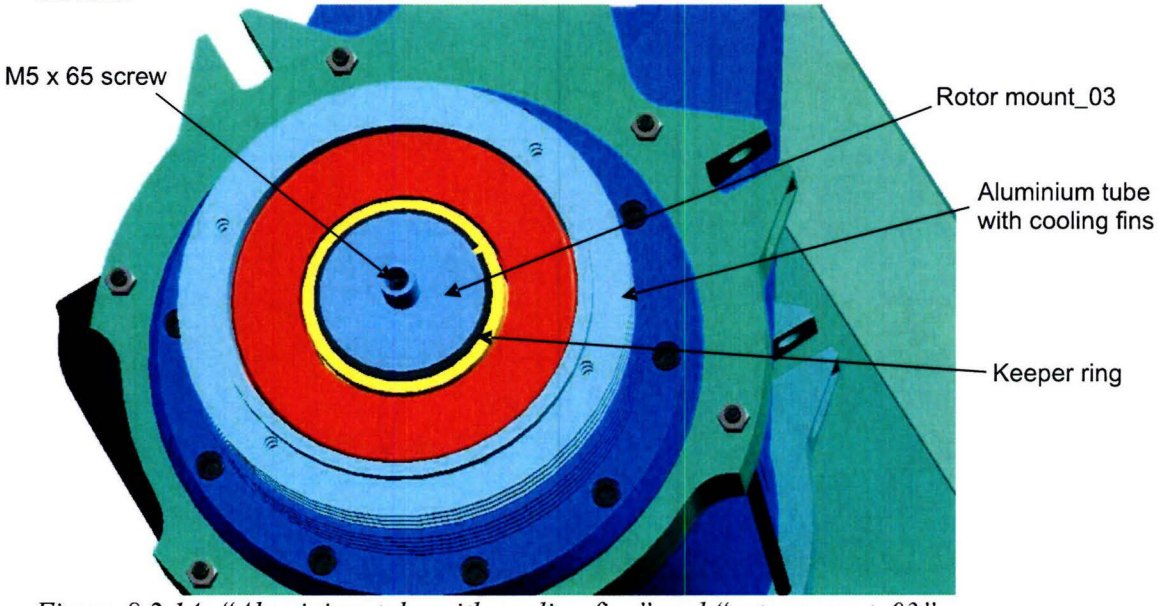

Figure 8.2.14: "Aluminium tube with cooling fins" and "rotor mount_03"

The motor housing is closed with the "aluminium disc motor housing" that is secured with 4 M5x80 screws. The encoder of the steering system is placed onto the motor housing disc and its rotating part is attached to the "rotor mount_03", see figure 8.2.15.

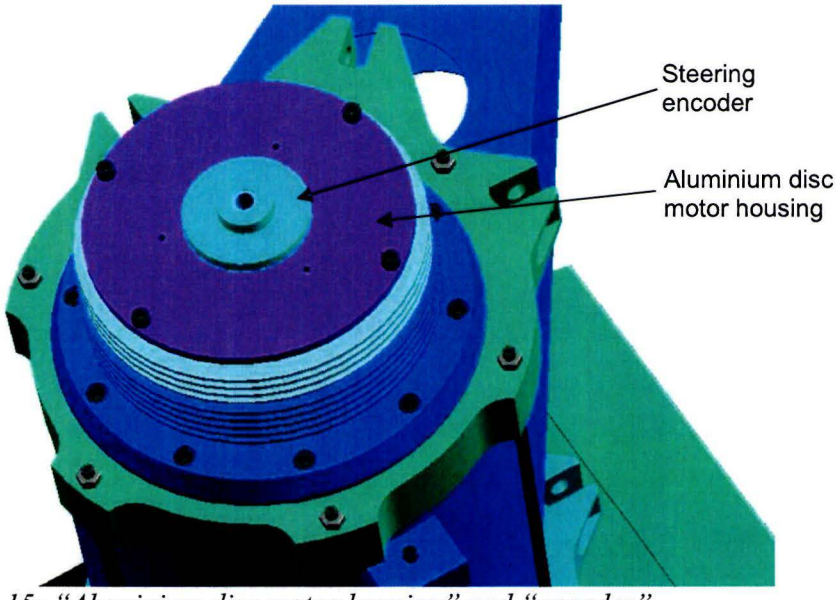

Figure 8.2.15: "Aluminium disc motor housing" and "encoder"

The steering encoder is secured and covered by the "cover lid" that is secured with 3 M4x20 screws, see figure 8.2.16.

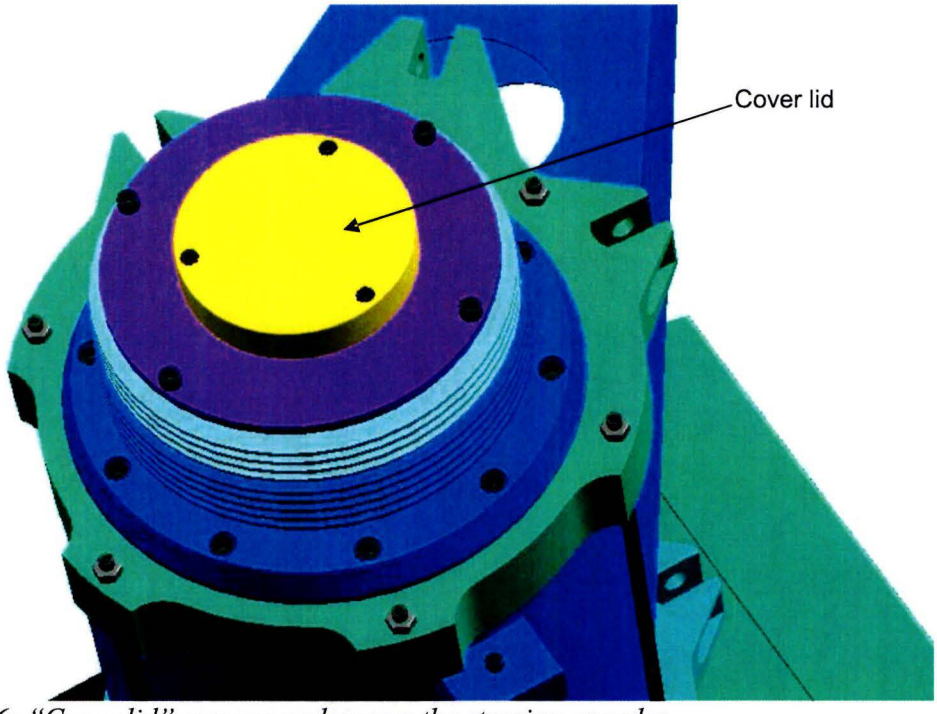

Figure 8.2.16: "Cover lid" secures and covers the steering encoder

When the suspension rods are attached, see figure 8.2.17 and 8.2.18, the wheel unit is ready to be connected to the main frame of the robot vehicle.

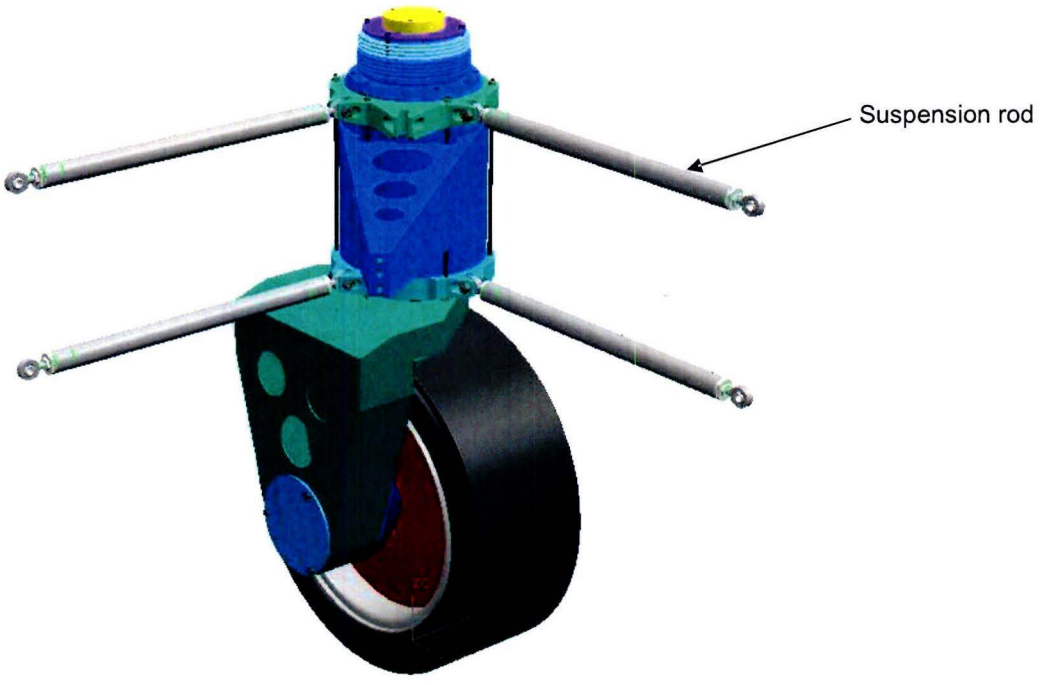

Figure 8.2.17: Wheel unit complete with suspension rods

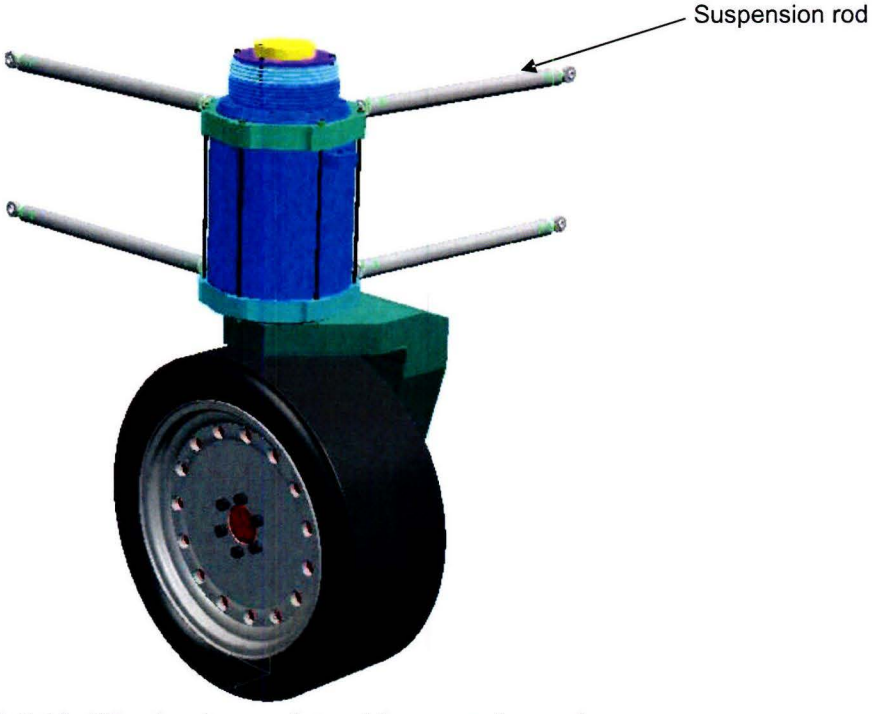

Figure 8.2.18: Wheel unit complete with suspension rods

§ 8.3 Construction of the main frame

There are four wheel units that have to be connected to form a vehicle, see figure 8.3.1 and 8.3.2.

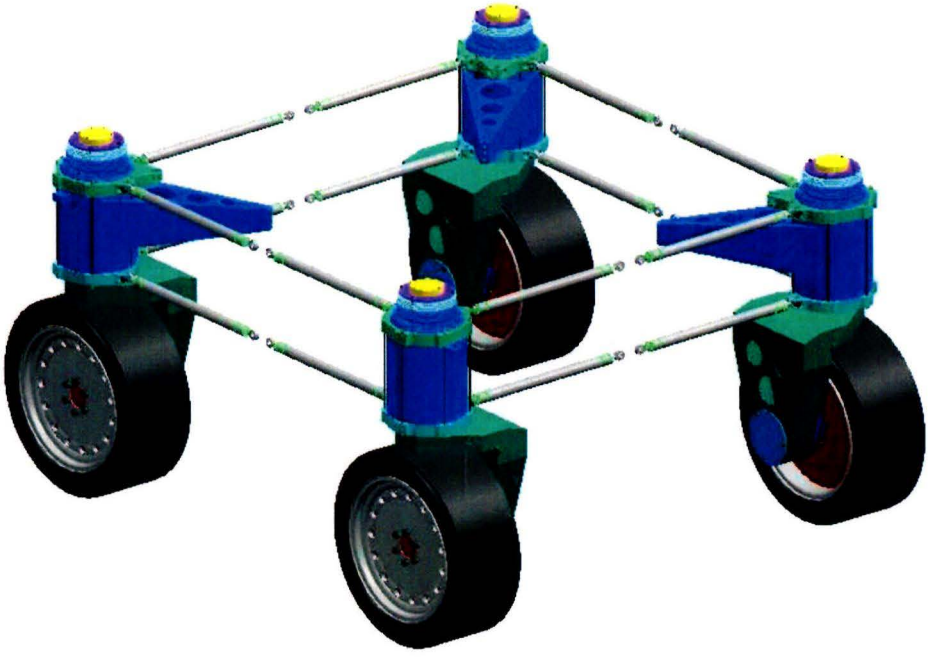

Figure 8.3.1: Four wheel units at their respective positions

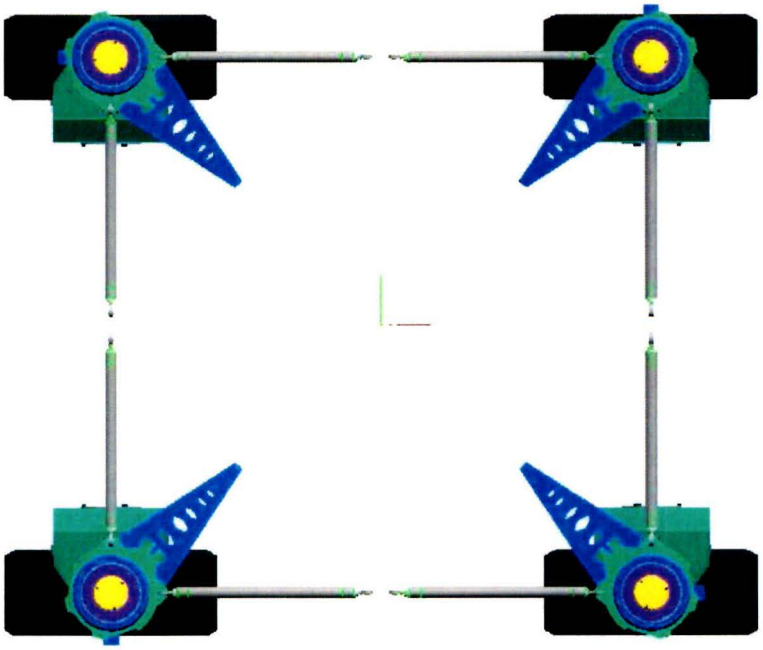

Figure 8.3.2: Four wheel units, top view

The main frame has to connect all the suspension rods to make one vehicle from the four separate wheel units. The connection has to be stiff and the frame has to withstand all the forces that are generated in different vehicle manoeuvres. All the vehicle components that are not in the wheel units will be mounted onto the main frame. All these components will be placed as low as possible in the main frame to minimize the height of the centre of gravity. The centre of gravity will be low and certainly below the lowest suspension rods, so the inertia forces from the centre of gravity are transferred through the frame up to the suspension rods and through the wheel carrying arm, wheel motor, wheel and tire to the road. The frame has to be compact, since a compact frame results in a low inertia around the yaw axis. And, as with all components, a low mass is important.

The most stiff and compact way of connecting the suspension rods and transferring the forces from the centre of gravity to the suspension rods is with the use of steel sheets between the ends of the suspension rods, like in the top view of figure 8.3.3. The steel sheets are placed vertically and go from 60 [mm] above the ground, which is the ride height, to the upper suspension rods. The intersection of two sheets is at the centre line of the suspension rods. In this way all forces from the suspension rods are transferred directly into the sheets. At the bottom, the four steel sheets are connected with a horizontal sheet. In this way an open box is created. The easiest way of improving the frame is to close the open box with a sheet on the top. But this is not desirable since the main frame should be accessible from the top. Another acceptable way of stiffening the open box is by creating a frame at the top edge.

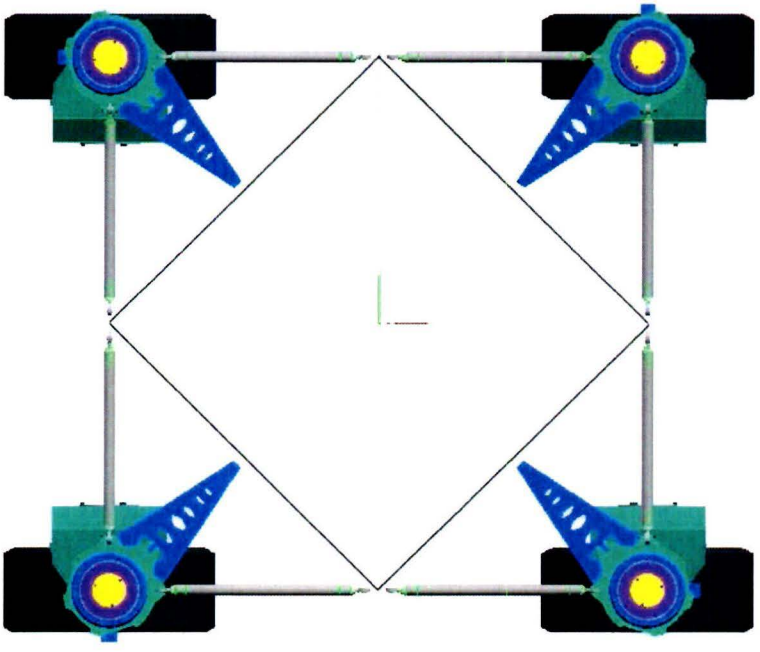

Figure 8.3.3: Four wheel units with an outline of the main frame

The reinforcement frame at the top edge of the open box construction helps to keep the box in its form when loads are exerted to the frame. The more the reinforcement frame approaches a completely closed box, the better it fulfils its task. But for accessibility a certain area has to be free. The chosen area allows the battery to fit through it, see figure 8.3.4. The width of the edge is 150 [mm] and the height is 260 [mm]. This height is chosen, because like this, the bottom side of the reinforcement frame is at the same height as the lower suspension rods and helps to transfer the forces through the frame.

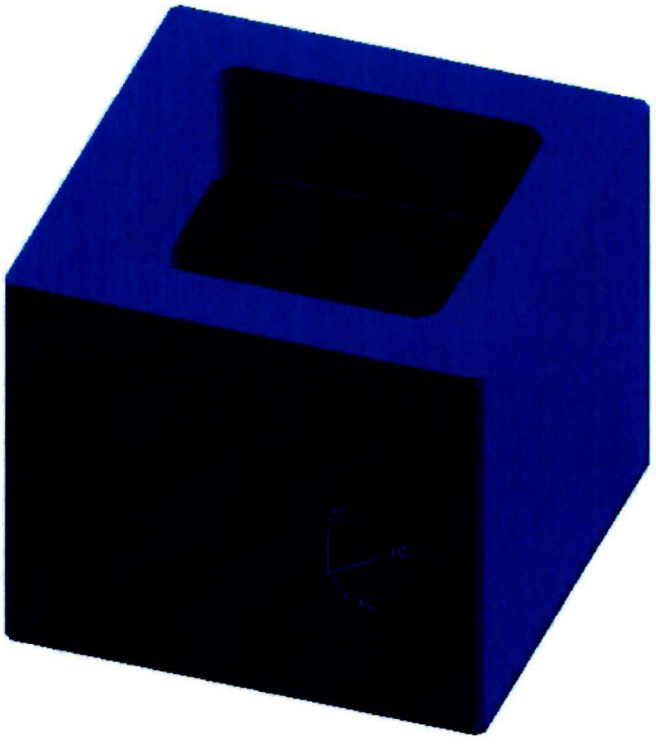

Figure 8.3.4: Open box construction with a reinforcement frame at the top edge

In the corners of the frame there has to be a connection of the steel sheets and each corner needs fixing points for the suspension rods. This can be done in various ways and some possibilities are shown in appendix T [Main frame corner concepts]. From these options, concept D is chosen, because it uses a tube with a small cross section which has a relatively low mass and because the part with the connection points for the rod ends can be easily dismounted. Moreover this concept has three mounting positions for each suspension rod, so adjustment of the suspension geometry is possible. The frame with the mounting points at the corners is shown in figure 8.3.5. A close-up of a corner of the frame is shown in figure 8.3.6. In this close up the tube is still open, so the mounting block inside the tube can be seen. In the final assembly this tube will be closed with a cover.

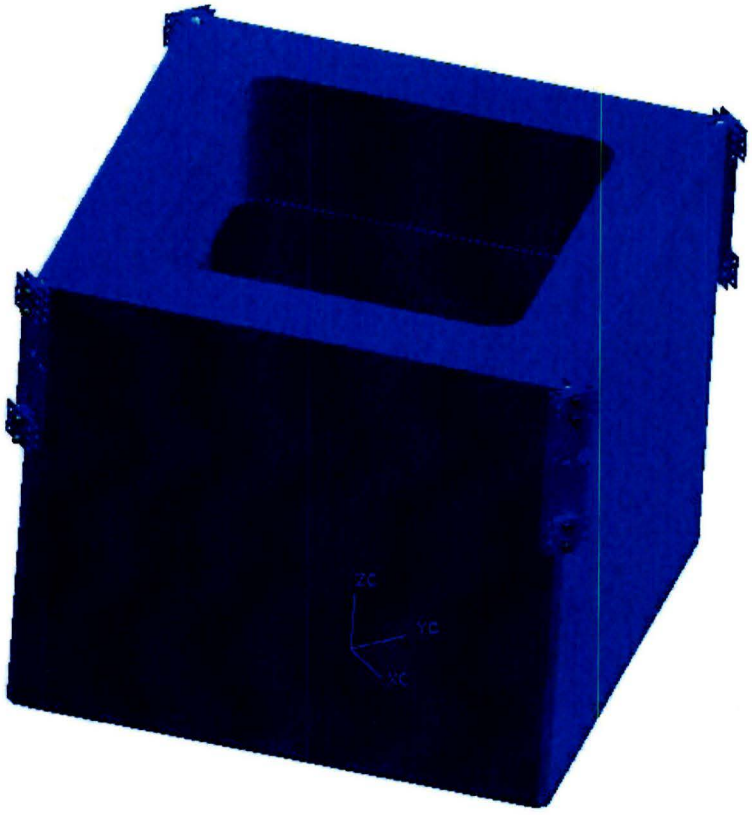

Figure 8.3.5: Main frame with connection points for the suspension rods at the corners

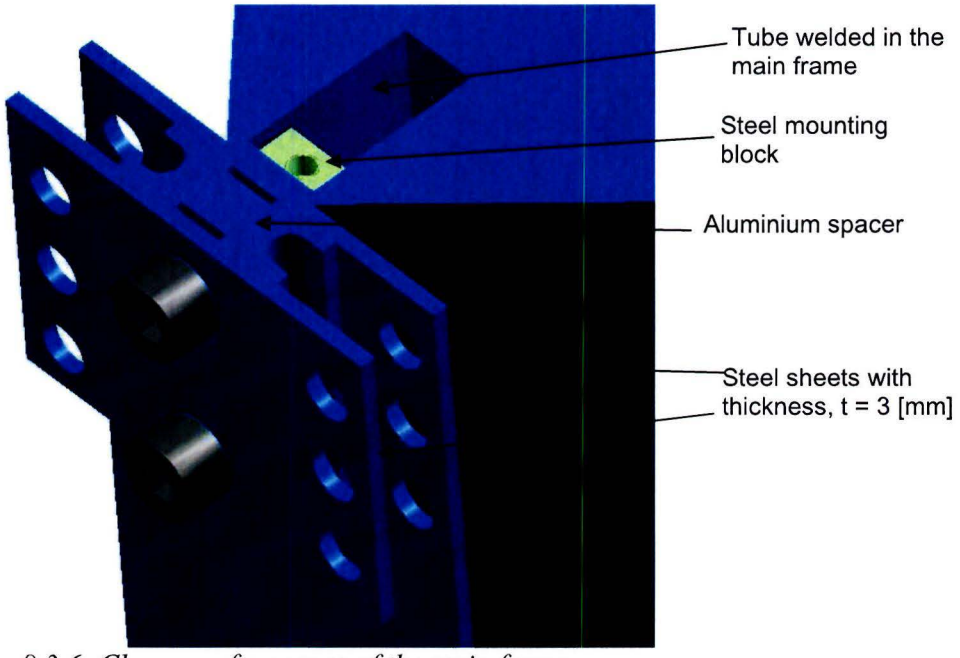

Figure 8.3.6: Close up of a corner of the main frame

This main frame is modelled with the finite element program ALGOR to investigate the behaviour of the frame under load, see appendix U [Main frame analysis]. From this analysis it becomes clear that the highest stress occurs in the corners of the main frame, so the version of the frame with added material in the sheets in the corners will be used. The frame will also be improved with omega-profiles as described in the appendix. For the support of the shock-absorbers and for the mounting of parts like batteries and motor drives an extra tube will be made at the bottom of the frame. Furthermore some holes will be made in areas where the stress is low to save mass and for the accessibility of the parts in the frame. The complete frame is shown in figure 8.3.7. The total mass of this frame is 62 [kg]

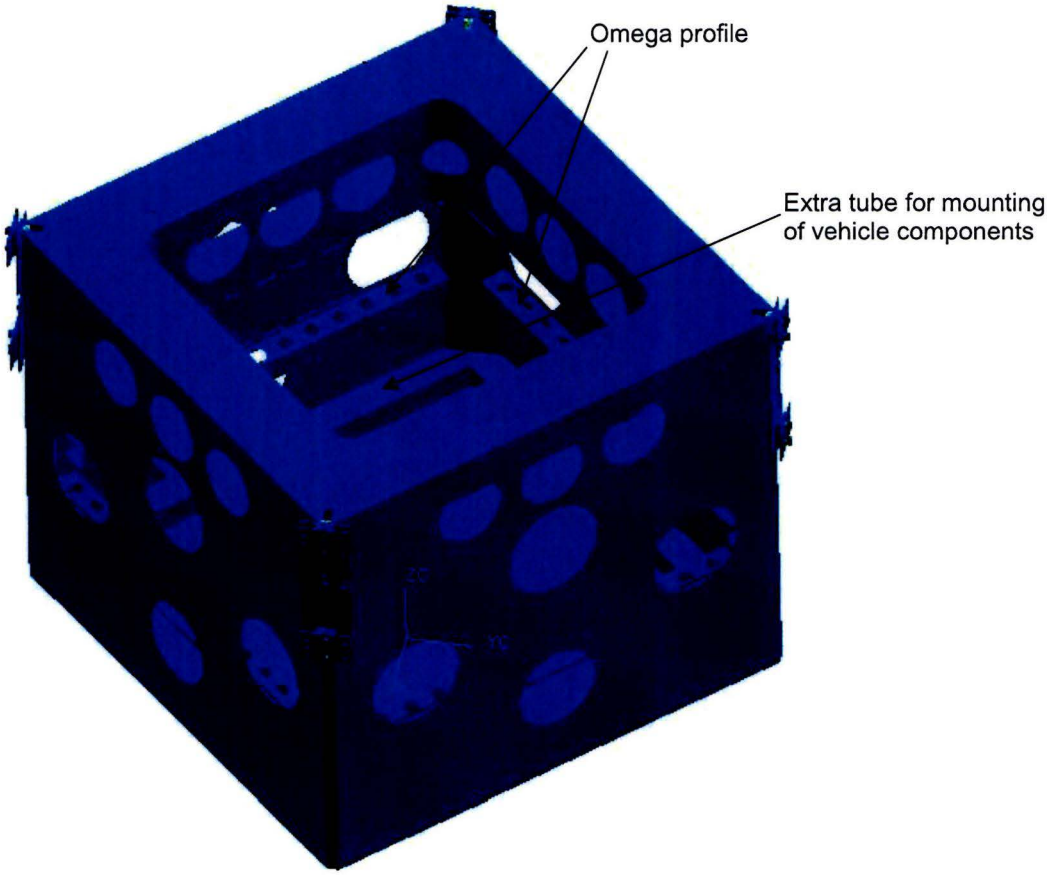

Figure 8.3.7: Main frame complete

§ 8.4 Total assembly

In this paragraph all the separate parts and subassemblies are put together to make the total vehicle. In figure 8.4.1 and 8.4.2 the four wheel units are mounted to the main frame. In this figure also the shock absorber module is added to the frame. Pull rods connect the wheel units with the rockers. The conical tube for the anti rotation system is connected to the frame with a steel rod. The mass of this assembly is 350 [kg], but a substantial amount of mass will be added with all the parts that will be mounted inside the main frame.

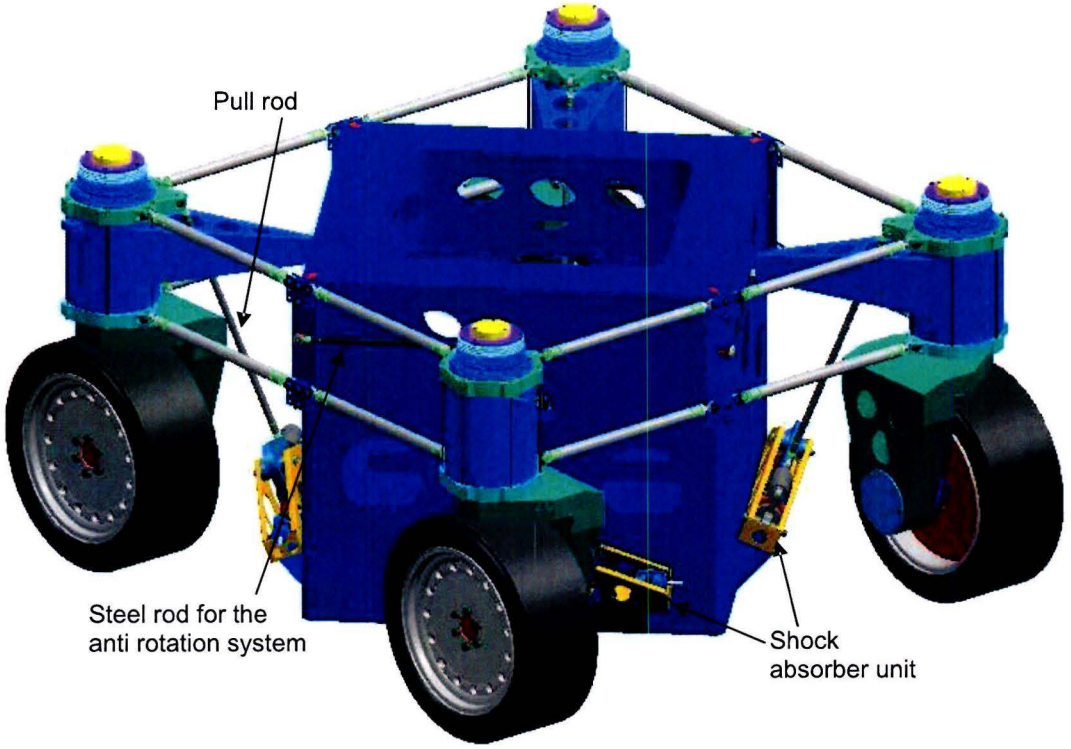

Figure 8.4.1: Total vehicle, but without the parts mounted in the frame

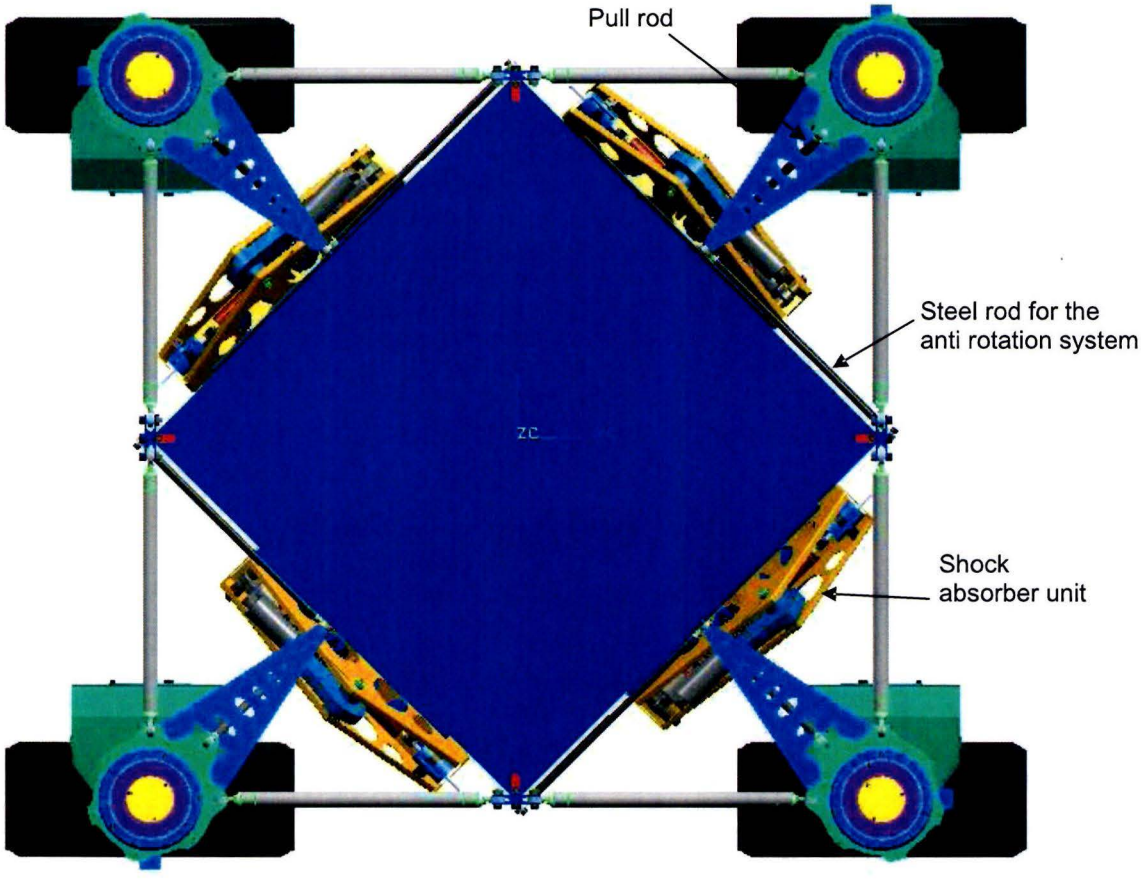

Figure 8.4.2: Total vehicle, but without the parts mounted in the frame; Top view

All the other parts will be mounted in the main frame. To keep the height of the centre of gravity as low as possible, parts with a large mass will be mounted at the bottom of the main frame.

Two batteries from the Toyota Prius TSH2 are placed in the middle and at the bottom of the frame, see figure 8.4.3 and 8.4.4. They are mounted with vertical sheets to the tube at the bottom of the frame, so forces in all directions are directly transferred. On top of the batteries are the super capacitor modules and the DC-DC-converter, because they are part of the energy system. The drive electronics for the drive motors are placed in pairs beside the battery. The drivers for the steering motors are also placed beside the battery, one at each side. The safety box is placed in a corner of the frame, also beside the battery. In the opposite corner is the adapter box with the control system ControlCIT. This one is rather big, so it is placed above the battery. In the current Moving Base is another box with relays, fuses and other electrical components. The components of this unit should be redesigned and placed distributed in the frame. For remote communication with the vehicle control system a W-LAN router is used. This one is placed to the top of the frame for the reception of the data signals. The accelerometer and the gyroscope are mounted to the omega sections.

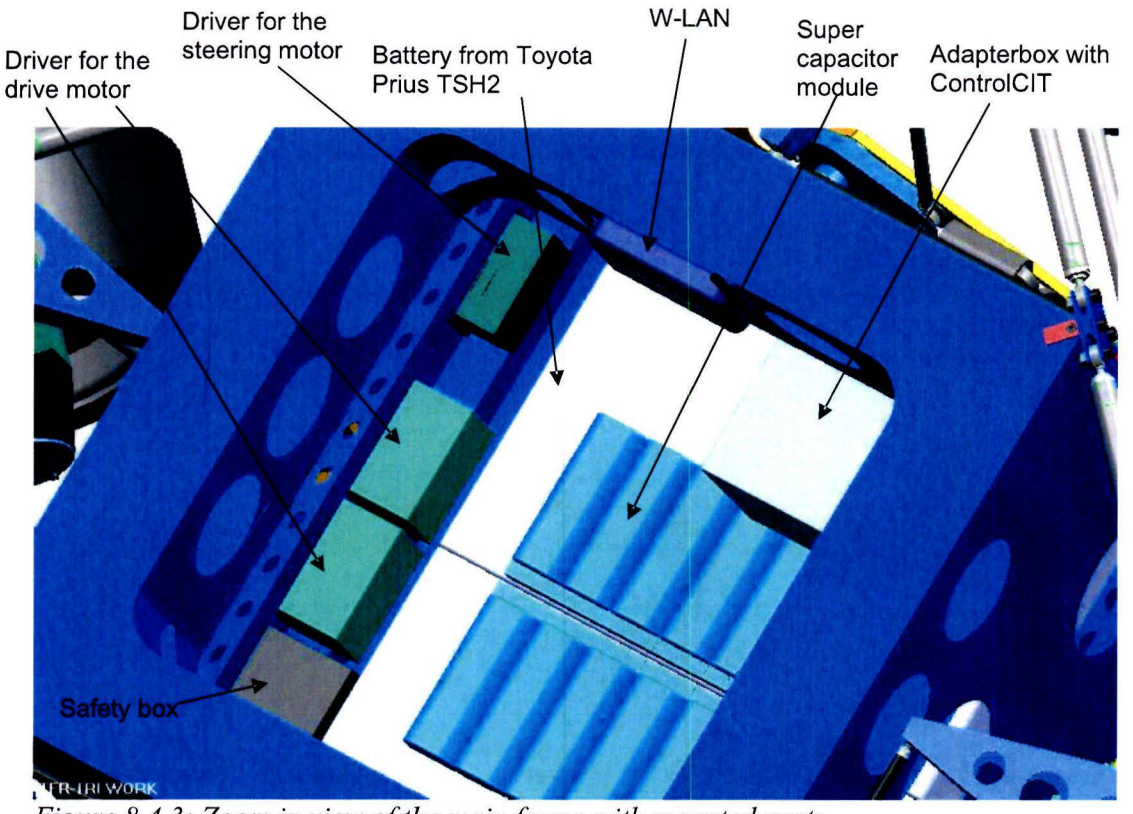

Figure 8.4.3: Zoom in view of the main frame with mounted parts

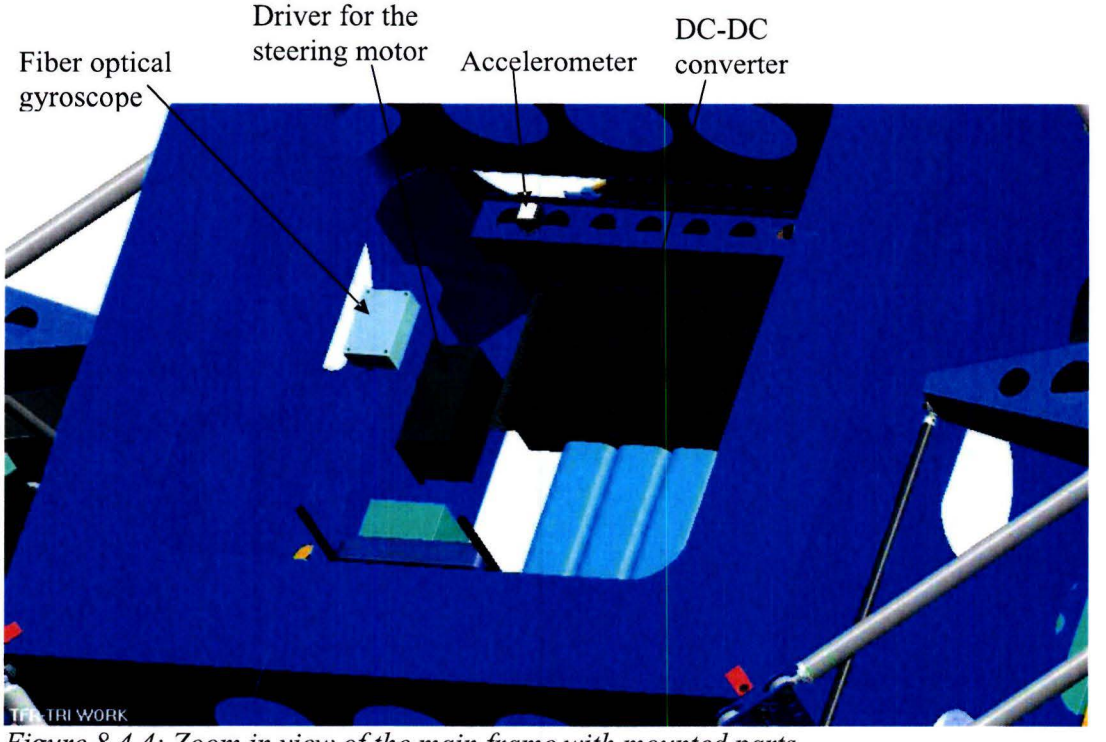

Figure 8.4.4: Zoom in view of the main frame with mounted parts

The complete vehicle is shown In figure 8.4.5. The mass of the vehicle is 496 [kg] and the centre of gravity is only 4 [mm] out of the centre of the vehicle. The height of the centre of gravity is 0,42 [m]. The total vehicle mass will increase due to the wiring of the vehicle. More detailed information about the used vehicle components can be found in appendix L [Specifications Moving Base version D].

A cost estimation of this robot vehicle can be found in appendix V [Cost prediction for various vehicle configurations] table: version D. This appendix contains tables with the cost prediction for various vehicle configurations. In appendix W [Drive line cost comparison] only the drive lines of these vehicle configurations are listed for better comparison between the various versions.

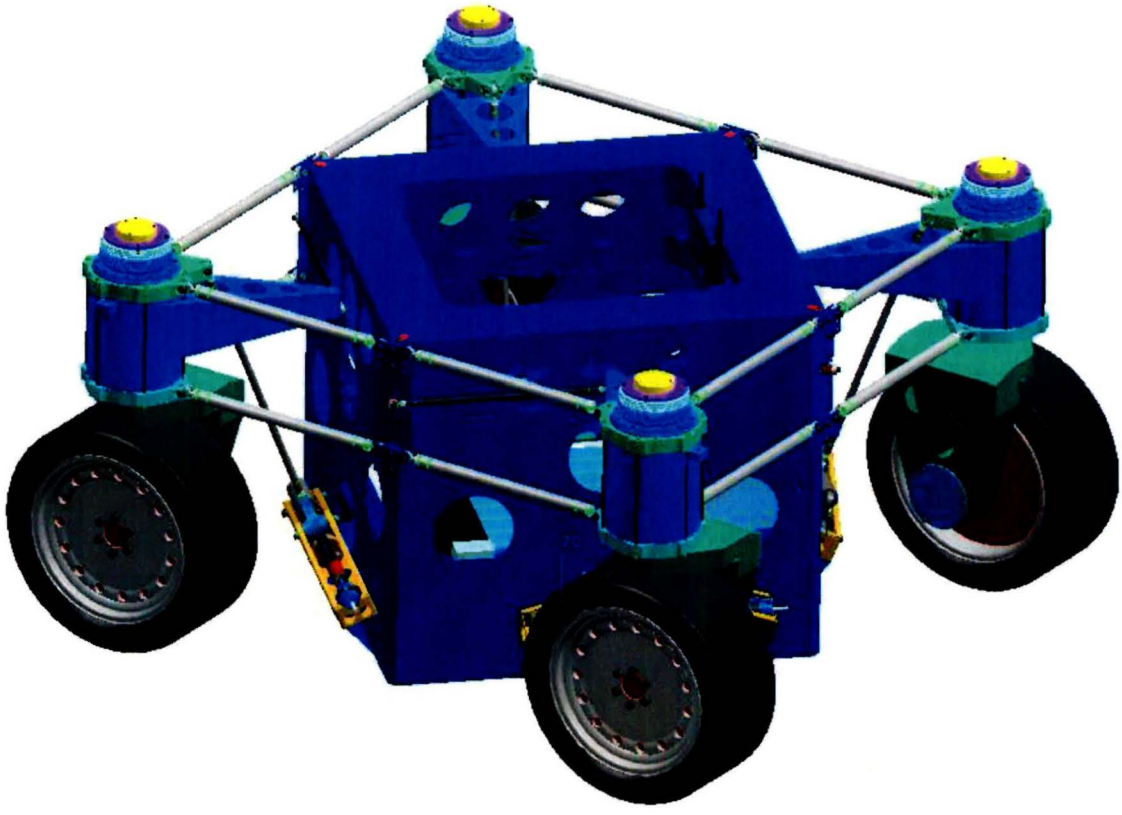

Figure 8.4.5: The complete robot vehicle

Conclusions and Recommendations

For the use in the VEHIL test facility of TNO Automotive and for other possible applications a new robot vehicle has been designed. The design of this robot vehicle incorporates primary suspension. This improves the road holding of the vehicle and reduces the vertical accelerations of the main frame with all the electronics. All four wheels of the robot vehicle are driven and can be steered without a limitation in the steering angle, so complex movements in the horizontal plane are possible. The maximum acceleration of the vehicle is 10 [m/s^2] and the maximum driving speed is 50 [km/h]. The suspension is adaptable for different ride heights and situations. The robot vehicle is capable of carrying loads up to 300 [kg]. The design is made with cost in mind to achieve high performance at acceptable cost.

For further development the following issues should be considered:

Adapt the control system and implement the vertical movements of the vehicle and the actions of the anti roll system.

Devise a system for rapidly changing of batteries, to improve the availability of the robot vehicle. The energy density becomes less important when the battery can be changed rapidly. With a smaller battery, the total vehicle mass will be considerably reduced

Keep up with the developments of wheel motors, because prices will drop and performance will increase.

Look for wheel motors with drivers that are suitable for 13 inch wheels, since this helps in lowering the height of the centre of gravity.

With the new design for the robot vehicle, the track width and wheel base can be easily varied. This can be done by changing suspension rods by rods with a different length, but it may be possible to make suspension rods which can vary in length while they are being used.

Literature

[4007] Lecture notes 4007, "Constructieprincipes", Technische Universiteit Eindhoven, 2003

[Bastow] Donald Bastow, Geoffrey Howard, "Car Suspension and Handling", 3rd editon, Pentech Press ltd. and SAE, 1993, ISBN: 1-56091-404-1

[Berkhout] Wouter J. Berkhout, "Design for a Formula Student race car", Master's thesis, Technische Universiteit Eindhoven, 2004

[Besselink] Igo Besselink, "college sheets Vehicle Dynamics", course 4L150, Technische Universiteit Eindhoven, 2004

[Chan] C.C. Chan and K.T. Chau, "Modern electric vehicle technology", Oxford University Press, 2001, ISBN: 0-19-850416-0

[Dixon] John C. Dixon, "Tires, Suspension and Handling" 2nd edition, SAE International, 1996, ISBN: 1-56091-831-4

[Jacek] Jacek F. Gieras, Mitchell Wing, "Permanent Magnet Motor Technology" ISBN:0-8247-0739-7

[Jana] Wiliam S. Jana, "Engineering Heat Transfer", 2nd edition, CRC Press, 2000, ISBN: 0-8493-2126-3

[Kenjo] Tak Kenjo, "Electric motors and their controls", Oxford Science Publications, 1991, ISBN: 0-19-856240-3

[Matschinsky] Wolfgang Matschinsky, "Road Vehicle Suspensions", Professional Engineering Publishing Ltd., 2000, ISBN: 1-86058-202-8

[Ploeg] Jeroen Ploeg, Dirk J. Verburg, Albert C.M. van der Knaap, "ATS/AGV: Design, Implementation and Evaluation of a High Performance AGV", IEEE Intelligent Vehicle Symposium (IV'2002), Versailles, France, June 18-20, 2002

[Schmeitz] Private communication with Dr.ir. A.J.C. Schmeitz

[Tertoolen] Simone F. Tertoolen, "Innovation in the film industry, A new application and a new user interface for a highly manoeuvrable robot", Technische Universiteit Delft, 2005

[TNO ControlCIT] Brochure TNO Automotive: "ControlCIT, Control system design and real-time implementation for intelligent automated vehicles"

[TNO MB] Brochure TNO Automotive: "VEHIL moving bases: the ultimate roadbots"

[TNO VEHIL] Brochure TNO Automotive: "Vehicle Hardware In the Loop (VEHIL), Intelligent test facility"

[Pat. Cannondale] Patent WO0043261A1, Cannondale

[Verburg] Dirk J. Verburg, Albert C.M. van der Knaap, Jeroen Ploeg, "VEHIL, Developing and testing intelligent vehicles", IEEE Intelligent Vehicle Symposium (IV'2002), Versailles, France, June 18-20, 2002